PARAMETRIC FINITE ELEMENT ANALYSIS OF STEEL BEAMS SUBJECTED TO LATERAL TORSIONAL BUCKLING

by

Tuğkan Şengül

B.S., Civil Engineering, Boğaziçi University, 2008

Submitted to the Institute for Graduate Studies in
Science and Engineering in partial fulfillment of
the requirements for the degree of
Master of Science

Graduate Program in Civil Engineering

Boğaziçi University

2014

ACKNOWLEDGEMENTS

I would like to express the deepest appreciation to Prof. Gülay Altay, who has the attitude and multi dimensional engineering perspectives. She continually and convincingly conveyed a spirit of adventure in regard to research and an excitement in regard to teaching. Without her guidance, advices, criticisms, encouragements and insight throughout the research, this dissertation would not have been possible.

Besides my thesis supervisor, I would like to thank the rest of my thesis committee: Prof. Cengiz Dökmeci and Assist. Prof. Serdar Soyöz and for their encouragements, insightful comments.

Also, I owe my gratitude to my family, for giving birth to me at the first place and supporting me spiritually throughout my life.

In addition, I present my deep thankful attributions to Duygu Gül, who was the most motivational spark effect throughout all my thesis research.

ABSTRACT

PARAMETRIC FINITE ELEMENT ANALYSIS OF STEEL BEAMS SUBJECTED TO LATERAL TORSIONAL BUCKLING

Lateral torsional buckling is a failure criteria for beams in flexure. The AISC defines lateral torsional buckling as the buckling mode of a flexural member involving deflection normal to the plane of bending occurring simultaneously with twist about the shear center of the cross-section. This failure criteria occurs when the compression portion of a beam is no longer sufficient in strength and instead the beam is restrained by the tension portion of the beam, which causes deflection or twisting to occur. The purpose of this study is to determine whether the allowable lateral torsional buckling stresses defined in AISC are conservative with eigenfunction finite element analyses. In this scope, four compact I-Sections were modeled, each of them with double symmetrical dimensions separately for parametric analyses. Besides, loading condition performed via constant bending moment and trianbular bending moment distribution. Beam models on which linear analyses were performed by using finite element analysis software, ANSYS R14.5/Structural to observe the lateral torsional buckling of steel beams were constructed as simply supported and cantilever beams. Therefore, a 4-Dimensional global structural string with 1(I-section) x 4(double symmetric parametric models) x 2(loading conditions) x 1(software) x 2(analyses) x 4 (span lengths)= 64 entries was progressed to cover all thesis researches. To simulate the actual beam behavior, solver operators in ANSYS is manually optimized instead of performing default configurations. Error spectrum lies between the limits of 1.92% and 43.74% for the simply supported beam models, beam models these limits are bounded with very close values as 0.22% and 1.37%. Finally, it has been obserbed that, ANSYS software converges to AISC standarts with an absolute average error value of 11.16%.

ÖZET

YANAL BURULMALI BURKULMA ETKİLERİNE MARUZ KALAN ÇELİK KİRİŞLERİN PARAMETRİK SONLU ELEMANLAR ANALİZİ

Yanal burulmalı burkulma, kirişler için burkulma açısından bir göçme kriteridir. AISC, yanal burulmalı burkulmayı, elastik halde, eğilme düzlemine dik yerdeğiştirme ile en kesitin kayma merkezi etrafında dönmesinin aynı anda oluşmasını içeren burkulma durumu olarak tanımlar. Bu göçme kriteri, kirişin basınç kısmının artık taşıma kapasitesi açısından yeterli olmadığı, kirişin yerdeğiştirme ve dönmeye neden olan, gerilme kısmı tarafından sınırlandırılması durumunda oluşur. Bu çalışmanın amacı, oluşturulan modellerin sonlu eleman analizleriyle elde edilen sonuçların, AISC yönetmeliğinde tanım lanan yanal burulmalı burkulma emniyet gerilmeleri ile karşılaştırarak, bu yanal burkulma ifadelerinin tutarlılığını belirleyebilmektir. Bu kapsamda, herbiri ayrı ayrı, çift simetrik dört kompakt I kesitleri parametrik analizler için modellenmiştir. Ayrıca, sabit ve üçgensel eğilme momentleriyle, iki farklı yükleme durumu uygulanmıştır. Çelik kirişin yanal burulmalı burkulma davranışını gözlemlemek için ANSYS R14.5/Structural sonlu eleman analiz yazılımı kullanılmış, doğrusal analizleri yapılan kiriş modelleri basit mesnetli ve ankastre olarak oluşturulmuştur. Böylece, 1(kesit) x 4(parametrik simetrik model) x 2(yükleme) x 1(yazılım) x 4(kiriş aıçıklığı) x 2 (analiz)=64 elemanlı, 4 boyutlu geniş bir yapısal sicim, tüm tez çalışmalarını kapsayacak biçimde geliştirilmiştir. Gerçek kiriş davranışının benzeşimini görmek için, ANSYS öntanımlı çözüm operatör lerini kullanmak yerine, bu operatörler probleme uygun şekilde düzenlenmiştir. Hata spektrumu basit mesnetli kiriş için 1.92% ve 43.74%; ankastre kiriş için de 0.22% ile 1.37% arasında yer almıştır. Sonuç olarak, ANSYS yazılımının, AISC standartlarına, 11.16%'lık mutlak ortalama hata değeriyle yaklaştığı saptanmıştır.

TABLE OF CONTENTS

LIST OF FIGURES

LIST OF TABLES

LIST OF SYMBOLS

A	Area
A_f	Flange area
A_s	Area of steel cross section
A_w	Web area
b	Width of a cross sectional element
b_f	Flange width
C_b	Moment fradient factor for lateral-torsional buckling strength
C_w	Warping constant
E	Modulus of elasticity
E_s	Modulus of elasticity of structural steel
G	Shear modulus of elasticity
h	Width of web
I	Moment of inertia
I_s	Moment of inertia of steel section
I_x,I_y	Moments of inertia about a and y axes
L_b	Unbraced beam length
L_p	Largest unbraced beam length for which lateral torsional buckling
M	Bending moment
M_1, M_2	Bending moments at the end of a beam
M_c	Available moment strength
M_{cx}, M_{cy}	Available moment strengths for x and y axes
M_{cr}	Critical moment for lateral-torsional buckling
M_n	Nominal bending strength
M_{nx}, M_{ny}	Nominal bending strengths fort he x and y axes
M_p	Plastic moment
M_r	Yield moment
M_x, M_y	Moments about the x and y axes
P	Concentrated force

P_{cr}	Critical buckling load
r	Radius of gyration
R_a	Allowable strength
S	Elastic section modulus
S_x, S_y	Elastic section modulus for a and y axes
t	Thickness of cross-sectional element
t_b	Thickness of beam flange
t_f	Thickness of flange
t_w	Thickness of web
V	Shear force
Z	Plastic section modulus
Z_x, Z_y	Plastic section modulus for x and y axes

δ	Axial deformation
Δ	Deflection
ε	Deformation
λ	Width-thickness ratio
σ	Stress

LIST OF ACRONYMS/ABBREVIATIONS

AISC	American Institue of Steel Construction
AISI	American Iron and Steel Instute
APDL	ANSYS Parametric Design Language
ASCE	American Society of Civil Engineers
ASD	Allowable Stress Design
BC	Boundary Condition
BUCOPT	Block Lanczos
LESIZE	Element Edge Size
EQSLV	Equation solver with Sparse Solver
ES	Error Spactrum
FEA	Finite Element Analysis
FEM	Finite Element Method
MEXPAND	Number of Modes to Expand
PSTRES	Prestress Effects
SCI	Steel Construction Institue

1. INTRODUCTION

1.1. Theory Background

Beams are essential components of steel construction. A satisfactory design should ensure that the beam is stable and has enough strength and stiffness against the applied loads. For steel beams having an I-shaped cross section, global buckling and local buckling are typical modes of instability [1].

Global instability is in the form of lateral torsional buckling of the beam as a whole while local instability could be in the form of web or flange buckling. Design codes present capacity equations for lateral torsional buckling of I-Section members. Local buckling is usually precluded by limiting the width-thickness ratio of the compression elements web or flange [2].

In account, for such furthermore complex analyses, this thesis aims to present a detailed investigation of lateral torsional buckling phenomenia, by using advanced finite element software ANSYS. As indicated in Figure 1.1 and in Figure 1.2, ANSYS R14.5/Structural is performed during the structural pre-processing via 3D, deformable and solid extrusion techniques and also a postprocessing simulation.

Comparision of the simulated ANSYS data with theoretical solutions is the main idea of this research of which mostly consists of statistical error analyses. In order to cosntruct a detailed analysis, relative and average error values are calculated. Not only the statistical but also the analytical techniques are apllied throught the whole thesis research.

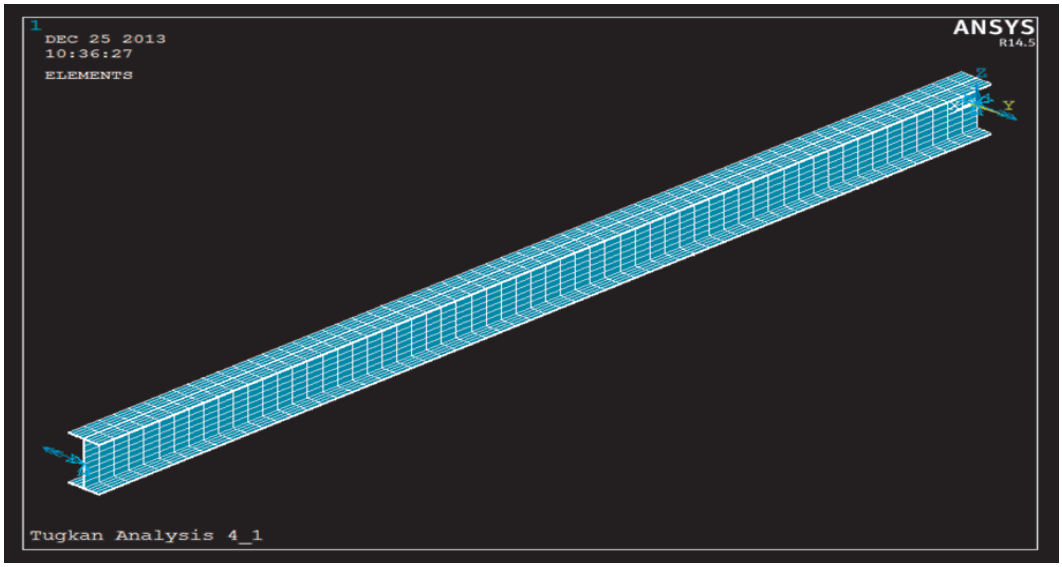

Figure 1.1. ANSYS R14.5/Structural 3D Beam Modeling.

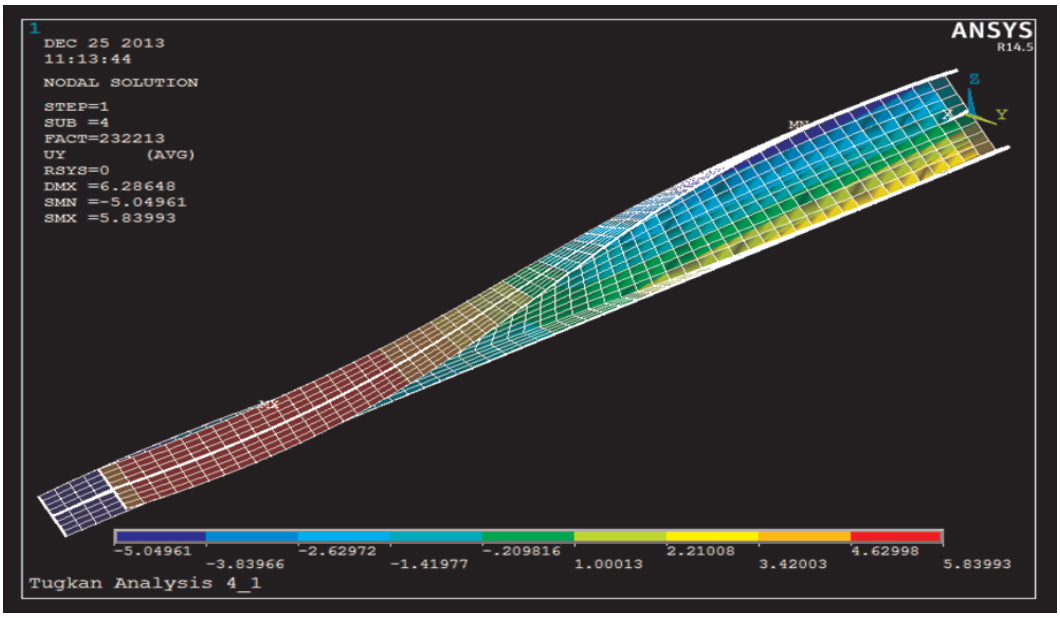

Figure 1.2. ANSYS R14.5/Structural Lateral Torsional Buckling Simulation.

1.2. Literature Survey

The slender members loaded by transversal loads or ended moments acting around the major axis of inertia, may collapse by lateral-torsional buckling before reaching the full plastic resistant moment, Mpl. As Figure 1.3 shows lateral-torsional buckling of a beam, exaggerated as a result of fire, in a flour-mill building in Minnesota[3].

Figure 1.3. Lateral Torsional Beam Buckling Exaggerated by Fire.

Lateral torsional buckling should be taken into account during the design of steel structures. The phrase "lateral torsional buckling" is appropriate because the cross-section both rotates and displaces laterally. It is also a buckling phenomenon because the lateral stiffness is affected by the intensity of the load that is applied to the beam. In fact, the buckling load is determined by the lateral stiffness being zero. To account for the effect of the applied load on the lateral stiffness it is necessary to consider equilibrium in the displaced configuration [3].

1.2.1. Lateral instability of elliptical hollow section beams (Law, Gardner, 2012)

Lateral instability of elliptical hollow section(EHS) members in bending is studied through eight laterally unrestrained EHS beams, with a constant cross-sectional aspect

of two, were tested in three-point bending. The test set-up, material properties, section geometry, residual stress measurements and full load-deformation responses of the test specimens are reported. To supplement the esperimental data, numerical models were also developed and validated against the test results.

Parametric studies were then performed, to assess the influence of cross-sectional aspect ration and member slenderness on lateral stability. Based on the assmbled structural performance data, lateral torsional buckling curves for elliptical hollow section beams have been developed and statistically verified. Limit-buckling curves for elliptical hollow section beams have been developed and statistically verified.

Member instability in hot-finished EHS beams has been examined in this study. An experimental programme comprising 6 tensile coupon tests, longitudional residual stress measurements ans in-palne major axis bending tests was undertaken. The key material properties, geometric measurements and test results from the lateral torsional buckling tests have been verified via numerical iterations. To generate additional results to assess EHS member instability for a range of cross-sectional aspect ratios and member slenderness, an extensive numerical modelling was undertaken. Satisfactory aggreement between the test results and those obtained from the numerical models was achieved.

A series of parametric studies were the conducted using the validated numerical models to investigate the influence of cross-secional aspects ratios ranging from 2 to 6 slendernessess from 2 to 12 on the lateral torsional buckling behavior.

1.2.2. Thin-Walled Structures (Camotim, Andrade, Basaglia, 2012)

This technical note addresses a surprising result conceerning the lateral-torsional buckling of monosymmetric I-section beams: amongst all bending moment diagrams caused by any combination of applied end moments and transverse loads acting at the shear sentre, the lowest critical moment does not necessarily correspond to uniform bending, which is at odds with the “intuitive expectation” of most engineers that such

bending moment distribution is the most unfavourable with respect to lateral-torsional buckling.

It is shown, by means of several illustrative examples, that this may not be the sac efor I-section beams with unequal flanges(monosymmetric cross-section symmetry with respect to the minor axis).

Moreover, the critical inspection of the terms associated with the cross-section monosymmetry and appearing in the beam potential energy expression and differential equilibrium equation provides the mechanical/mathematical explanation fort this surprising behavioural feature.

Based on the experience with doubly symmetric I-section beams, the lowest critical moment always corresponds to a uniform bending moment diagram, provided that no transverse load is applied away from the shear centre. The numerical results concerning the welded I-section beam with fork-type support condtions and the geometry showed that the critical buckling moment, M_{cr}, associated with the parabolic bending moment diagram caused by a uniformly distributed transverse load applied along the beam shear centre axis was lower than the value corresponding to the uniform bending moment diagram caused by equal end moments.

1.2.3. Lateral torsional buckling of rectangular beams using variational iteration method (Pınarbaşı, 2011)

This paper shows that complex beam buckling problems, such as lateral torsional buckling of narrow rectangular cantilever beams whose minor axis flexural and torsional rigidities vary exponentially along their lengths, can successfully be solved using variational iteration method (VIM). In order to see the convergence of the approximate solutions to the exact solutions, seventeen iterations are conducted for each algorithm and critical moments for the first three modes are computed.

Analysis results shows that all iteration algorithms yield exactly the same results

in all studied problems. Two fundamental beam buckling problems; lateral torsional buckling of (i) simply supported narrow rectangular beams under uniform moment and (ii) narrow rectangular cantilever beams carrying concentrated load at their free ends, are studied using variational iteration method (VIM). Exact solutions to these problems are available in literature only for beams of constant rigidities and some particular cases of linearly tapered beams.

In order to verify the effectiveness of VIM on solving beam buckling equations and to show the application of the method; firstly, the problems with constant rigidities are studied. The excellent match of the VIM results with the exact results verifies the efficiency of the technique in the analysis of lateral torsional buckling problems.

1.2.4. Lateral torsional buckling of castellated beams (Showkati, 2008)

In this paper, the bending behavior of unbraced CSB is investigated and some empirical equations are proposed to predict the bending coefficient of Cb. The acquired results are compared with some published papers in the technical literature, and by applying the proposed modification factor Cc on the relations of I-sections, a very good agreement is gained.

Castellated steel beams (CSB) are lightweight sections usually made from I-sections by the castellation process. When the distortional and local buckling of section components and overall lateral buckling of such beams are prevented, it may be possible to use their full plastic bending capacities.

If a local and overall lateral bracing is not provided, the bending behavior of the beam will be a function of some of the slenderness parameters . In this paper, a model of the eigenvalue buckling analysis is presented for unbraced CSB using the finite element method.

The beam models are made of lightweight wide-flange steel sections (IPE) by the castellation process, with an original depth of d varying from 100mm to 300mm. So the

ultimate section heights are between 150mm to 450mm (CPE10 CPE30). On lateral buckling of plane-webbed steel beams, several published investigations are available, like Chen and Lui , Hitahori and Kubo and N. S. Trahair. Nethercot and Kerdal performed two series of tests on the lateral stability of CSB.

1.2.5. Lateral buckling of overhanging beams (Özdemir, 2004)

Lateral torsional buckling should be taken into account during the design of overhanging steel beams. One special type of overhanging beams is the crane trolley monorails. Lateral buckling of overhanging monorails under idealized loading and boundary conditions has been studied in the past using classical mathematical procedures. This thesis aims to present a detailed investigation of overhanging monorails using finite element analysis. Effects of different loading and boundary conditions were studied in detail.

It was found out that the location of loading and supports on the cross section have significant effects on the buckling capacity. Beams having different warping and torsional properties were analyzed.

The effects of cross section distortion on buckling capacity were investigated for beams with single and double overhangs. The reduction in capacity due to cross section distortion has been quantified. Based on the analysis results simple design recommendations were developed for lateral buckling of overhanging monorails and they are presented herein.

In this thesis, the buckling of overhanging monorails was studied in detail. First, the effects of load position and support location among the cross section were investigated and the results were compared with the findings of previous research. Then, a detailed analysis of boundary conditions at exterior support was conducted.

In addition, the performance of beams having different warping and torsional stiffness properties were investigated. The influence of cross section distortion on buckling

capacity of overhanging monorails was explored. Finally, the investigations performed for single overhanging beams were extended to double overhanging beams.

1.3. Theory Application

Lateral torsional buckling of I-beams is a complex phenomenon. If a simply supported beam is subjected to equal and opposite end moments as shown in Figure 1.3, the compression flange of the beam can move sideways when a certain value of applied moment is reached. In this undesirable behavior the tension flange tries to restrain the flange in compression and the resulting buckling mode is lateral-torsional indicating a lateral displacement together with a rotation of the cross section. Closed form solution of the critical buckling moment M_{cr0} has been developed by Timoshenko and Gere, and was adopted by many design codes (AISC 2001) in different forms [3,5].

Lateral torsional buckling may occur in an unrestrained beam. A beam is considered to be unrestrained when its compression flange is free to displace laterally and rotate. When an applied load causes both lateral displacement and twisting of a member lateral torsional buckling has occurs as shown in Figure 1.4 [1].

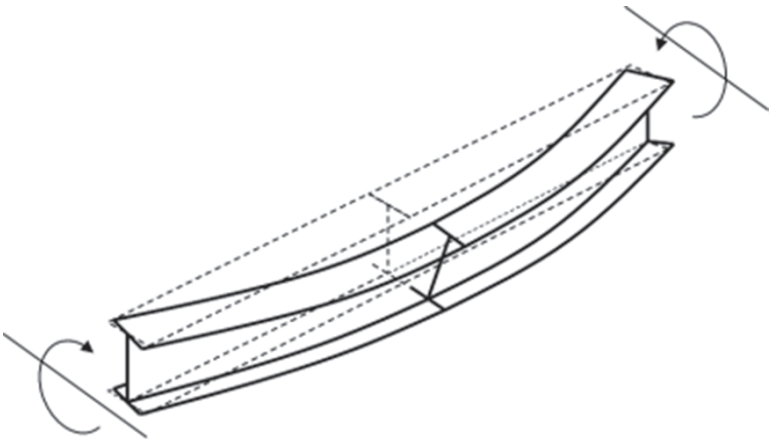

Figure 1.4. I-Section Beam in Buckled Configuration [1].

In the derivation of Equation 1.1 it is assumed that the cross section is prevented

from lateral movement and twist at the ends of the beam [1].

$$M_{cr} = C_b \frac{\pi}{L} \sqrt{EI_x GJ + C_w I_x \left(\frac{\pi E}{L}\right)^2} \tag{1.1}$$

Where, L is the unbraced length, E is the modulus of elasticity, I_y is the minor axis moment of inertia, G is the shear modulus, J is the torsional constant, C_w warping constant. Due to the complexity of the problem it is difficult to come up with closed form solutions for cases with different loading and boundary conditions. Only a few closed form solutions exist for the lateral torsional buckling problem and mostly numerical methods are used for the solution of such problems [2].

The vertical distance between the load application point and the shear centre of the section affects the susceptibility of the section to the effects of lateral torsional buckling. If the load is applied at a location above the shear centre of a section it is more susceptible to lateral torsional buckling than if the load was applied through the shear centre. Applying the load at a location below the shear centre of a section reduces the susceptibility of the section to the effects of lateral torsional buckling [2].

When the load is applied above the shear centre it is known as a destabilising load, with loads applied at or below the shear centre called non-destabilising loads. The effect of a destabilising load is considered by the use of effective, where the effective lengths are longer for destabilising loads compared to the non-destabilising loads [2].

Buckling resistance for a section subject to a uniform bending moment distribution along its length is less than the buckling resistance obtained for the same section subjected to a different bending moment distribution. Factors are included in design guidance to allow for the effect of different bending moment distributions. The boundary conditions also play an effective within this phenomenia. The more constraints the model have, the higher lateral torsional buckling critical loads will appear. Especially cantilever beam models have highly relative critical load comapred to simply supoorted beam models [4].

The slenderness of a section is used in design checks for lateral torsional buckling. The following factors affect the slenderness of a section:

- Length of the beam
- Lateral bending stiffness of the flanges
- Torsional stiffness of the section.

In addition to the lateral movement of the section the forces within the flanges cause the section to twist about its longitudinal axis as shown in Figure 1.5. The twisting is resisted by the torsional stiffness of the section.

The torsional stiffness of a section is dominated by the flange thickness. That is why a section with thicker flanges has a larger bending strength (pb) than the same depth of section with thinner flanges [6].

Beam deflections are calculated using both the moment-area method and the principle of superposition. Although the moment-area method is fairly quick, it is easily prone to errors due to the complicated sign conventions.

The principle of superposition is performed by solving for the displacement at a single point along the beam by using formulas which are based on simpler beam problems, and then adding the results. This technique is also prone to arithmetic errors because of the large number of variables involved in the formulas [2].

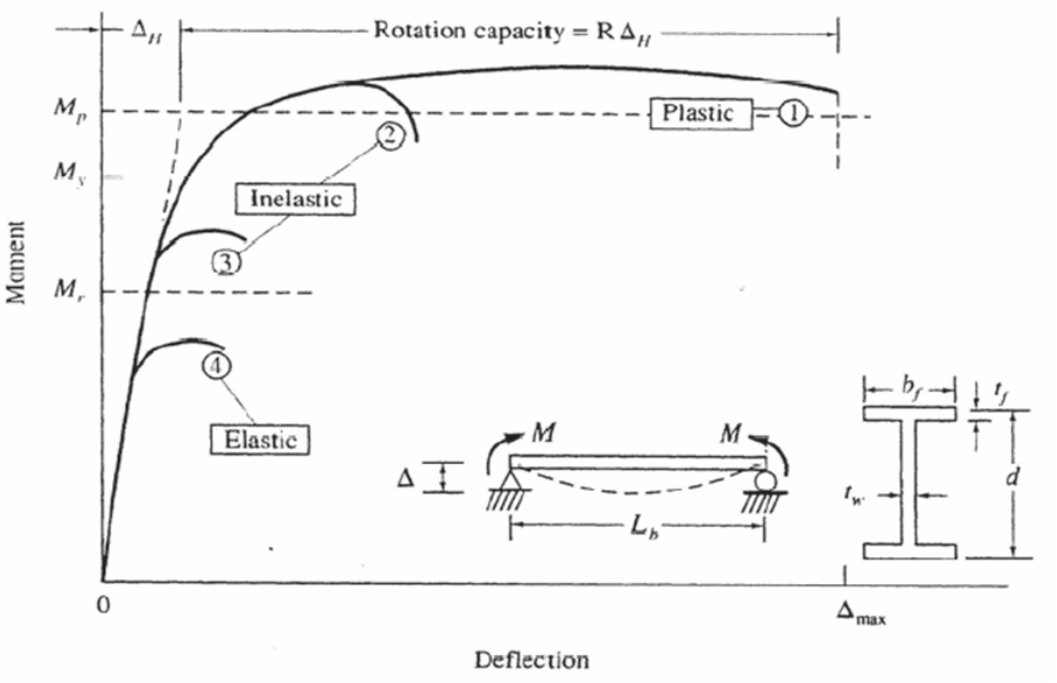

Figure 1.5. Beam Behaviour with Moment - Deflection Illustration [2].

When the beam is adequately supported against lateral buckling, the beam failure occurs by yielding of the material at the point of maximum moment. The beam is thus capable of reaching its plastic moment capacity under the applied loads. Thus the design strength is governed by yield stress and the beam is classified as laterally supported beam. Such conditions can be best simulated with softwares only if the fork-support parameters are defined [3].

Beams have much greater strength and stiffness while bending about the major axis. Unless they are braced against lateral deflection and twisting, they are vulnerable to failure by lateral torsional buckling prior to the attainment of their full in-plane plastic moment capasity. Such beams are classified as laterally supported beam [3].

The various factors affecting the lateral-torsional buckling strength are:

- Distance between lateral supports to the compression flange.
- Restraints at the ends and at intermediate support locations.
- Type and position of the loads.

- Moment gradient along the length.
- Type of cross-section.
- Initial perfections.
- Non-prismatic nature of the member.
- Material properties.

The classical lateral-torsional buckling solution using the Full Section properties results in the largest unbraced length in all the calculations. The addition of the load location term to the classical solution lowers the unbraced length nearly 10% and the Galambos solution lowers the value nearly 17%. When the lateral-torsional buckling solutions were evaluated using the Tee Section Assumption, the unbraced lengths decreased. However, the margin of difference between the different solutions decreased. Lastly, when the lateral-torsional buckling solutions were evaluated using the Weighted Section Assumption, the unbraced lengths fall between the previous two approaches as expected [3].

1.4. Problem Statement

As presented before little has been done to quantify the buckling capacity of steel beams especially with an inter-related comparision study of moren than two finite element softwares, numerical analyses and analytical computations. The design recommendations are based on a theoretical solution which only encompasses ideal support conditions.

In reality, the boundary conditions at the exterior support can also vary significantly. In addition, bottom flange loading is more commonly encountered in practice compared to the shear centre loading. This thesis aims to present a rigorous numerical study on buckling of steel beams compared based high performance simulation techniques and dynamic parametric studies.

Throught the research, direct analytical solutions will be calculated via ASCI standarts. Results will be plotted over succeeding Matlab graphical interfaces via

paramateric variables to compare with the simulation results over 96 analyses.

A detailed error spectrum will be constructed for each model and span case. Matlab codes will be used to construct the theoretical solution space. Not olny the ANSYS simulations bu also the theoretical solutions will be compared to create a relative error statistics perspective.

2. LATERAL TORSIONAL BUCKLING

2.1. Theory

In this type of instability, the member is loaded by forces in the plane of symmetry, and it deforms in this plane until, at a critical loading, the member both deflects out of its plane of symmetry and twists. This behaviour is typical of wide-flnage beams that are loaded so that the resulting bending moments act about the x-axis [2].

Lateral-torsional buckling is a limit-state of structural usefulness where the deformation of a beam changes from predominantly in-plane deflection to a combination of lateral deflection and twisting while the load capacity remains first constant, before dropping off due to large deflections. while the load capacity remains first constant, before dropping off due to large deflections [6].

The basic reference case for lateral-torsional buckling as shown in the Figure 2.1 attributes the following properties:

- The beam behaves elastically
- The cross-section is double symmetric (and thus the centroid and the shear center coincide).
- It is subjected to uniform moment about the major principal axis.
- Bending occurs about the major axis.
- It is simply supported

The member continues to deflect as M_0 is increased from zero, without any out-of-plane movement, until a critical moment M_{ocr} is reached. This moment represents the point of bifurcation when equilibrium is possible in both an unbuckled and in a buckled configuration. This condition is the same as the buckling of the ideal Euler column, cocenptually. In case of the pinned-end column, bifurcation is the transition from a perfectly straight to a laterally deflected geometry.

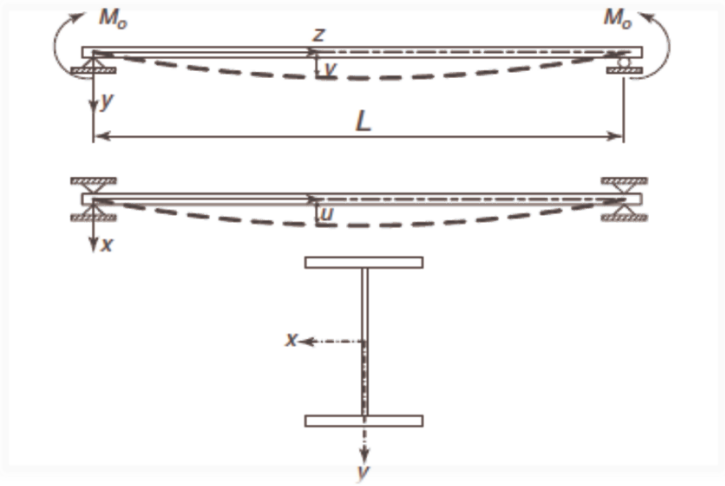

Figure 2.1. The Simplest Case of Lateral Torsional Buckling [1].

For the beam, the buckled deflection changes from an in-plane configuration at the critical moment M_{ocr} to an out-of-plane mode represented by a lateral deflection u and an angle of twist F. Because the buckled shape includes both a lateral deflection and an angle of twist, this case of instability is called lateraltorsional buckling [1].

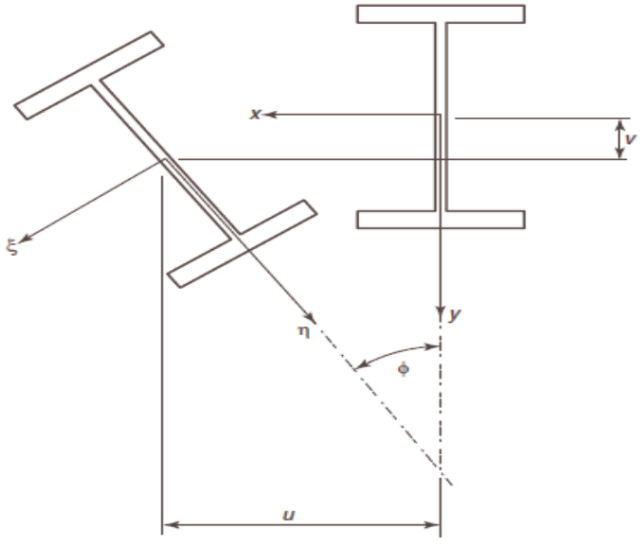

Figure 2.2. The Cross-Section Before and After Buckling [1].

The simply supported end of the beam is the idealized condition when lateral deflection and twist are prevented, the end is free to rotate laterally, and the end cross-section is free to warp.

Figure 2.2 illustrates the transition from the unbuckled configuration to the buckled location of the cross-section at the critical moment. The translated and rotated cross-section has moved from the pre-buckling state with a transverse deflection n, to a new location with a lateral deflection u, and an angle of twist Φ.

The original centroidal coordinates x and y of the crosssection in the buckled configuration are designated as ζ and η.

In the following derivation, these conditions are assumed:

- The deflections and angles of twist are small.
- The material is elastic, homogeneous and isotropic.
- There is no local buckling of the flanges and the web.
- There is no distortion of the cross section during buckling.

2.2. Formulations

For the simply supported beam models, Timoshenko formulation which is derived through differential equations will be used as shown with the Equation 2.1 is [4]:

$$M_{cr} = C_b \frac{\pi}{L} \sqrt{EI_x GJ + C_w I_x \left(\frac{\pi E}{L}\right)^2} \tag{2.1}$$

On the other hand, for the cantilever beam models, again Timoshenko formulation is used as reflected with the Equation 2.2 is[4];

$$\mathrm{P}_{cr} = \frac{4.013}{L^2} \sqrt{GJEI_x} \tag{2.2}$$

3. FINITE ELEMENT ANALYSIS

3.1. Theory

In mathematics, the finite element method (FEM) is a numerical technique for finding approximate solutions to boundary value problems for differential equations. It uses variational methods to minimize an error function and produce a stable solution. Analogous to the idea that connecting many tiny straight lines can approximate a larger circle, FEM encompasses all the methods for connecting many simple element equations over many small subdomains, named finite elements, to approximate a more complex equation over a larger domain [7].

Reviwing this fact, the finite element analysis method is not only a problem solving approach for the engineering problems but also a perspective to have an deep insight for the micro-space behaviours of the systems.

The problems are first converted to matrix and partial differential equation forms. Eventually the partial differential and integral equations are being solved to reach the solution of the problem. The volume of the equations to be solved is usually so large that arriving solution without using computer is practically impossible. And, this is the main phenomenia for the the need of different FEA software applications [8].

In spite of the great power of FEA, the disadvantages of computer solutions must be kept in mind when using this and similar methods: they do not necessarily reveal how the stresses are in?uenced by important problem variables such as materials properties and geometrical features, and errors in input data can produce wildly incorrect results that may be overlooked by the analyst.

Throught this research, statistical error analyses will be performed by optimizing the default operators which functions the finite element analyses over lateral torsional buckling concept. All the beam models will be fine meshed to increase the accuracy.

At the same time, the subdivision of a whole domain into simpler parts has several advantages [9]:

- Accurate representation of complex geometry.
- Inclusion of dissimilar material properties.
- Easy representation of the total solution.
- Capture of local effects.

3.2. Methodology

In this research, ANSYS 14.5/Structural avanced finite element software is performed. Ansys offers a comprehensive software suit that spans the entire range of physics, providing access to virtually any field of engineering simulations that a design process requires.

The ANSYS/Structural software has an high performance to rapidly solve complex structural engineering problems with ease. FEA analysis tools from ANSYS provide the ability to simulate every structural aspect of the structural systems such as:

- Linear static and eigenbuckling analysis options that provide stresses and deformations.
- Modal analyses that determines the dynamic structural characteristics.

With the aim of a fundamental understanding to observe the structural behaviours of the systems, these two aspects will be the vital importance in terms of the applications through the whole thesis research.

3.3. Process Algorithm

The method essentially consists of assuming the piecewise continuous function for the solution and obtaining the parameters of the functions in a manner that reduces the error in the solution. In this article, a brief introduction to finite element method is

provided. The method is illustrated with the help of the plane stress and plane strain formulation [8].

The Finite Element Method translates partial differential equation problems into a set of linear algebraic equations. The basis of the finite element method is the representation of a body or a structure by an assemblage of subdivisions called finite elements. The geometry is divided into a number of discrete subregions or elementsconnected at discrete points are called nodes as shown in Figure 3.1.

Figure 3.1. A Basic Represantation of Nodes and Elements.

3.4. Modelling Background

In this research, the lateral torsional buckling of steal beams was studied in detail using the finite element method. As mentioned before due to the complexity of loading and boundary conditions, it is difficult to come up with closed form solutions. Rather numerical methods are employed to investigate the instability behavior. Finite element analysis could be conducted using either solid or shell elements for this problem. Most of the beam elements developed can be used for ideal boundary conditions. On the other hand if complex boundary conditions exist such as presence of stiffeners; a global three dimensional modeling with shell elements is preferred but through the all processes, the default beam model, Beam-189, is used as shown in Figure 3.2 [10].

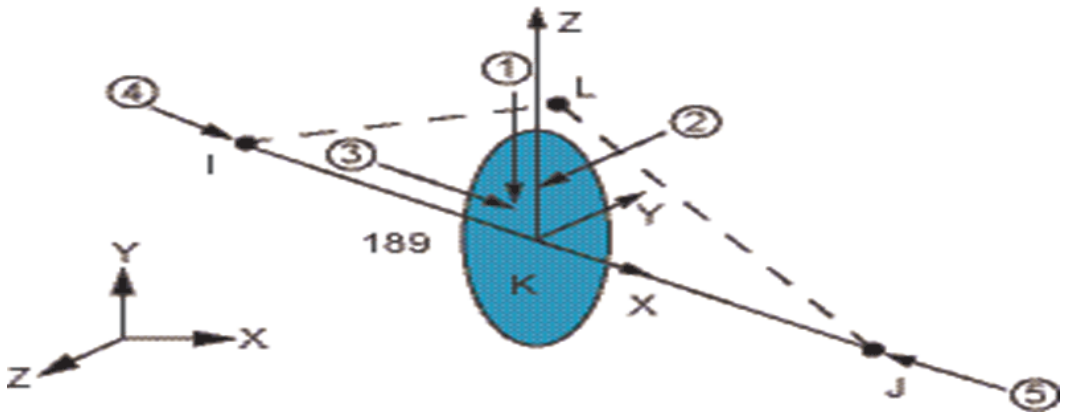

Figure 3.2. ANSYS Beam-189 Orientation.

The BEAM 189 element is suitable for analyzing slender to moderately stubby/thick beam structures. The element is based on Timoshenko beam theory which includes shear-deformation effects. The element provides options for unrestrained warping and restrained warping of cross-sections [10].

The element is a quadratic three-node beam element in 3-D. With default settings, six degrees of freedom occur at each node; these include translations in the x, y, and z directions and rotations about the x, y, and z directions. An optional seventh degree of freedom (warping magnitude) is available. The element is well-suited for linear, large rotation, and/or large-strain nonlinear applications [10].

The element includes stress stiffness terms, by default, in any analysis with NLGEOM,ON. The provided stress-stiffness terms enable the elements to analyze flexural, lateral, and torsional stability problems (using eigenvalue buckling, or collapse studies with arc length methods or nonlinear stabilization). Elasticity, plasticity, creep and other nonlinear material models are supported. A cross-section associated with this element type can be a built-up section referencing more than one material [10].

BEAM 189 is based on Timoshenko beam theory, which is a first-order shear-deformation theory: transverse-shear strain is constant through the cross-section; that is, cross-sections remain plane and undistorted after deformation. The element can be used for slender or stout beams. Due to the limitations of first-order shear-deformation

theory, slender to moderately thick beams can be analyzed. BEAM 189 does not use higher-order theories to account for variation in distribution of shear stresses [10].

The element can also be defined without the orientation node L. In this case, the element x-axis is oriented from node I (end 1) toward node J (end 2). When no orientation node is used, the default orientation of the element y-axis is automatically calculated to be parallel to the global X-Y plane [10].

3.5. Modelling Process

A typical flow chart of finite element algorithm is ullastrated at Figure 3.3.

The seven processes can be defined as [9]:

- Saving the 3D CAD Geometry in Neutral Format: First, the 3D CAD geometry in neutral format like IGES, STEP is valid. Though some of the ANSYS allow importing the CAD geometry directly from some of the 3D CAD packages. For example, the ProE geometry can be directly imported to ANSYS.
- Importing 3D CAD geometry to ANSYS: Starting the FEA pack ANSYS and importing the CAD geometry into the ANSYS.
- Defining Material Properties: Defining which material you are using for the part. By this process you have to tell modulus of elasticity, poissions ratio and all other necessary properties require for the ANSYS.
- Meshing: Meshing is a critical operation in FEA. In this operation, the CAD geometry is divided into large numbers of small pieces. The small pieces are called mesh. The analysis accuracy and duration depends on the mesh size and orientations. With the increase in mesh size, the finite element analysis speed increase but the accuracy decrease.

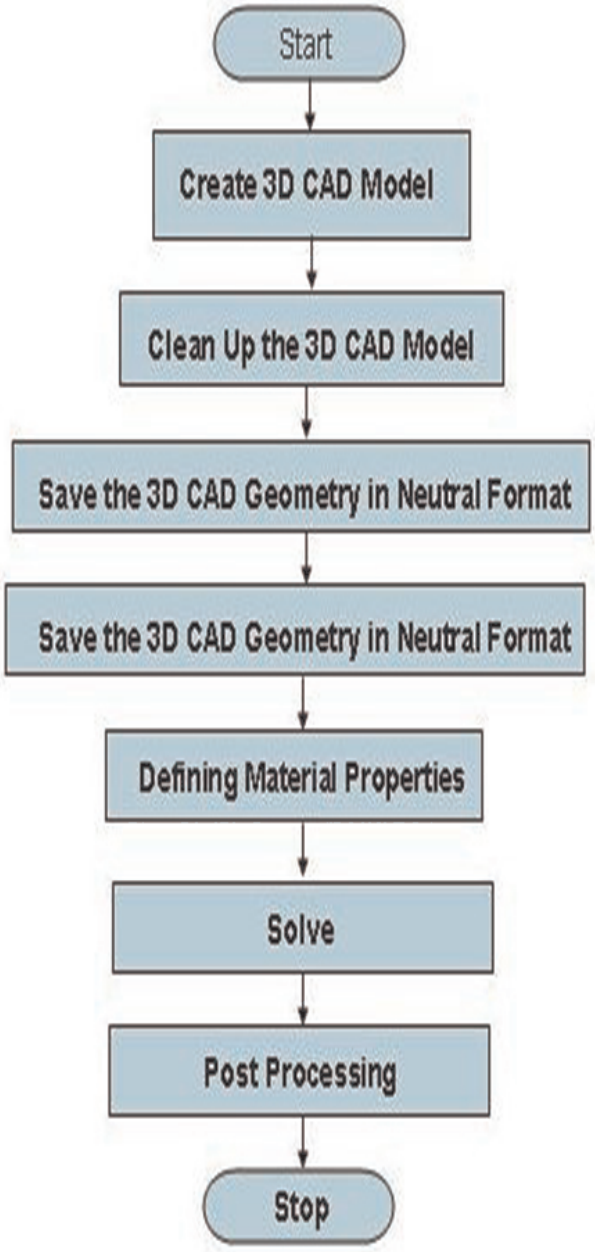

Figure 3.3. ANSYS Work Flow [9].

- Defining Boundary Condition: This conditon must be introduced to ANSYS where the loads are apllied and where you want to rest the part/assemble constraints.
- Solve: In this step ANSYS is leaded to solve the problem for the defined material properties, boundary conditions and mesh size.
- Post Processing: Finally, viewing the results of the solution is on the process. The result can be viewed in various formats: graph, value, animation etc.

3.6. Modelling Application

The process after choosing the BEAM-189 model is sectioning. In Figure 3.4 and Figure 3.5 a detailed illustration a fine-meshed section dimensions are of interest with Analysis-1111.

After choosing the default section models, dimensions data are inserted manually. It can be also noticed that fine-meshed option is on the process by choosing mesh-parameter as five. The meshed model is ready to be expaned in the weak-axis to have the third dimension span as shown in Figure 3.6.

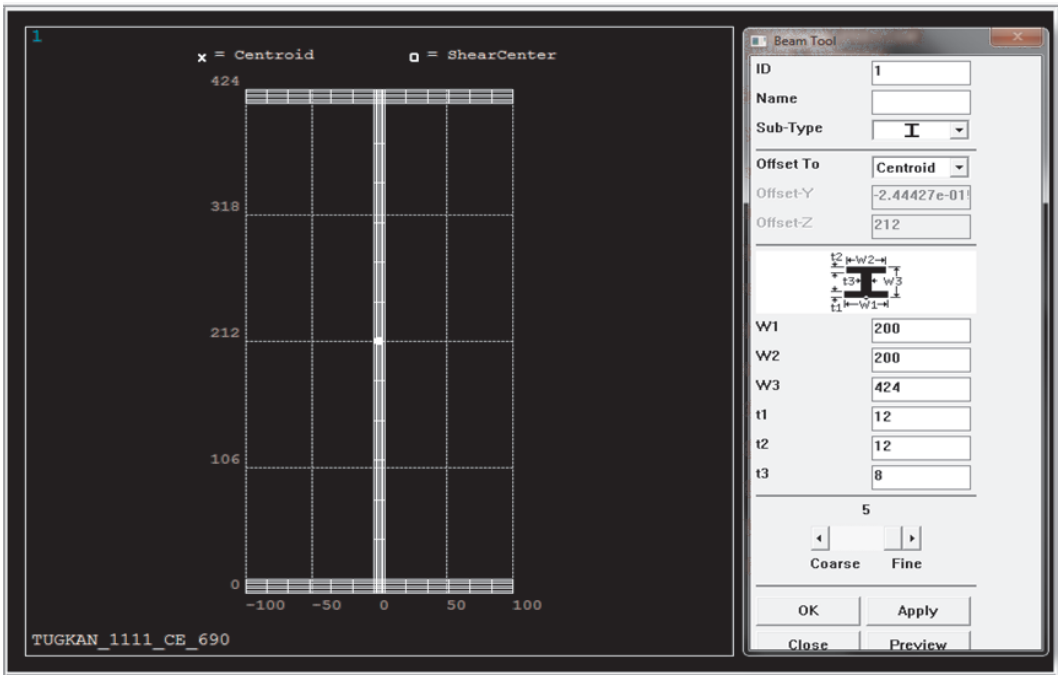

Figure 3.4. Sectioning and Fine-Meshing Process at Analysis-1111.

```
LIST SECTION ID SETS       1 TO      1 BY      1

SECTION ID NUMBER:         1
BEAM SECTION SUBTYPE:  I Section
BEAM SECTION NAME IS:
BEAM SECTION DATA SUMMARY:
 Area                  =  8000.0
 Iyy                   = 0.24642E+09
 Iyz                   =-0.91386E-08
 Izz                   = 0.16017E+08
 Warping Constant      = 0.67840E+12
 Torsion Constant      = 0.29711E+06
 Centroid  Y           =-0.24443E-14
 Centroid  Z           =  212.00
 Shear Center Y        =-0.22672E-09
 Shear Center Z        =  212.00
 Shear Correction-yy   = 0.50897
 Shear Correction-yz   = 0.30713E-11
 Shear Correction-zz   = 0.40111

 Beam Section is offset to CENTROID of cross section
```

Figure 3.5. Sectioning Output Data at Analysis-1111.

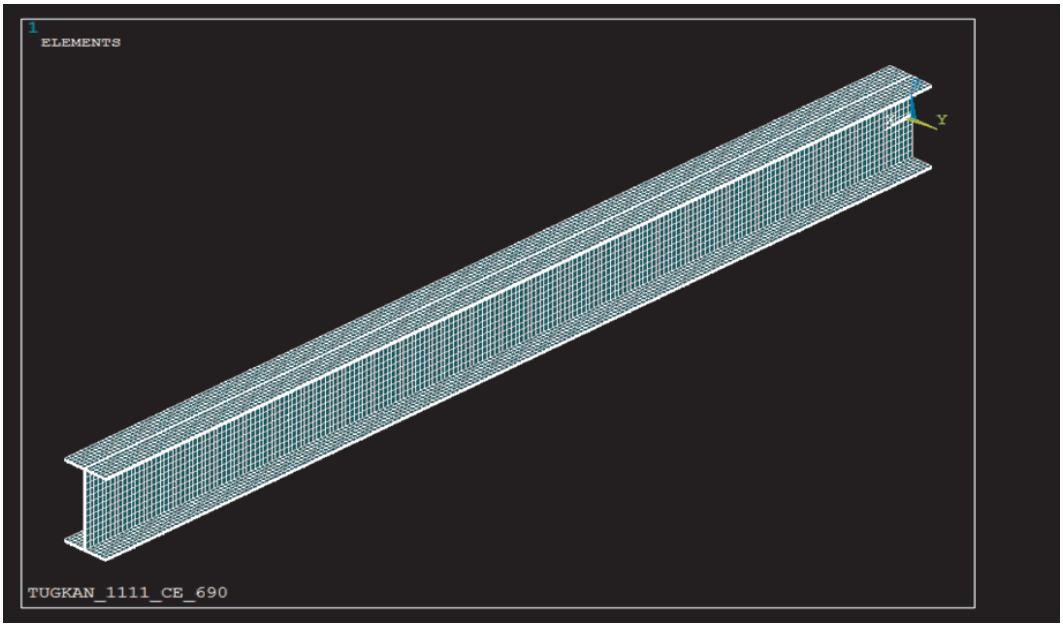

Figure 3.6. 3D View of at Analysis-1111.

3.7. Nonlinear Finite Element Analysis

Solution of many engineering problems is based on linear approximations. In structural analyses, these approximations are represented by consideration that:

- Displacements are small and can be neglected in equilibrium equations,

- The strain is proportional to the stress
- Loads are conservative, independent on displacements,
- Supports of the structure remain unchanged during loading.

Consequently, in the Finite Element Analysis (FEA) the set of equations, describing the structural behavior is then linear:

$$\{F\} = [K]\{d\} \tag{3.1}$$

where K is the stiffness matrix of the structure, d is the nodal displacements vector and F is the external nodal force vector. This augmented matrix is one of the main algorithms of ANSYS. The stifness properties of the material reflects the actual behaviours of the structural systems [10].

Characteristics of solution of this linear problem is that:

- The displacements are proportional to the loads.
- The stiffness of the structure is independent on the value of the load level.

In reality, behavior of structures is nonlinear, but divergences from linear response are usually small and may be neglected in most practical problems.

On other hand, solution of many engineering problems needs abandonment of linear approximations. For example, displacements of slender structures may be so large that changes of the structure shape (or configuration changes) cannot be neglected. Many materials behave nonlinearly or linear material model cannot be used if stress exceeds some value. Moreover, loads may change their orientations according to displacements and supports may change during loading [10].

Consequently, structure behaves nonlinearly. If these phenomena are included in a FEA, the set of equilibrium equations becomes nonlinear and instead of set of linear

Equation 3.1 we obtain a set of nonlinear algebraic equations:

$$R(d) = F \tag{3.2}$$

The load is divided into a set of small increments Δ F_i. Increments of displacements Δ d_i are calculated from the set of linear simultaneous equations:

$$K_{T(i-1)} \cdot \Delta d_i = \Delta F_i \tag{3.3}$$

and an updated solution is obtained as follows and illsutrated at Figure 3.7.

$$d_i = d_{i-1} + \Delta d \tag{3.4}$$

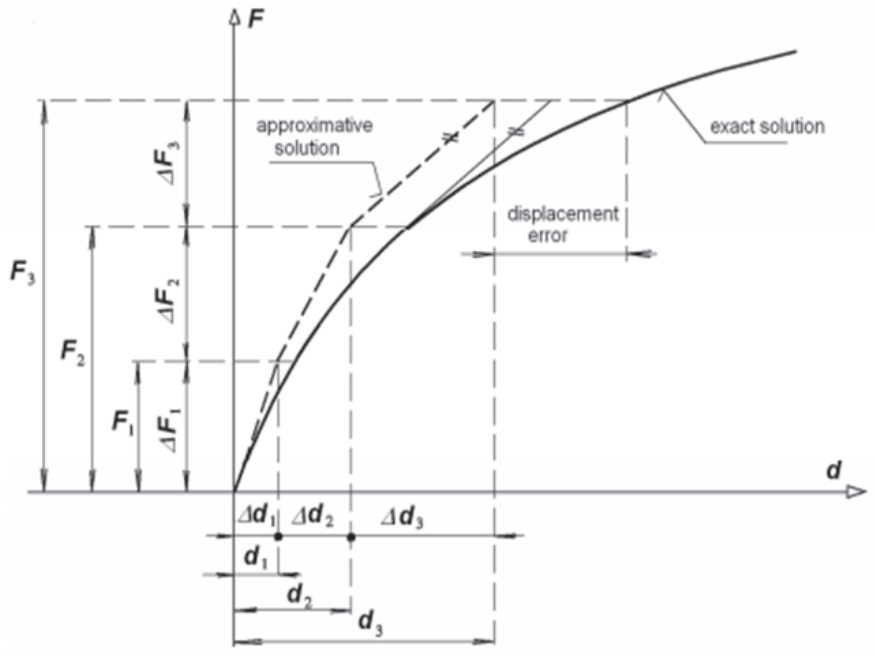

Figure 3.7. The Incremental Method [10].

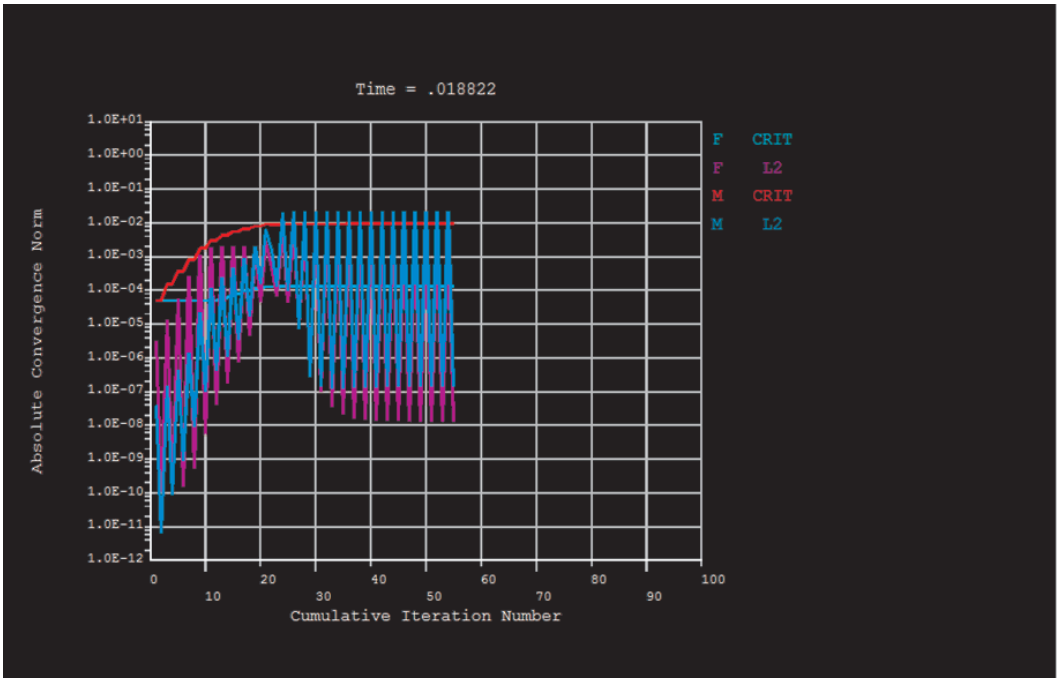

Figure 3.8. Absolute Convergence Norm at ANSYS 14.5 Mechanical APDL.

The procedure is shown in Figure 3.7 and Figure 3.8 ANSYS application. It is obvious that solution error difference from exact solution gradually cumulates. To reduce error, large number of small incremental steps has to be done that is inefficient. On the other hand, division of loading process into sufficiently small increments is necessary to model load path dependent behavior of a structure. Dependence of response on a manner of loading, not only of final values of loads is typical for problems with plastic deformation and with friction.

4. PARAMETRIC ANALYSES

4.1. Algorithm Perspective

Parametric analysis is an excellent technique to get accurate correlation about the influence of all parameters on the design objectives, such as structural performance with respect to section dimensions, loading conditions, material models and other variables. With this aspect, the structural engineer can make informed decisions throughout the design process, especially in the early conceptual stage. As a consequence of the parametric analysis, the designer also can react qucikly to any modification due to external constraints [11].

In this study, in order to be specific on the behaviour of lateral torsional buckling concept, parametric analyses were conducted over a global structural grid to investigate the effects of sectional dimensions, span lengths and boundary conditions. To do so, four dimensional global structural grid with:

- 4 symmetric, parametric I-Section models
- 4 different beam span lengths
- 2 boundary conditions with simply supported and cantilever beams
- 2 types of analyses with theoretical solutions and ANSYS simulations.

is detailly constructed as shown in Figure 4.1.

While x-axis denotes four different span lengths, on the other hand y-axis corresponds to four different parametric section models. Besides, the first boundary condition, BC-1, with simply supported beam operates the whole grid processes for one cycle as the second boundary condition, BC-2, with cantilever beam progresses also.

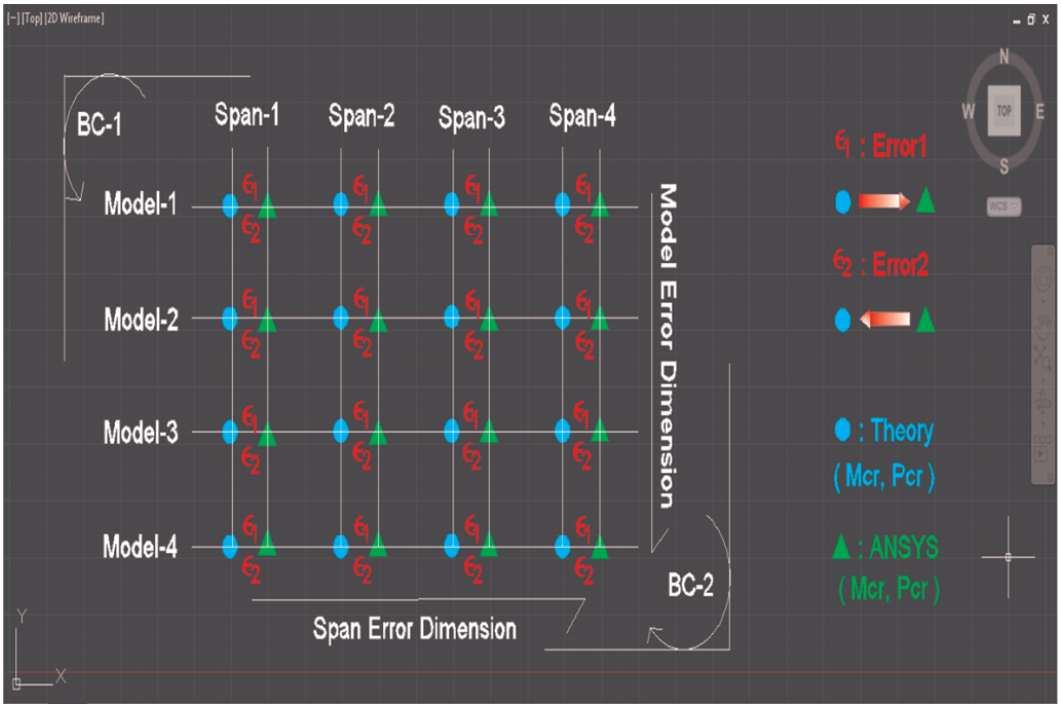

Figure 4.1. The General Algorithm of the Parametric Analyses.

Parametric analyses are classified as theoretical direct solutions of Timoshenko and ANSYS simulations via linear buckling operators. For each cycle process, 32 analyses exists through the concept of boundary conditions over simply supported and cantilever beams. The pairwise mutually independent error couples denotes the relative errors with respect to both theoretical and ANSYS calculations in terms of critical lateral torsional buckling loads. A detailed error statistics study is performed throughout 64 relative error data and 32 average convergence data so that expanding the error space over an dimensionless error spectrum with 96 error data.

A wide variety of parameters can be varied to study the impact of those changes on the design, but a major source of variation within the lateral torsional buckling phenomenia is the geometry itself. To simulate the actual beam behaviour to a full parametric scale, behavioral trends were illustrated via sensitivity analysis through finite-dimensional parameter spaces.

Morever, the default system configurations in ANSYS, such as operators, functions, constants are manually optimized to increase the accuracy level of the output

data through APDL which is called as Ansys Parametric Design Language.

4.2. Parametric Models

Four different, mutually related, symmetric I-Section profiles were modelled with the aim of a detailed parametric analysis through relative correspondences. All the dimension values are illustrated at Table 4.1.

Table 4.1. Parametric Model Dimensions.

	b(mm)	tf(mm)	hw(mm)	h(mm)	tw(mm)
Model-1	200	12	400	420	8
Model-2	200	12	420	432	10
Model-3	220	14	400	414	8
Model-4	220	14	420	434	10

To extend the graphical view, Figure 4.2. is drawn with AutoCAD Structural Detailing software. As an ultimate sense:

- Model-1 and Model-2 are related in flange dimensions with b and t_f.
- Model-1 and Model-3 are related in web dimensions with h_w and t_w.
- Model-3 and Model-4 are related in flange dimensions with b and t_f.
- Model-2 and Model-4 are related in web dimensions with h_w and t_w.

These four mutually related combinations will lead to relative parametric correlations through error statistics process. Morever, the physical senses will be observed while the dimensional changes of flange and web portions effect the critical loads of lateral torsional buckling phenomenia. The results of statistical parametric error analyses will indicate not only the geometrical effects but also the loading conditions resulting with the bucklings stresses which are affected by the variations in both design aspects.

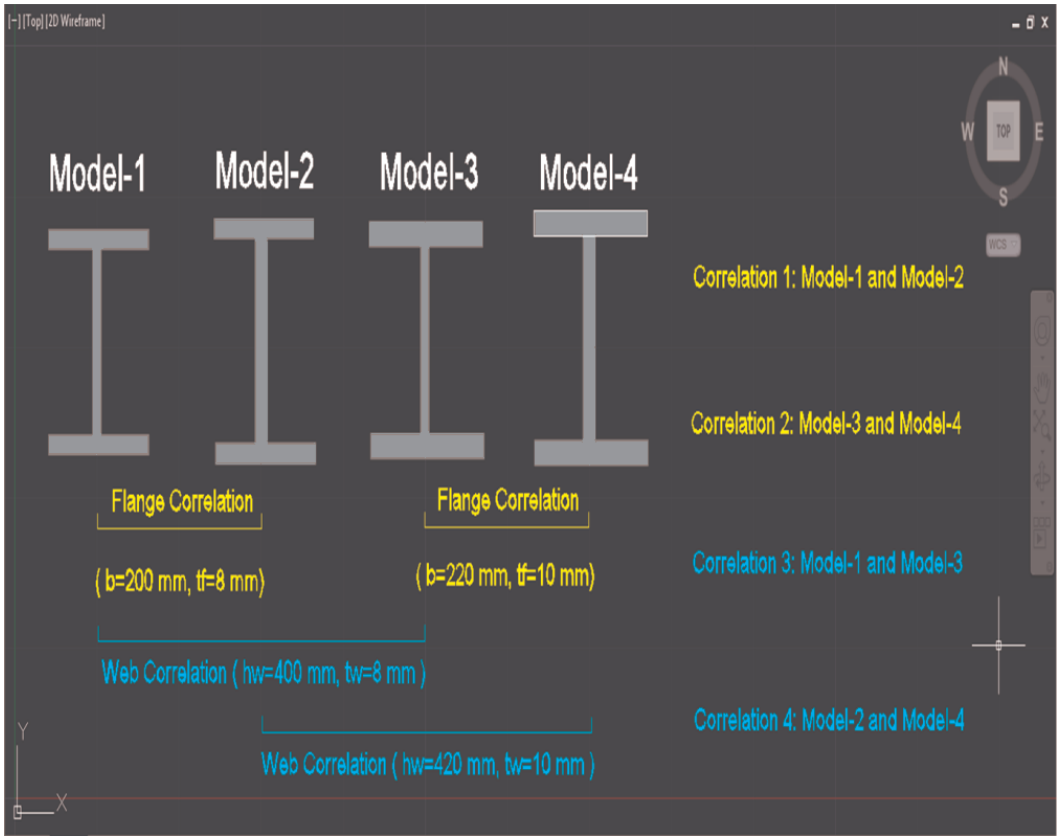

Figure 4.2. Parametric Section Correlations.

4.3. Parametric Notation Background

The system logic mainly incorporates between the span lengths and the section dimensions resulting with the critial stresses resulting with the critical loads. These ciritical loads are the critical moments for the simply supported beam models, M_{cr}, and the critical forces for the cantilever beam models, P_{cr}.

For each of the loading and boundary conditions, a pairwise symbolic logic notation can be formed to illustrate the lateral torsional buckling analysis output data as ashown in Table 4.2 and Table 4.3.

Table 4.2. M_{cr} Notations for the Simply Supported Models with BC-1.

	Span-1	Span-2	span-3	Span-4
Model-1	$M_{cr}11$	$M_{cr}21$	$M_{cr}31$	$M_{cr}41$
Model-2	$M_{cr}12$	$M_{cr}22$	$M_{cr}32$	$M_{cr}42$
Model-3	$M_{cr}13$	$M_{cr}23$	$M_{cr}33$	$M_{cr}43$
Model-4	$M_{cr}14$	$M_{cr}24$	$M_{cr}34$	$M_{cr}44$

Table 4.3. P_{cr} Notations for Cantilever Models with BC-2.

	Span-1	Span-2	span-3	Span-4
Model-1	$P_{cr}11$	$P_{cr}21$	$P_{cr}31$	$P_{cr}41$
Model-2	$P_{cr}12$	$P_{cr}22$	$P_{cr}32$	$P_{cr}42$
Model-3	$P_{cr}13$	$P_{cr}23$	$P_{cr}33$	$P_{cr}43$
Model-4	$P_{cr}14$	$P_{cr}24$	$P_{cr}34$	$P_{cr}44$

The fundamental idea is to create an effective relative sense over the parametric space through relative errors which are calculated from the corresponding theoretical direct solutions and ANSYS outputs for each model and span length condition.

While passing from critical loads, M_{cr} and P_{cr}, to evaluated error values, the notation for each analysis case will expand into three-digid form for which the first number will reveal the boundary conditions BC-1 or BC-2, through which is considered in the performed analysis. The three-digid error notations are tabulated in Table 4.4 and Table 4.5 respectively.

Table 4.4. The Pure Error Coding Set of Simple Supported Models (BC-1).

	Span-1	Span-2	span-3	Span-4
Model-1	Error-111	Error-121	Error-131	Error-141
Model-2	Error-112	Error-122	Error-132	Error-142
Model-3	Error-113	Error-123	Error-133	Error-143
Model-4	Error-114	Error-124	Error-134	Error-144

Table 4.5. The Pure Error Coding Set of Cantilever Models (BC-2).

	Span-1	Span-2	span-3	Span-4
Model-1	Error-211	Error-221	Error-231	Error-241
Model-2	Error-212	Error-222	Error-232	Error-242
Model-3	Error-213	Error-223	Error-233	Error-243
Model-4	Error-214	Error-224	Error-234	Error-244

The motivation is both analytic and quantitative to visualize the error outputs related with the analysis code; that is, in some circumstances it is advantageous to form the notations in an artistic fashion by ordered integers as presented in Error-111 or Error-211.

All the error data codes which starts with the integer “1” denotes the analyses processed with the first boundary condition of simply supported beam models, whereas they start with the integer “2” when the point of interest is the second boundary condition with cantilever beam models.

A mathematical illustration can be constructed to define the error and analysis coding subscripts within the expressions of set theory. The variation over the integer values of the subscripts define the expandation of the mutually independent error axes

which orhotogonally span the error space, such as:

$$E_{ijkl} \rightarrow i \in \{1,2\} \cup j \in \{1,2\} \cup k \in \{1,2,3,4\} \cup l \in \{1,2,3,4\} \tag{4.1}$$

The physical global matrices can be set through the error statistics to demonsrate the accuracy and precision between the theoretical calculations and Ansys simulations. Since the theoretical solutions mainly based on assumptions, a fine meshed finite element method analysed through the optimised ANSYS operators will reflect the actual structural behviour in a more realiable sensitivity.

These global matrices can be furthermore expanded into the relative sense of error scope according not only to the model type, span length and boundary conditions but also to the analysis type which is considered as the base reference error data. Tabular forms are illustrated through Table 4.6 and Table 4.7 for ANSYS analyses; Table 4.8 and Table 4.9 for theoretical analyses respectively.

Morever, with the aim of a certain perceptual intensity over the whole thesis research, representative parametric error spaces for ANSYS and theoretical solutions are detailly drawn by AutoCAD, as shown in Figure 4.3 and Figure 4.4. Furthermore, analysis codes are tabulated for each error calculation through Table 4.9, Table 4.10, Table 4.11, and Table 4.12.

Table 4.6. The Error Coding Set of BC-1 with ANSYS.

	Span-1	Span-2	span-3	Span-4
Model-1	Error-1111	Error-1121	Error-1131	Error-1141
Model-2	Error-1112	Error-1122	Error-1132	Error-1142
Model-3	Error-1113	Error-1123	Error-1133	Error-1143
Model-4	Error-1114	Error-1124	Error-1134	Error-1144

Table 4.7. The Error Coding Set of BC-2 with ANSYS.

	Span-1	Span-2	span-3	Span-4
Model-1	Error-1211	Error-1221	Error-1231	Error-1241
Model-2	Error-1212	Error-1222	Error-1232	Error-1242
Model-3	Error-1213	Error-1223	Error-1233	Error-1243
Model-4	Error-1214	Error-1224	Error-1234	Error-1244

Table 4.8. The Error Coding Set of BC-1 with Theory.

	Span-1	Span-2	span-3	Span-4
Model-1	Error-2111	Error-2121	Error-2131	Error-2141
Model-2	Error-2112	Error-2122	Error-2132	Error-2142
Model-3	Error-2113	Error-2123	Error-2133	Error-2143
Model-4	Error-2114	Error-2124	Error-2134	Error-2144

Table 4.9. The Error Coding Set of BC-2 with Theory.

	Span-1	Span-2	span-3	Span-4
Model-1	Error-2211	Error-2221	Error-2231	Error-2241
Model-2	Error-2212	Error-2222	Error-2232	Error-2242
Model-3	Error-2213	Error-2223	Error-2233	Error-2243
Model-4	Error-2214	Error-2224	Error-2234	Error-2244

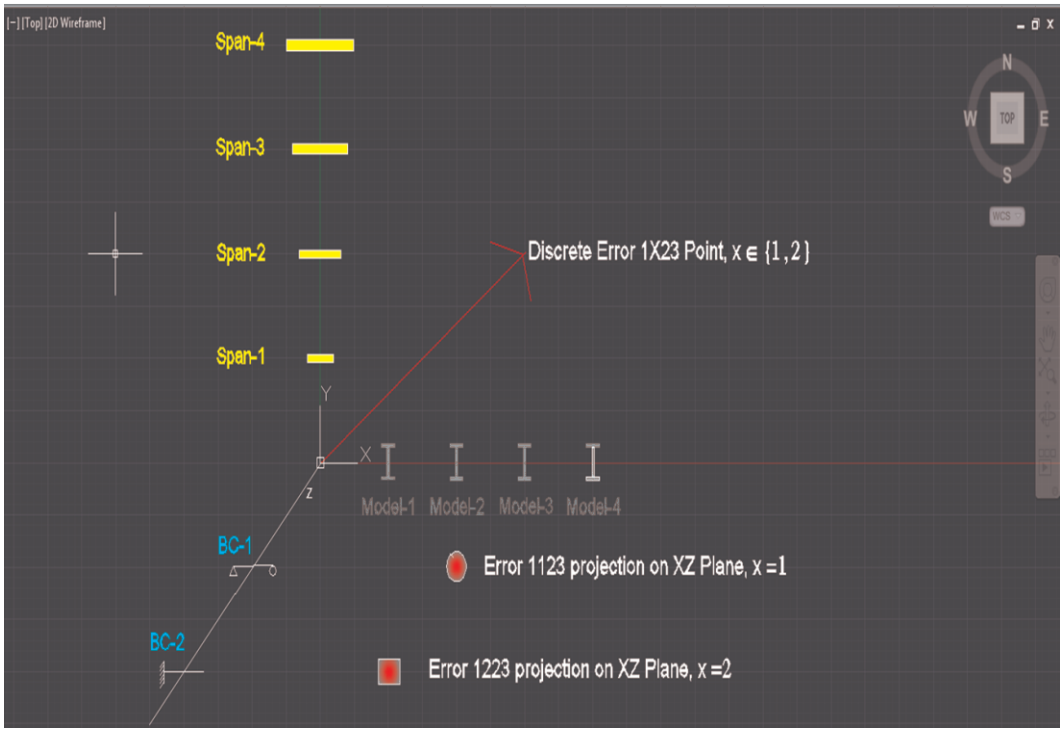

Figure 4.3. Parametric ANSYS Error Space.

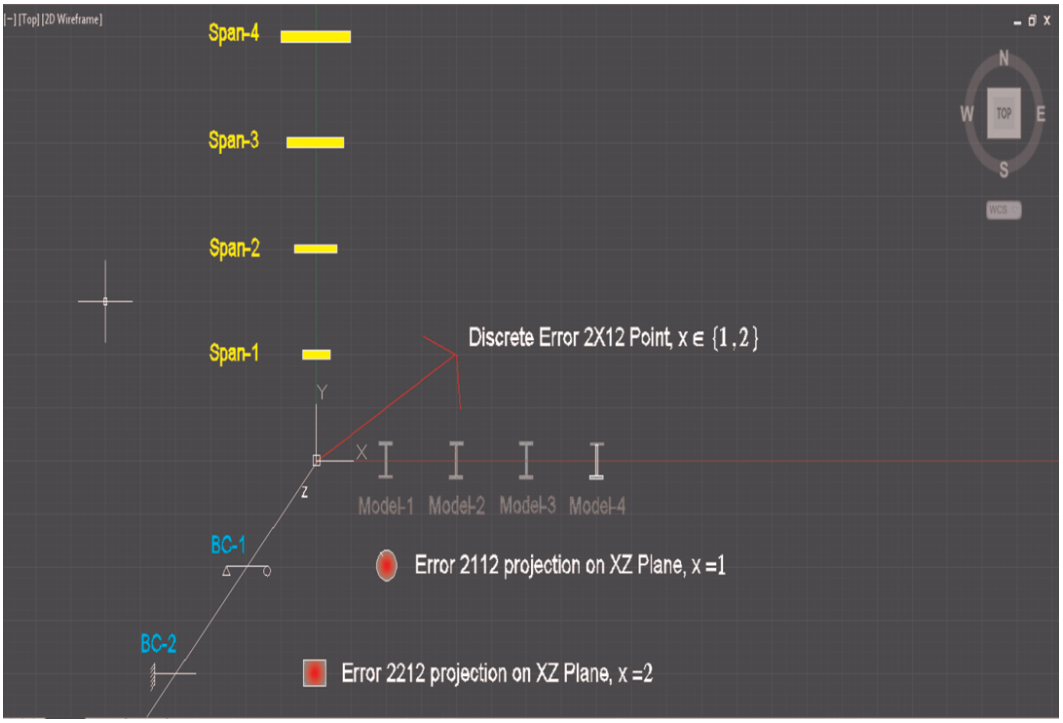

Figure 4.4. Parametric Theoretical Error Space.

Table 4.10. The Analysis Notation Set with ANSYS and BC-1.

	Span-1	Span-2	span-3	Span-4
Model-1	Analysis-1111	Analysis-1121	Analysis-1131	Analysis-1141
Model-2	Analysis-1112	Analysis-1122	Analysis-1132	Analysis-1142
Model-3	Analysis-1113	Analysis-1123	Analysis-1133	Analysis-1143
Model-4	Analysis-1114	Analysis-1124	Analysis-1134	Analysis-1144

Table 4.11. The Analysis Notation Set with ANSYS and BC-2.

	Span-1	Span-2	span-3	Span-4
Model-1	Analysis-1211	Analysis-1221	Analysis-1231	Analysis-1241
Model-2	Analysis-1212	Analysis-1222	Analysis-1232	Analysis-1242
Model-3	Analysis-1213	Analysis-1223	Analysis-1233	Analysis-1243
Model-4	Analysis-1214	Analysis-1224	Analysis-1234	Analysis-1244

Table 4.12. The Analysis Notation Set with THEORY and BC-1.

	Span-1	Span-2	span-3	Span-4
Model-1	Analysis-2111	Analysis-2121	Analysis-2131	Analysis-2141
Model-2	Analysis-2112	Analysis-2122	Analysis-2132	Analysis-2142
Model-3	Analysis-2113	Analysis-2123	Analysis-2133	Analysis-2143
Model-4	Analysis-2114	Analysis-2124	Analysis-2134	Analysis-2144

Table 4.13. The Analysis Notation Set with THEORY and BC-2.

	Span-1	Span-2	span-3	Span-4
Model-1	Analysis-2211	Analysis-2221	Analysis-2231	Analysis-2241
Model-2	Analysis-2212	Analysis-2222	Analysis-2232	Analysis-2242
Model-3	Analysis-2213	Analysis-2223	Analysis-2233	Analysis-2243
Model-4	Analysis-2214	Analysis-2224	Analysis-2234	Analysis-2244

4.4. Critical Load Calculations with Theoretical Solutions

In this section, the critical load calculations of:

- Analysis-2111 (Theoretical/BC-1/Span-1/Model-1)
- Analysis-2122 (Theoretical/BC-1/Span-2/Model-2)
- Analysis-2233 (Theoretical/BC-2/Span-3/Model-3)
- Analysis-2244 (Theoretical/BC-2/Span-4/Model-4)

will be samply progressed under the contents of Analysis-2111 Calculations (Theoretical Solution / BC-1 / Span-1 / Model-1), Analysis-2122 Calculations (Theoretical Solution/BC-1/Span-2/Model-2), Analysis-2233 Calculations (Theoretical Solution / BC-2 / Span-3 / Model-3), and Analysis-2244 Calculations (Theoretical Solution / BC-2 / Span-2 / Model-4). subheadings respectively. These calculations are numerically stated by applying the direct solution techniques of lateral torsional buckling formulas derived by Timoshenko. As a perceptual sense, it is obvious that these analysis types are chosen to illustrate the relative correlations including each model, span and loading types. These analyses and their corresponded error values lies on the diagonal rows within the related matrices due to symmetry condition.

Finally, the all 32 critical load calculations including the four sample solutions are performed by Matlab/R2011a software which compiled the theoretical mathematical algorithm of the lateral torsional buckling concept precisely. The screenshots of both

algorithm flow and the resultant critical loads will be arranged systematically through the figures and tabulated data structures within the subheading content of Matlab Solutions.

4.4.1. Analysis-2111 Calculations (Theoretical Solution / BC-1 / Span-1 / Model-1)

Table 4.14. Analysis-2111 inputs.

	Geometric Inputs						Material Properties	
	b[mm]	bf[mm]	hw[mm]	h[mm]	tw[mm]	L[mm]	E[N/mm^2	G[N/mm^2]
Analysis 211 Inputs	200	12	400	412	8	4000	2.10E+05	80769

The calculation procedure is provided in accordance with Table 4.13. which expresses the numerical values to be used in pre-calculations, that is, M_{cr} constants [11]:

- Torsional Constant:
  $J = \frac{1}{3}(2bt_f{}^3 + ht_w{}^3) = \frac{1}{3}(2 \times 200 \times 12^3 + 412 \times 8^3) = 300710\text{mm}^4$
- Warping Constant:
  $C_w = \frac{t_f b^3 h^2}{24} = \frac{12 \times 200^3 \times 412^2}{24} = 6.7898\text{e} + 011\text{mm}^6$
- Moment of Inertia (Weak Axis):
  $I_X = 2t_f \frac{b^3}{12} = 2 \times 12 \times \frac{200^3}{12} = 16\text{e} + 006\text{mm}^4$
  $M_{cr} = C_b \frac{\pi}{L} \sqrt{EI_x GJ + C_w I_x \left(\frac{\pi E}{L}\right)^2} = 482.32\text{kN.m}$

4.4.2. Analysis-2122 Calculations (Theoretical Solution/BC-1/Span-2/Model-2)

Table 4.15. Analysis-2122 Inputs.

	Geometric Inputs						Material Properties	
	b[mm]	bf[mm]	hw[mm]	h[mm]	tw[mm]	L[mm]	E[N/mm^2	G[N/mm^2]
Analysis 2122 Inputs	200	12	420	432	10	6000	2.10E+05	80769

The calculation procedure is provided in accordance with Table 4.14. and M_{cr} pre-calculation constants are as follows:

- Torsional Constant:
  $J = \frac{1}{3}(2bt_f{}^3 + ht_w{}^3) = \frac{1}{3}(2 \times 200 \times 12^3 + 432 \times 10^3) = 374400\text{mm}^4$
- Warping Constant:
  $C_w = \frac{t_f b^3 h^2}{24} = \frac{12 \times 200^3 \times 432^2}{24} = 7.4650\text{e} + 011\text{mm}^6$
- Moment of Inertia (Weak Axis):
  $I_X = 2t_f \frac{b^3}{12} = 2 \times 12 \times \frac{200^3}{12} = 16\text{e} + 006\text{mm}^4$
  $M_{cr} = C_b \frac{\pi}{L} \sqrt{EI_x GJ + C_w I_x \left(\frac{\pi E}{L}\right)^2} = 259.70\text{kN.m}$

4.4.3. Analysis-2233 Calculations (Theoretical Solution / BC-2 / Span-3 / Model-3)

Table 4.16. Analysis-2233 Inputs.

	Geometric Inputs						Material Properties	
	b[mm]	bf[mm]	hw[mm]	h[mm]	tw[mm]	L[mm]	E[N/mm^2]	G[N/mm^2]
Analysis 2233 Inputs	220	14	400	414	8	8000	2.10E+05	80769

The calculation procedure is provided in accordance with Table 4.15 and P_{cr} pre-calculation constants are as follows:

- Torsional Constant:
  $J = \frac{1}{3}(2bt_f{}^3 + ht_w{}^3) = \frac{1}{3}(2 \times 220 \times 14^3 + 414 \times 8^3) = 473110\text{mm}^4$
- Warping Constant:
  $C_w = \frac{t_f b^3 h^2}{24} = \frac{14 \times 220^3 \times 414^2}{24} = 1.0646\text{e} + 012\text{mm}^6$
- Moment of Inertia (Weak Axis):
  $I_X = 2t_f \frac{b^3}{12} = 2 \times 14 \times \frac{220^3}{12} = 2.4845\text{e} + 007\text{mm}^4$
  $P_{cr} = \frac{4.013}{L^2} \sqrt{GJEI_x} = 27.73\text{kN}$

4.4.4. Analysis-2244 Calculations (Theoretical Solution / BC-2 / Span-2 / Model-4)

Table 4.17. Analysis-2244 Inputs.

	Geometric Inputs						Material Properties	
	b[mm]	bf[mm]	hw[mm]	h[mm]	tw[mm]	L[mm]	E[N/mm^2	G[N/mm^2]
Analysis 2244 Inputs	220	14	420	434	10	10000	2.10E+05	80769

The calculation procedure is provided in accordance with Table 4.16 and P_{cr} pre-calculation constants are as follows:

- Torsional Constant:
  $J = \frac{1}{3}(2bt_f{}^3 + ht_w{}^3) = \frac{1}{3}(2 \times 220 \times 14^3 + 434 \times 10) = 547120\text{mm}^4$
- Warping Constant:
  $C_w = \frac{t_f b^3 h^2}{24} = \frac{14 \times 220^3 \times 434^2}{24} = 1.1699\text{e} + 012\text{mm}^6$
- Moment of Inertia (Weak Axis):
  $I_X = 2t_f \frac{b^3}{12} = 2 \times 14 \times \frac{220^3}{12} = 2.4845\text{e} + 007\text{mm}^4$
  $P_{cr} = \frac{4.013}{L^2}\sqrt{GJEI_x} = 19.161\text{kN}$

4.4.5. Matlab Solutions

All the previous calculation algorithms are performed by Matlab arithmetic operators and are illustrated between the Figure A.1 and A.8 at the Appendix Part. To have an insight, shows not only the pre-calculations of the lateral torsional buckling variables and constants but also the error analyses over the critical load results of Ansys and theory.

Consequently, an effective storage of the critical load data are both tabulated abd illustrated through Table 4.17, Table 4.18 and Figure 4.6, Figure 4.7. The crossed X(Model) and Y(Span) variables, distributed from 1 to 4 in an algebraic manner, which refers to additional third and fourth dimensions in the view of notation representation.

Table 4.18. Theoretical M_{cr} (kN.m) values for BC-1.

	M_{cr}-21Y1 X=1	M_{cr}-21Y2 X=2	M_{cr}-21Y3 X=3	M_{cr}-21Y4 X=4
M_{cr}-211X Y=1	482.32	512.90	752.88	793.72
M_{cr}-212X Y=2	241.62	259.70	377.27	399.45
M_{cr}-213X Y=3	154.85	167.91	241.84	256.98
M_{cr}-214X Y=4	112.79	123.12	176.18	187.73

Table 4.19. Theoretical P_{cr} (kN) values for BC-2.

	M_{cr}-22Y1 X=1	M_{cr}-22Y2 X=2	M_{cr}-22Y3 X=3	M_{cr}-22Y4 X=4
M_{cr}-221X Y=1	71.65	79.95	111.99	120.43
M_{cr}-222X Y=2	31.85	35.53	49.77	53.53
M_{cr}-223X Y=3	17.91	19.99	28.00	30.11
M_{cr}-224X Y=4	11.46	12.79	17.92	19.27

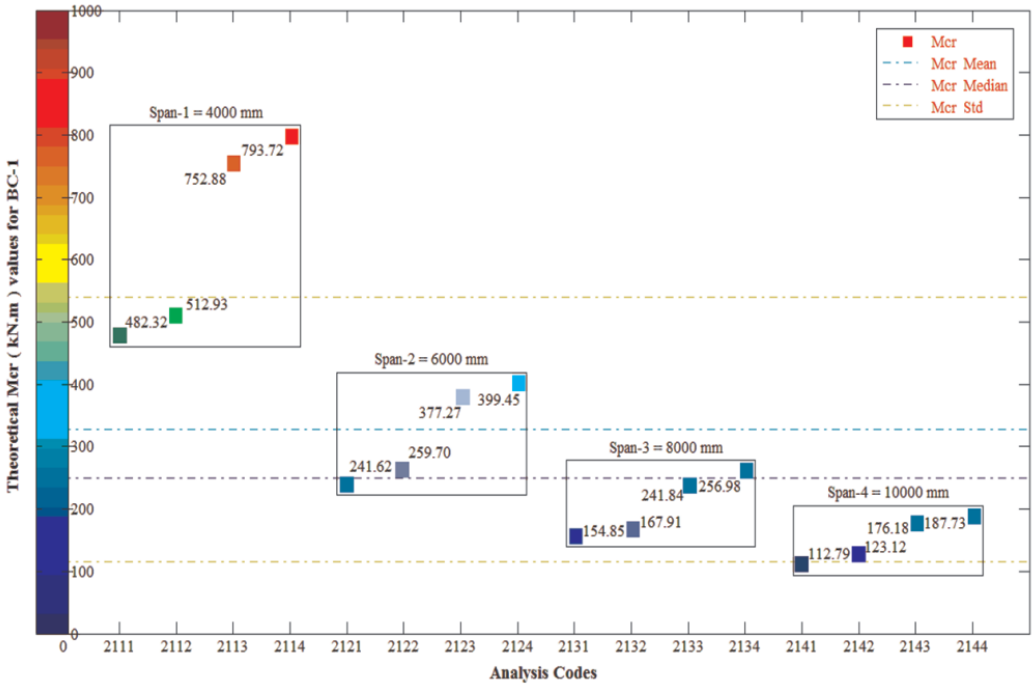

Figure 4.5. Theoretical M_{cr} (N.mm) Spectrum for BC-1.

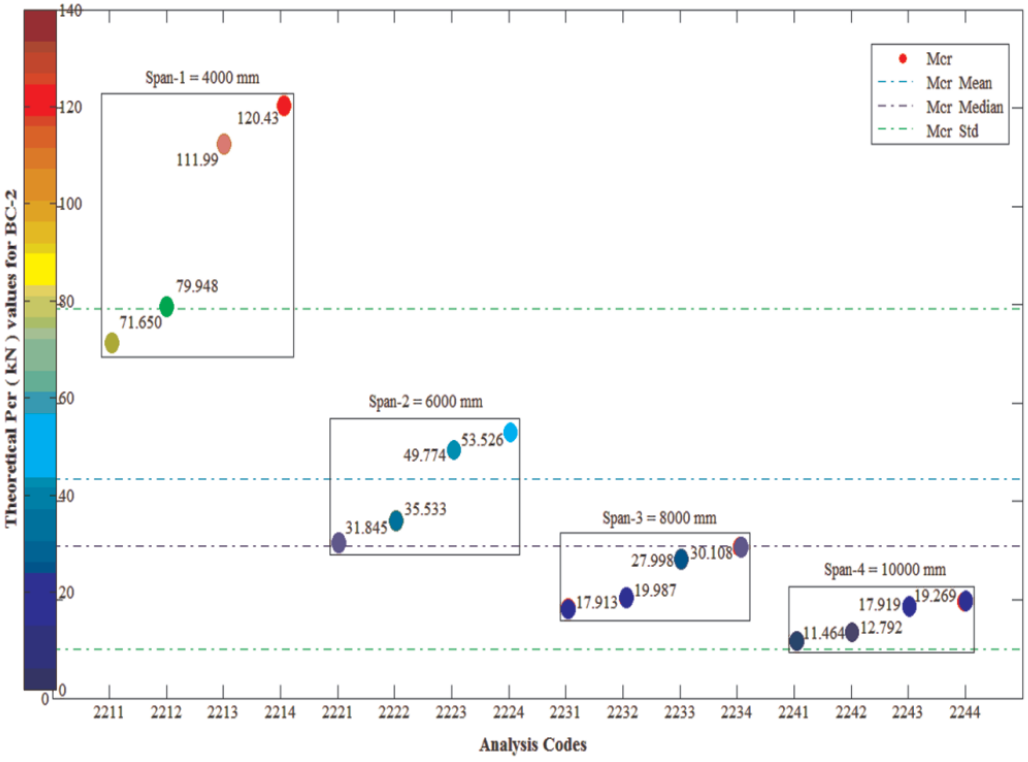

Figure 4.6. Theoretical P_{cr} (kN) Spectrum for BC-2.

4.5. Critical Load Calculations with ANSYS

4.5.1. Optimization of ANSYS Default Algorithm for Lateral Torsional Buckling

A fundamental understanding of developing the pre-process configurations over meshing options, default constants and solution functions with dynamic operators is of vital importance for a manually optimized beam behaviour simulation under various lateral torsional buckling effects.

Six manually optimized default settings and their related "Ansys Commands" through the whole simulation processes are:

- Command [EQSLV]: Equation solver with "Sparse solver"
- Command [BUCOPT]: Mode extraction method with "Block Lanczos"
- Command [MEXPAND]: Number of modes to expand with "1"
- Command [PIVCHECK]: Pivot check with "On"
- Command [PSTRES]: Include prestress effects with "Yes"
- Command [LESIZE]: Element edge length with "10 mm"

The ongoing operation process after the system base solution, "Steady-State" analysis, is the "Eigen Buckling" analysis with the expanded mode number of 1. To observe the critical loads, mode data should be set to 1, otherwise more than one critical loads will exists and error calculations will be highly complex.

GUI option windows are illustrated from Figure 4.8 to Figure 4.11 to reflect the manually optimized steps through the whole simulation perspectives.

Figure 4.7. Optimization of [EQSLV]. Equation Solver with "Sparse solver".

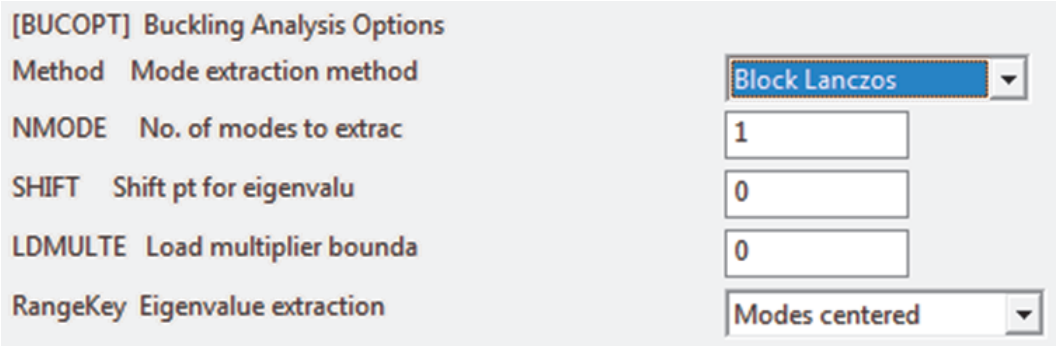

Figure 4.8. Optimization of [BUCOPT]. Mode Extraction with "Block Lanczos".

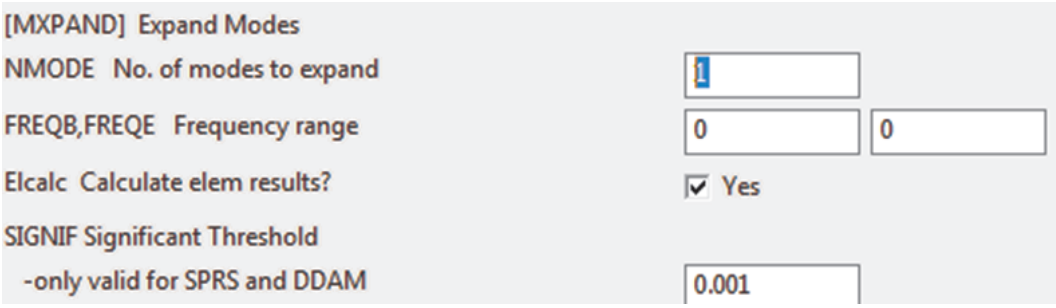

Figure 4.9. Optimization of [MEXPAND]. Number of Modes to Expand with "1".

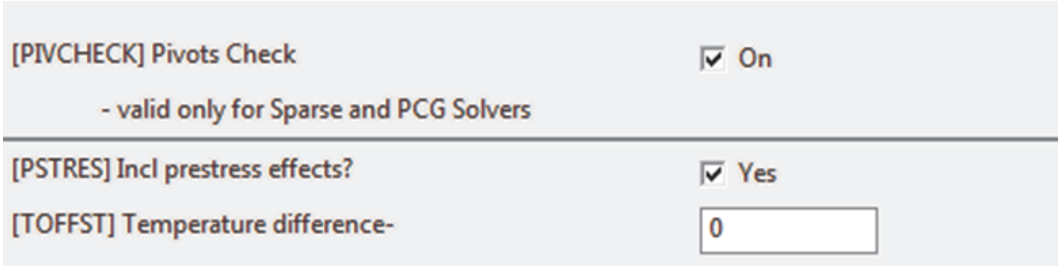

Figure 4.10. Optimizations of [PIVCHECK], and [PSTRES], with "On" and "Yes".

Once the default system configuration is optimized for lateral torsional buck-

ling simulations, running the analysis storages the processed output data under the processor of "General Postprocessing" which includes the plotting of contours, vector displays, deformed shapes and listing of the results in tabular formats

The both moment and force values initialy applied for both loading conditions have the scalar value of "1". Since the load value is only a magnitude of 1, this will not skew the eigenvalue matrix because eigenvalues are calculated by a factor of load applied. Results file with Figure 4.11. represents the M_{cr} value of ANSYS for the Analysis-1111. TIME/FREQ is the lowest eigenvalue representing the lowest load to cause lateral torsional buckling with the consistent SI units [N.mm]. for BC-1 moment and [N]. for BC-2 force.

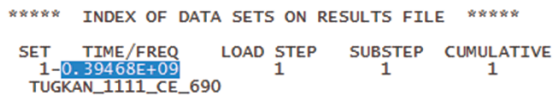

Figure 4.11. ANSYS M_{cr} Output Value of Analysis-1111. Accessed via the Path of Main Menu>General Postprocessing>List Results>Detailed Summary.

4.5.2. ANSYS M_{cr} and P_{cr} Values

While Figure 4.12 respresenting the pure raw integration of 16 "SET lis" post-processing files, Figure 4.14 illustrates these M_{cr} output data for the BC-1 condition.

SET	TIME/FREQ	LOAD STEP	SUBSTEP	CUMULATIVE
1	-0.39468E+09	1	1	1
	Mcr_ANALYSIS_1111			
1	0.44210E+09	1	1	1
	Mcr_ANALYSIS_1112			
1	0.61463E+09	1	1	1
	Mcr_ANALYSIS_1113			
1	-0.66353E+09	1	1	1
	Mcr_ANALYSIS_1114			
1	-0.26325E+09	1	1	1
	Mcr_ANALYSIS_1121			
1	0.26479E+09	1	1	1
	Mcr_ANALYSIS_1122			
1	0.41000E+09	1	1	1
	Mcr_ANALYSIS_1123			
1	0.44262E+09	1	1	1
	Mcr_ANALYSIS_1124			
1	-0.19747E+09	1	1	1
	Mcr_ANALYSIS_1131			
1	-0.22120E+09	1	1	1
	Mcr_ANALYSIS_1132			
1	-0.30757E+09	1	1	1
	Mcr_ANALYSIS_1133			
1	0.33203E+09	1	1	1
	Mcr_ANALYSIS_1134			
1	-0.15799E+09	1	1	1
	Mcr_ANALYSIS_1141			
1	0.17697E+09	1	1	1
	Mcr_ANALYSIS_1142			
1	-0.24608E+09	1	1	1
	Mcr_ANALYSIS_1143			
1	0.26565E+09	1	1	1
	Mcr_ANALYSIS_1144			

Figure 4.12. ANSYS M_{cr} Outputs of BC-1 between Analysis-1111 and Analysis-1144.

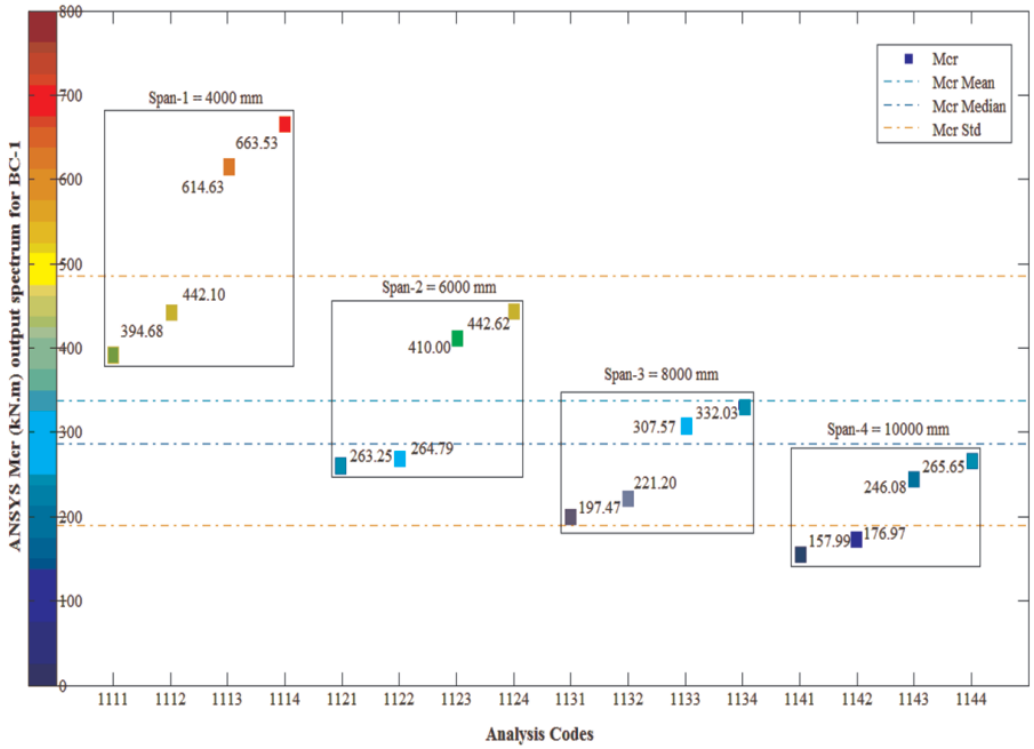

Figure 4.13. ANSYS M_{cr} Output Spectrum for BC-1.

In the same manner, Figure 4.14 and Figure 4.15 represents the 16 P_{cr} [N]. output values of 16 ANSYS simulations for the BC-2 condition with 16 cantilever beam models.

All the parametric comparative error simulations are illustrated through Appendix B, reflecting the von mises stress values.

It is obvious that stress gradient varies at high frequency towards constrained boundary locations. The color spectrum helps the stress phenomena to be understood in terms of symbolic localized sections.

SET	TIME/FREQ	LOAD	STEP	SUBSTEP	CUMULATIVE
1	-71124.		1	1	1
	Pcr_ANALYSIS_1211				
1	-79670.		1	1	1
	Pcr_ANALYSIS_1212				
1	0.11074E+06		1	1	1
	Pcr_ANALYSIS_1213				
1	0.11880E+06		1	1	1
	Pcr_ANALYSIS_1214				
1	-31642.		1	1	1
	Pcr_ANALYSIS_1221				
1	-35444.		1	1	1
	Pcr_ANALYSIS_1222				
1	49276.		1	1	1
	Pcr_ANALYSIS_1223				
1	53130.		1	1	1
	Pcr_ANALYSIS_1224				
1	-17805.		1	1	1
	Pcr_ANALYSIS_1231				
1	19944.		1	1	1
	Pcr_ANALYSIS_1232				
1	-27730.		1	1	1
	Pcr_ANALYSIS_1233				
1	29934.		1	1	1
	Pcr_ANALYSIS_1234				
1	11396.		1	1	1
	Pcr_ANALYSIS_1241				
1	12777.		1	1	1
	Pcr_ANALYSIS_1242				
1	-17751.		1	1	1
	Pcr_ANALYSIS_1243				
1	19161.		1	1	1
	Pcr_ANALYSIS_1244				

Figure 4.14. ANSYS P_{cr} Outputs of BC-2 between Analysis-1211 and Analysis-1244.

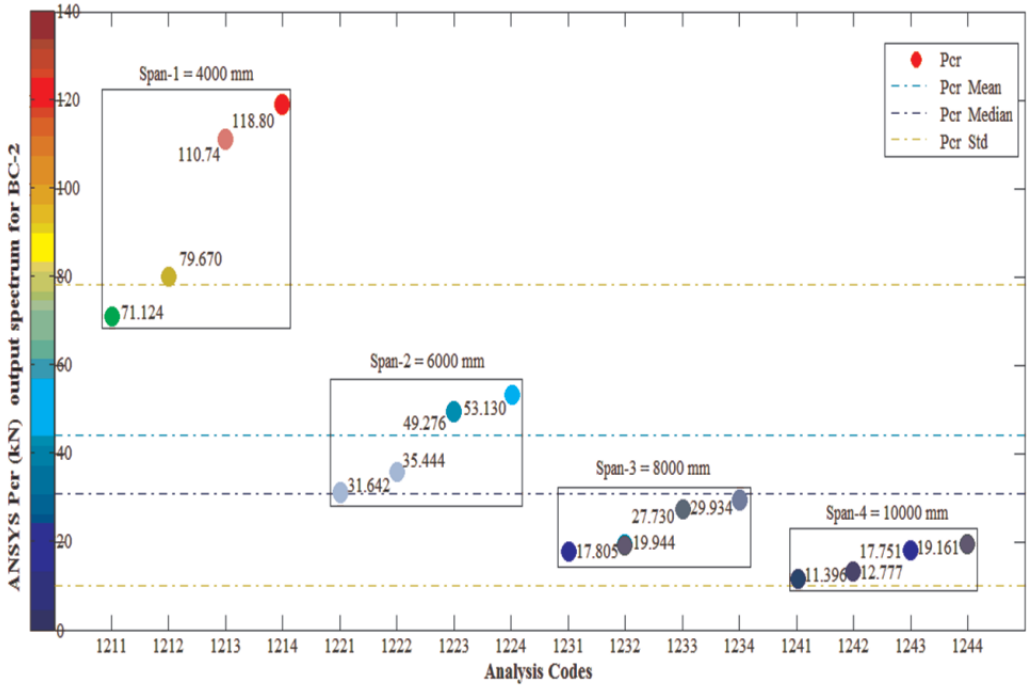

Figure 4.15. ANSYS P_{cr} Output Spectrum for BC-2.

Consequently, an effective storage of the critical load output data are tabulated through Table 4.20. and Table 4.21. for both M_{cr} and P_{cr} respectively. The crossed X(Model) and Y(Span) variables, distributed from as before.

Table 4.20. ANSYS M_{cr} (kN.m) Values for BC-1.

	M_{cr}-21Y1 X=1	M_{cr}-21Y2 X=2	M_{cr}-21Y3 X=3	M_{cr}-21Y4 X=4
M_{cr}-211X Y=1	394.68	442.10	614.63	663.53
M_{cr}-212X Y=2	263.25	264.79	410.00	442.62
M_{cr}-213X Y=3	197.47	221.20	307.57	332.03
M_{cr}-214X Y=4	157.99	176.97	246.08	264.65

Table 4.21. ANSYS P_{cr} (kN) Values for BC-2.

	P_{cr}-22Y1 X=1	P_{cr}-22Y2 X=2	P_{cr}-22Y3 X=3	P_{cr}-22Y4 X=4
P_{cr}-221X Y=1	71.12	79.67	110.74	118.80
P_{cr}-222X Y=2	31.64	35.44	49.28	53.13
P_{cr}-223X Y=3	17.81	19.94	27.73	29.93
P_{cr}-224X Y=4	11.40	12.78	17.75	19.16

4.6. Error Spectrum Analyses comparing the ANSYS and Theoretical Solutions

In numerical simulation or modeling of real structural systems, error analysis is concerned with the changes in the output of the model as the parameters to the model vary about a mean through different analysis types with the purpose of explaining how and why the results deviate from the expectations resulted by different analysis types. In this perspective, theoretical direct solutions and ANSYS simulations will be detailly compared through different various parameters and correlations.

As Figure 4.17 reflects the error bars, Figure 4.18 illustrates the closely matching error points in the same manner. According to the comperative analyses results, simply supported beam models with different spans serves an error spectrum between 1.92% and 43.74% and cantilever beam models has between 0.21% and 1.37%, that is, as the constraints decrease in terms of the boundary conditions, ANSYS simulations and theoretical solutions has neglegible relative error values.

To observe the multidimensional effects of the parameters, while Figure 4.19 and

Figure 4.20 are plotted on the basis of span perspectives on the hand Figure 4.21 constructed on model types. As the beam span length increases, both M_{cr} and P_{cr} values decreases resulting the sensitive error values.

Determining the behaviour of the error space, not only the relative errors but also the average error values are tabulated through Table 4.22 and Table 4.23. The detailed error statistic tabulations and graphics reveals the main effective behaviours of the parameters which were set at the begining of this section.

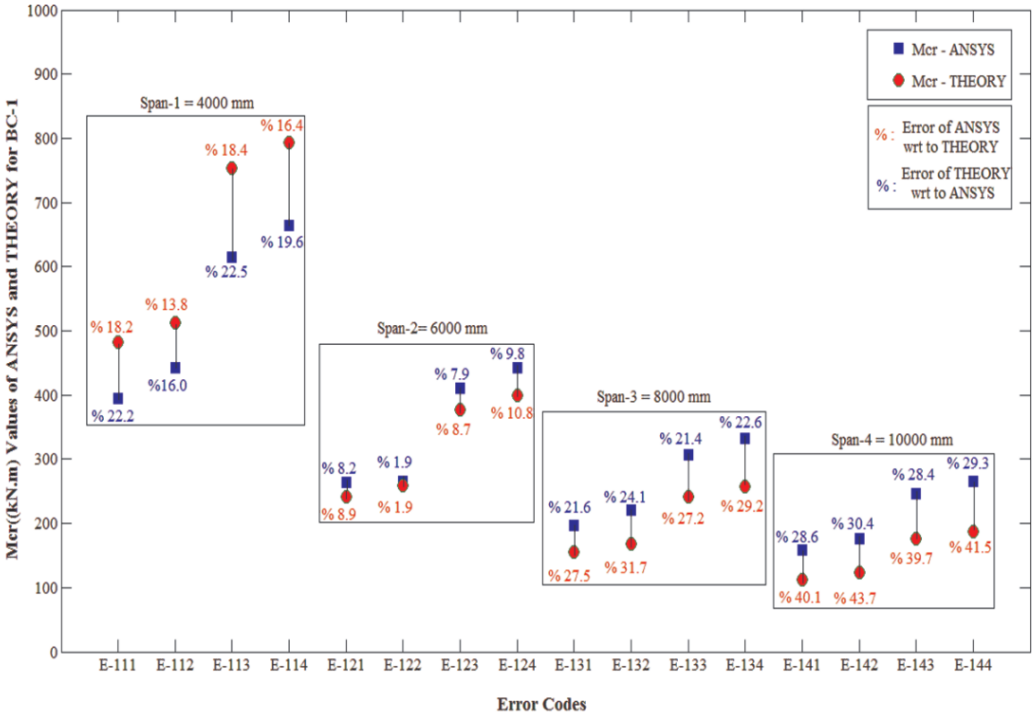

Figure 4.16. M_{cr} Error Bars between ANSYS and Theoretical Solutions for BC-1.

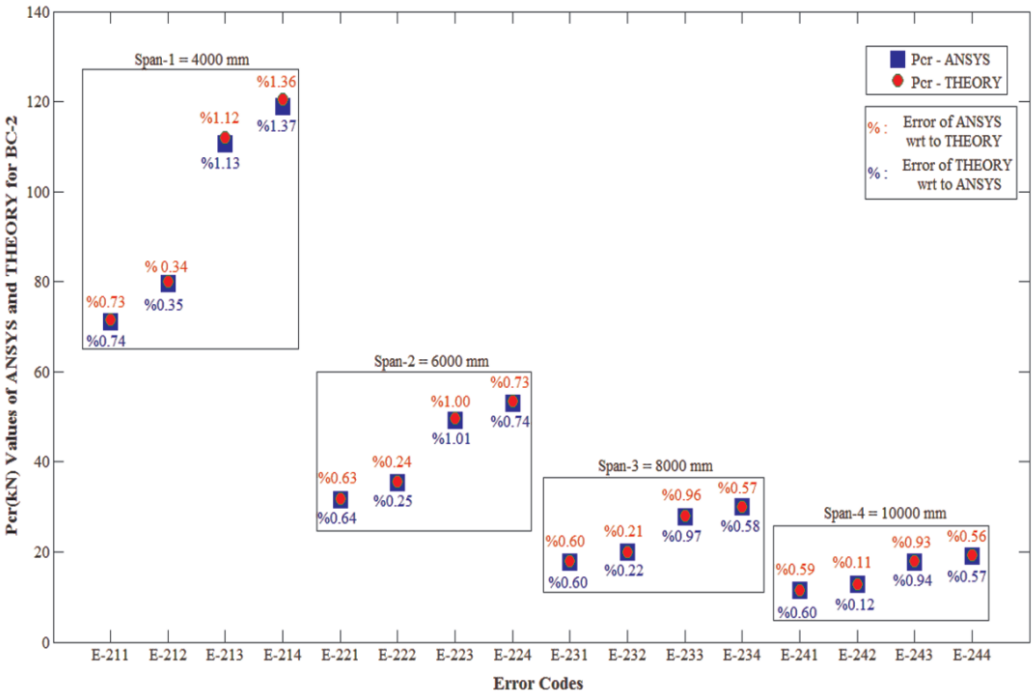

Figure 4.17. P_{cr} Error Poins between ANSYS and Theoretical Solutions for BC-2.

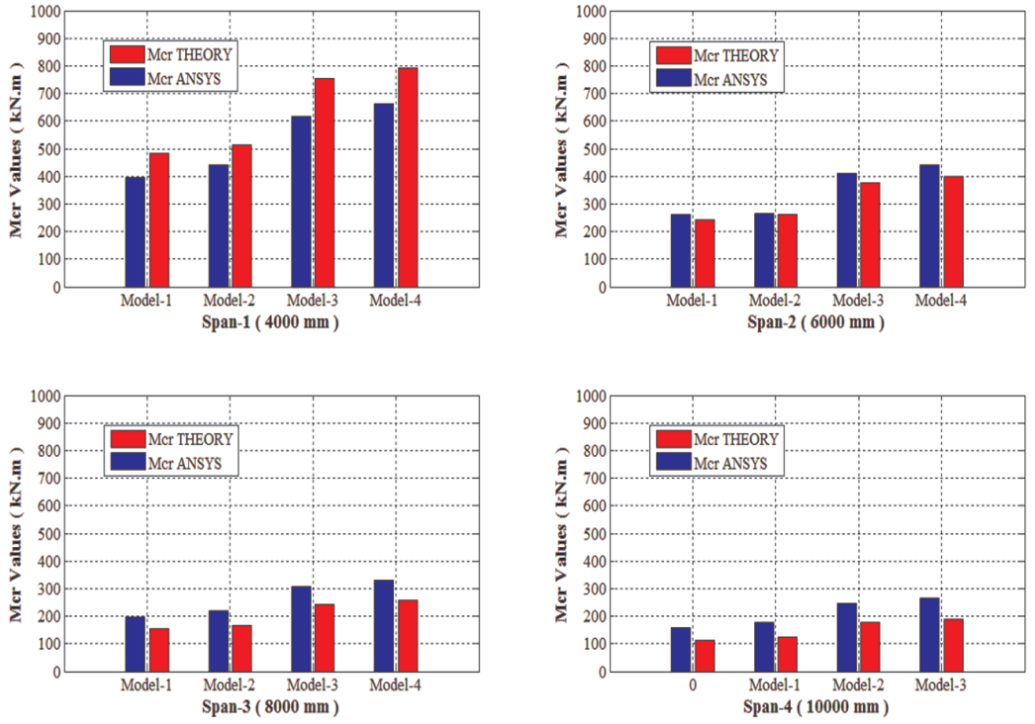

Figure 4.18. Span-Based M_{cr} Bars of ANSYS and Theoretical Solutions for BC-1.

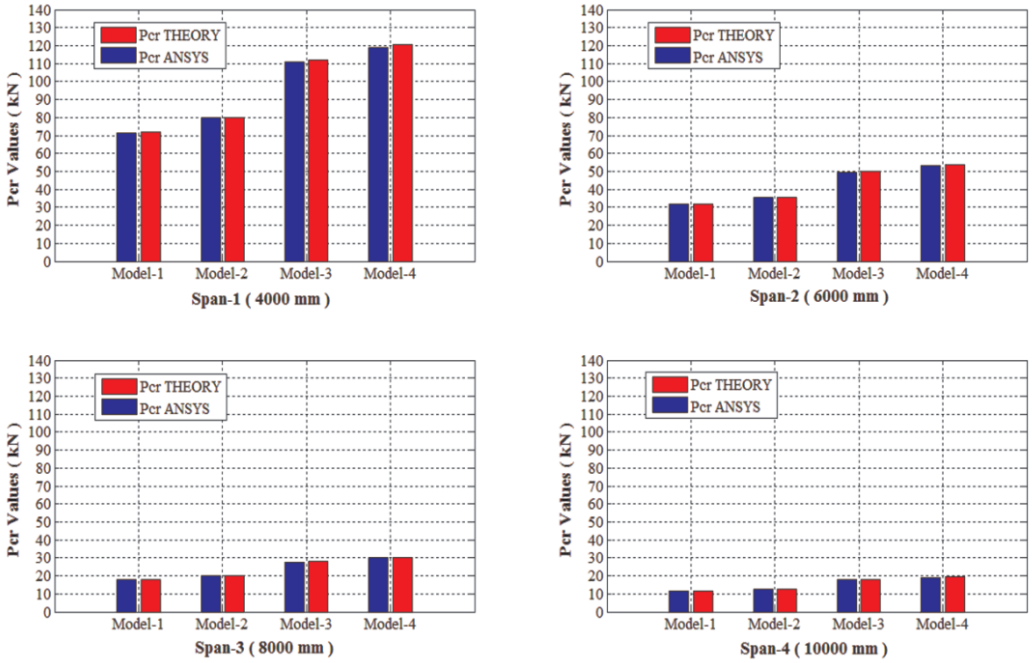

Figure 4.19. Span-Based P_{cr} Bars of ANSYS and Theoretical Solutions for BC-2.

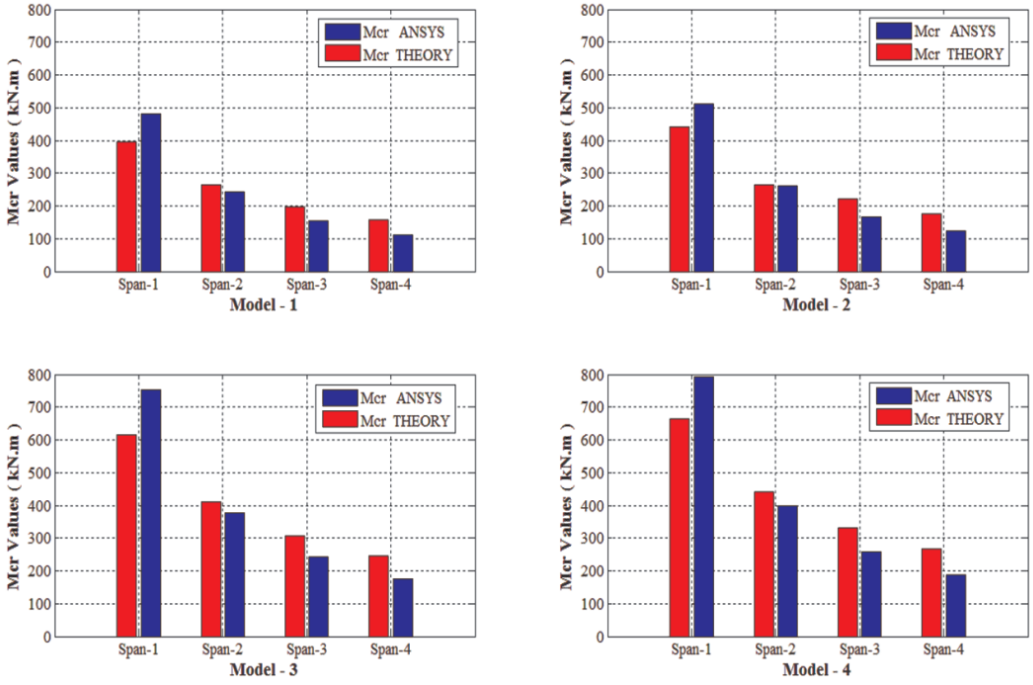

Figure 4.20. Model-Based M_{cr} Bars of ANSYS and Theoretical Solutions for BC-1.

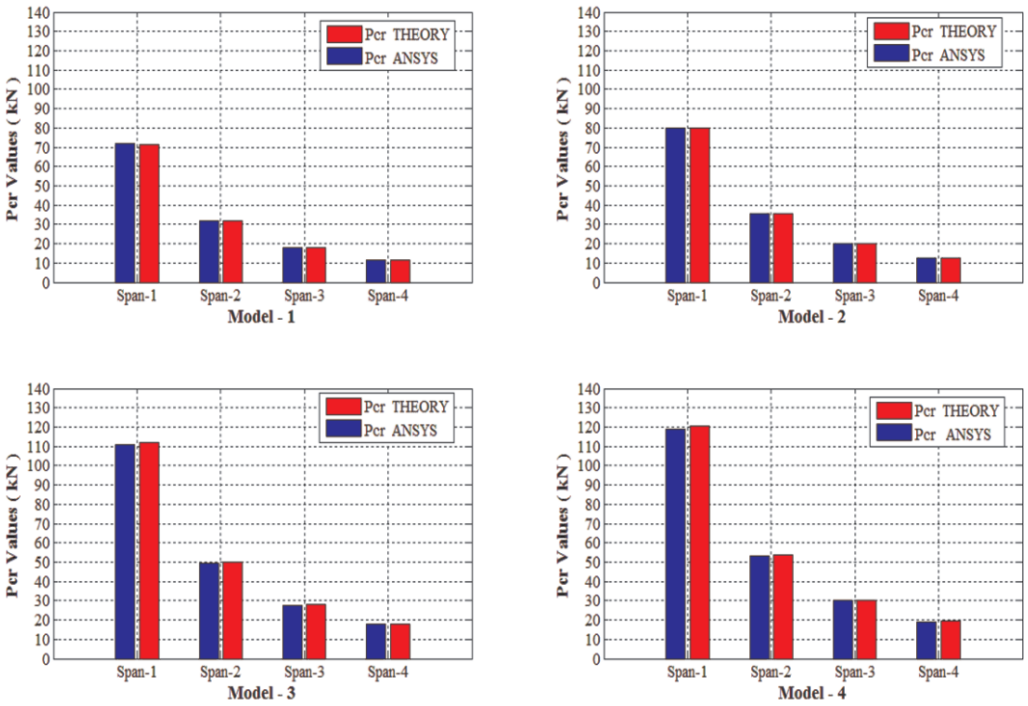

Figure 4.21. Model-Based P_{cr} Bars of ANSYS and Theoretical Solutions for BC-2..

Not only the relative errors values, but also the average error values are calculated through the arithmetic definiton of error consept. Appendix A contains all the Matlab error calculations.

Taking all into account, the figures shows that, while both span-based and model-based analyses has negligible relative error results for cantilever beam models; on the other hand simply supported beam model applications has obvious errorous values. With the aim of a parametric comparision result, the most effective factor in error calculations is the boundary conditions. These calculatioıns are skipped but performed externally by multiplying the P_{cr} values by the span lengths and comparing them with the M_{cr} values. After on, span lengths has the most effective factor on error analyses. At last, beam models with parametric correlations has the least error factors. So we can set the flow of the parametric effects as boundary conditions, span lengths, parametric models through descending error order. All the calculations are performed by the following equations.

Table 4.22. Error Variations with BC-1.

	Error-2	Error-1	Averge Error
E-111	22.21%	18.17%	20.19%
E-112	16.02%	13.81%	14.92%
E-113	22.49%	18.36%	20.43%
E-114	19.62%	16.40%	18.01%
E-121	8.21%	8.95%	8.58%
E-122	19.21%	19.59%	19.40%
E-123	7.98%	8.68%	8.33%
E-124	9.75%	10.81%	10.28%
E-131	21.58%	27.52%	24.55%
E-132	24.09%	31.73%	27.91%
E-133	21.37%	27.18%	24.28%
E-134	22.60%	29.20%	25.90%
E-141	28.61%	40.08%	34.34%
E-142	30.43%	43.74%	37.08%
E-143	28.40%	39.67%	34.04%
E-144	29.33%	41.51%	35.42%

Table 4.23. Error Variations with BC-2.

	Error-2	Error-1	Averge Error
E-211	0.740%	0.735%	0.737%
E-212	0.349%	0.348%	0.349%
E-213	1130%	1117%	1124%
E-214	1374%	1356%	1365%
E-221	0.640%	0.636%	0.638%
E-222	0.250%	0.249%	0.250%
E-223	1011%	1000%	1005%
E-224	0.745%	0.739%	0.742%
E-231	0.604%	0.601%	0.603%
E-232	0.216%	0.216%	0.216%
E-233	0.966%	0.957%	0.961%
E-234	0.582%	0.579%	0.580%
E-241	0.597%	0.594%	0.596%
E-242	0.115%	0.115%	0.115%
E-243	0.944%	0.935%	0.940%
E-244	0.565%	0.562%	0.563%

Error-1, Error-2 are the relative errors which are calculated by the formulas of:

$$Error-1=\left[\frac{|M_{cr}\_Theoretical-M_{cr}\_ANSYS|}{M_{cr}\_Theoretical}\right]\times 100 \tag{4.2}$$

$$Error-1=\left[\frac{|P_{cr}\_Theoretical-P_{cr}\_ANSYS|}{P_{cr}\_Theoretical}\right]\times 100 \tag{4.3}$$

$$Error-2=\left[\frac{|M_{cr}\_ANSYS-M_{cr}\_Theoretical|}{M_{cr}\_ANSYS}\right]\times 100 \tag{4.4}$$

$$Error-2=\left[\frac{|P_{cr}\_ANSYS-P_{cr}\_Theoretical|}{P_{cr}\_ANSYS}\right]\times 100 \tag{4.5}$$

The convergence error which is also called as average error is calculated by:

$$Average\_Error=\frac{(Error-1+Error-2)}{2} \tag{4.6}$$

5. CONCLUSION

This thesis has presented the details of an extensive investigation aimed at widening the scope of parametric analysis to include the design of steel structures subjected to lateral torsional buckling effects. A comprehensive literature review was undertaken related to both numerical and parametric analyses and lateral torsional buckling. The investigation on the structural beam's lateral torsional buckling behaviour involved a large amount of finite element analyses of simply supported and catilever beam models.

96 analyses of I-Section beams with four parametric models and two types of analyses were conducted via eigenbuckling loading operators through ANSYS Academic Research R14.5/Structural finite element software.

It is essential for the advanced structural analysis method to be able to deal with software packages. The lateral torsional buckling failures are complex phenomena. They are diffucult to account for transient analyses. The state-of-the-art finite element analysis methods are able to explicitly deal for this failure mode but they are not applicable to general design practice. A practical advanced software analysis option provides a more efficient alternative to the current direct theoretical direct solutions methods over millions of meshes. However, before the advanced software analysis can realise its potential as a tool for a practical lateral torsional buckling analysis; a number of opereator, default constant, solver function optimizations must be manually progressed. Without focusing this issue, the use of advanced software analysis as a pratical simulating tool will be severely restricted.

Based on the finite element analyses, an actual wide spectrum simulation behaviour has been developed over an average number of meshes limiting to 150.000. The finite element method results of simply supported and cantilever beam models were used to verify the theoretical direct solution of AISC formulations. Not only the parametric analyses but also the steady-state analyses are conducted to reveal the buckling effect via simulations.

The following is a statistical summary of the most significant findings arising this thesis research.

- The absolute convergence error average between ANSYS and theoretical solutions over all 96 analyses performed through the thesis research is 11.16%.
- The convergence error average between ANSYS and theoretical solutions over the 48 simply supported beam model analyses is 21.64%.
- The convergence error average between ANSYS and theoretical solutions over the 48 cantilever beam model analyses is 0.67%
- The maximum error is 43.74% with the Error-142.
- The minimum error is 0.22% with the Error-232.
- ANSYS simulations has averagelly 32.3 times better correlations with cantilever beam models compared to simply supoorted beam models.
- While spectrum error lies between the limits of 1.92% and 43.74% for the simply supported beam models, on the hand for the cantilever beam models these limits are bounded with very close values as 0.22% and 1.37%.

The following is a theoretical summary of the most significant findings arising this thesis research:

- Sections having different torsional and warping properties exhibit different responses.
- Lateral torsional buckling capacity of I-section beams tend to decrease as the web slenderness increases. The reduction in buckling capacity due to increasing web slenderness has been observed through the post processing animations.
- Future research should extend the findings of this study to different section types. U beams require additional treatment.
- Lateral torsional buckling of beams are greatly influenced by the location of loading, span length and section dimensions.
- Effects of initial geometrical imperfections were investigated and through the modelling process, this item has been taken into consideration via geometry optimizers.

- Stress gradiant flows are observed through simulation animations which were generelly arising from boundary regions to to the centroidal nodes of the beams.
- Throughout the post-processing, different eigenbuckling modes were analysed seperatedly to observe the mode frequency effects over the lateral torsional buckling zone.
- Parametric analyses were conducted through 4 compact sections to reveal the slenderness ratio effect on lateral torsional buckling behaviour of beams.

APPENDIX A: MATLAB CODES FOR THEORETICAL SOLUTIONS AND ERROR CALCULATIONS

A.1. Analysis-2.1.1.1 M_{cr} and E-1.1.1 Calculations

```
>> E=210000; G=80769; % Elastic/Shear M. [N/mm^2]
>> b=200;tf=12; hw=400;tw=8; h=412;L=4000; % Geometric Dimensions [mm]
>> J=(1/3)*[2*b*tf^3+h*tw^3]; % Torsional Constant [mm^4]
>> Cw=(tf*b^3*h^2)/24; % Warping Constant [mm^6]
>> Ix=2*tf*(b^3/12); % Moment of Inertia [mm^4]
>> Mcr Theoretical=(pi/L)*sqrt(E*Ix*G*J+Cw*Ix*[(pi*E)/L]^2)
Mcr Theoretical =
4.8232e+008
>>
>> Mcr ANSYS= 0.39468E+09; % ANSYS-Critical Moment [N.mm]
>>
>> Error1=[abs(Mcr ANSYS-Mcr Theoretical)/Mcr ANSYS]*100 Error1=
22.2059
>>
>> Error2=[abs(Mcr Theoretical-Mcr ANSYS)/Mcr Theoretical]*100 Error2 =
18.1709
>>
>> Average Error=( Error1+ Error2)/2
Average Error=
20.1884
```

A.2. Analysis-2.1.1.2 Mcr and E-1.1.2 Calculations

```
>> E=210000; G=80769; % Elastic/Shear M. [N/mm^2]
>> b=200;tf=12; hw=420;tw=10; h=432;L=4000; % Geometric Dimensions [mm]
>> J=(1/3)*[2*b*tf^3+h*tw^3]; % Torsional Constant [mm^4]
>> Cw=(tf*b^3*h^2)/24; % Warping Constant [mm^6]
>> Ix=2*tf*(b^3/12); % Moment of Inertia [mm^4]
>> Mcr Theoretical=(pi/L)*sqrt(E*Ix*G*J+Cw*Ix*[(pi*E)/L] ^2)
Mcr Theoretical =
5.1293e+008
>>
>> Mcr ANSYS= 0.44210E+09; % ANSYS-Critical Moment [N.mm]
>>
>> Error1=[abs(Mcr ANSYS-Mcr Theoretical)/Mcr ANSYS]*100
Error1=
16.0214
>>
>> Error2=[abs(Mcr Theoretical-Mcr ANSYS)/Mcr Theoretical]*100
Error2=
13.8090
>>
>> Average Error=( Error1+ Error2)/2
Average Error Convergence =
14.9152
```

A.3. Analysis-2.1.1.3 Mcr and E-1.1.3 Calculations

```
>> E=210000; G=80769; % Elastic/Shear M. [N/mm^2]
>> b=220;tf=14; hw=400;tw=8; h=414;L=4000; % Geometric Dimensions [mm]
>> J=(1/3)*[2*b*tf^3+h*tw^3]; % Torsional Constant [mm^4]
>> Cw=(tf*b^3*h^2)/24; % Warping Constant [mm^6]
```

```
>> Ix=2*tf*(b^3/12); % Moment of Inertia [mm^4]
>> Mcr Theoretical=(pi/L)*sqrt(E*Ix*G*J+Cw*Ix*[(pi*E)/L] ^2)
Mcr Theoretical =
7.5288e+008
>>
>> Mcr ANSYS= 0.61463E+09; % ANSYS-Critical Moment [N.mm]
>>
>> Error1=[abs(Mcr ANSYS-Mcr Theoretical)/Mcr ANSYS]*100
Error1=
22.4930
>>
>> Error2=[abs(Mcr Theoretical-Mcr ANSYS)/Mcr Theoretical]*100
Error2=
18.3627
>>
>> Average Error=( Error1+ Error2)/2
Average Error Convergence =
20.4279
```

A.4. Analysis-2.1.1.4 Mcr and E-1.1.4 Calculations

```
>> E=210000; G=80769; % Elastic/Shear M. [N/mm^2]
>> b=220;tf=14; hw=420;tw=10; h=434;L=4000; % Geometric Dimensions [mm]
>> J=(1/3)*[2*b*tf^3+h*tw^3]; % Torsional Constant [mm^4]
>> Cw=(tf*b^3*h^2)/24; % Warping Constant [mm^6]
>> Ix=2*tf*(b^3/12); % Moment of Inertia [mm^4]
>> Mcr Theoretical=(pi/L)*sqrt(E*Ix*G*J+Cw*Ix*[(pi*E)/L] ^2)
Mcr Theoretical =
7.9372e+008
>>
>> Mcr ANSYS= 0.66353E+09; % ANSYS-Critical Moment [N.mm]
```

```
>>
>> Error1=[abs(Mcr ANSYS-Mcr Theoretical)/Mcr ANSYS]*100
Error1=
19.6202
>>
>> Error2=[abs(Mcr Theoretical-Mcr ANSYS)/Mcr Theoretical]*100
Error2=
16.4021
>>
>> Average Error=( Error1+ Error2)/2
Average Error Convergence =
18.0111
```

A.5. Analysis-2.1.2.1 Mcr and E-1.2.1 Calculations

```
>> E=210000; G=80769; % Elastic/Shear M. [N/mm^2]
>> b=200;tf=12; hw=400;tw=8; h=412;L=6000; % Geometric Dimensions [mm]
>> J=(1/3)*[2*b*tf^3+h*tw^3]; % Torsional Constant [mm^4]
>> Cw=(tf*b^3*h^2)/24; % Warping Constant [mm^6]
>> Ix=2*tf*(b^3/12); % Moment of Inertia [mm^4]
>> Mcr Theoretical=(pi/L)*sqrt(E*Ix*G*J+Cw*Ix*[(pi*E)/L] ^2)
Mcr Theoretical =
2.4162e+008
>>
>> Mcr ANSYS= 0.26325E+09; % ANSYS-Critical Moment [N.mm]
>>
>> Error1=[abs(Mcr ANSYS-Mcr Theoretical)/Mcr ANSYS]*100
Error1=
8.2149
>>
>> Error2=[abs(Mcr Theoretical-Mcr ANSYS)/Mcr Theoretical]*100
```

```
Error2=
8.9501
>>
>> Average Error Convergence=( Error1+ Error2)/2
Average Error Convergence =
8.5825
```

A.6. Analysis-2.1.2.2 Mcr and E-1.2.2 Calculations

```
>> E=210000; G=80769; % Elastic/Shear M. [N/mm^2]
>> b=200;tf=12; hw=420;tw=10; h=432;L=6000; % Geometric Dimensions [mm]
>> J=(1/3)*[2*b*tf^3+h*tw^3]; % Torsional Constant [mm^4]
>> Cw=(tf*b^3*h^2)/24; % Warping Constant [mm^6]
>> Ix=2*tf*(b^3/12); % Moment of Inertia [mm^4]
>> Mcr Theoretical=(pi/L)*sqrt(E*Ix*G*J+Cw*Ix*[(pi*E)/L] ^2)
Mcr Theoretical =
2.5970e+008
>>
>> Mcr ANSYS= 0.26479E+09; % ANSYS-Critical Moment [N.mm]
>>
>> Error1=[abs(Mcr ANSYS-Mcr Theoretical)/Mcr ANSYS]*100
Error1=
1.9213
>>
>> Error2=[abs(Mcr Theoretical-Mcr ANSYS)/Mcr Theoretical]*100
Error2 =
1.9589
>>
>> Average Error=( Error1+ Error2)/2
Average Error Convergence =
1.9401
```

A.7. Analysis-2.1.2.3 Mcr and E-1.2.3 Calculations

```
>> E=210000; G=80769; % Elastic/Shear M. [N/mm^2]
>> b=220;tf=14; hw=400;tw=8; h=414;L=6000; % Geometric Dimensions [mm]
>> J=(1/3)*[2*b*tf^3+h*tw^3]; % Torsional Constant [mm^4]
>> Cw=(tf*b^3*h^2)/24; % Warping Constant [mm^6]
>> Ix=2*tf*(b^3/12); % Moment of Inertia [mm^4]
>> Mcr Theoretical=(pi/L)*sqrt(E*Ix*G*J+Cw*Ix*[(pi*E)/L] ^2)
Mcr Theoretical =
3.7727e+008
>>
>> Mcr ANSYS= 0.41000E+09; % ANSYS-Critical Moment [N.mm]
>>
>> Error1=[abs(Mcr ANSYS-Mcr Theoretical)/Mcr ANSYS]*100
Error1=
7.9831
>>
>> Error2=[abs(Mcr Theoretical-Mcr ANSYS)/Mcr Theoretical]*100
Error2 =
8.6756
>>
>> Average Error=( Error1+ Error2)/2
Average Error Convergence =
8.3293
```

A.8. Analysis-2.1.2.4 Mcr and E-1.2.4 Calculations

```
>> E=210000; G=80769; % Elastic/Shear M. [N/mm^2]
>> b=220;tf=14; hw=420;tw=10; h=434;L=6000; % Geometric Dimensions [mm]
```

```
>> J=(1/3)*[2*b*tf^3+h*tw^3]; % Torsional Constant [mm^4]
>> Cw=(tf*b^3*h^2)/24; % Warping Constant [mm^6]
>> Ix=2*tf*(b^3/12); % Moment of Inertia [mm^4]
>> Mcr Theoretical=(pi/L)*sqrt(E*Ix*G*J+Cw*Ix*[(pi*E)/L] ^2)
Mcr Theoretical =
3.9945e+008
>>
>> Mcr ANSYS= 0.44262E+09; % ANSYS-Critical Moment [N.mm]
>>
>> Error1=[abs(Mcr ANSYS-Mcr Theoretical)/Mcr ANSYS]*100
Error1=
9.7539
>>
>> Error2=[abs(Mcr Theoretical-Mcr ANSYS)/Mcr Theoretical]*100
Error2 =
10.8081
>>
>> Average Error=( Error1+ Error2)/2
Average Error Convergence =
10.2810
```

A.9. Analysis-2.1.3.1 M_{cr} and E-1.3.1 Calculations

```
>> E=210000; G=80769; % Elastic/Shear M. [N/mm^2]
>> b=200;tf=12; hw=400;tw=8; h=412;L=8000; % Geometric Dimensions [mm]
>> J=(1/3)*[2*b*tf^3+h*tw^3]; % Torsional Constant [mm^4]
>> Cw=(tf*b^3*h^2)/24; % Warping Constant [mm^6]
>> Ix=2*tf*(b^3/12); % Moment of Inertia [mm^4]
>> Mcr Theoretical=(pi/L)*sqrt(E*Ix*G*J+Cw*Ix*[(pi*E)/L] ^2)
Mcr Theoretical =
1.5485e+008
```

```
>>
>> Mcr ANSYS= 0.19747E+09; % ANSYS-Critical Moment [N.mm]
>>
>> Error1=[abs(Mcr ANSYS-Mcr Theoretical)/Mcr ANSYS]*100
Error1=
21.5830
>>
>> Error2=[abs(Mcr Theoretical-Mcr ANSYS)/Mcr Theoretical]*100
Error2 =
27.5234
>>
>> Average Error=( Error1+ Error2)/2
Average Error Convergence =
24.5532
```

A.10. Analysis-2.1.3.2 Mcr and E-1.3.2 Calculations

```
>> E=210000; G=80769; % Elastic/Shear M. [N/mm^2]
>> b=200;tf=12; hw=420;tw=10; h=432;L=8000; % Geometric Dimensions [mm]
>> J=(1/3)*[2*b*tf^34+h*tw^3]; % Torsional Constant [mm^4]
>> Cw=(tf*b^34*h^2)/24; % Warping Constant [mm^6]
>> Ix=2*tf*(b^3/12); % Moment of Inertia [mm^4]
>> Mcr Theoretical=(pi/L)*sqrt(E*Ix*G*J+Cw*Ix*[(pi*E)/L] ^2)
Mcr Theoretical =
1.6791e+008
>>
>> Mcr ANSYS= 0.22120E+09; % ANSYS-Critical Moment [N.mm]
>>
>> Error1=[abs(Mcr ANSYS-Mcr Theoretical)/Mcr ANSYS]*100
Error1=
24.0892
```

```
>>
>> Error2=[abs(Mcr Theoretical-Mcr ANSYS)/Mcr Theoretical]*100
Error2 =
31.7336
>>
>> Average Error=( Error1+ Error2)/2
Average Error Convergence =
27.9114
```

A.11. Analysis-2.1.3.3 M_{cr} and E-1.3.3 Calculations

```
>> E=210000; G=80769; % Elastic/Shear M. [N/mm^2]
>> b=220;tf=14; hw=400;tw=8; h=414;L=8000; % Geometric Dimensions [mm]
>> J=(1/3)*[2*b*tf^3+h*tw^3]; % Torsional Constant [mm^4]
>> Cw=(tf*b^3*h^2)/24; % Warping Constant [mm^6]
>> Ix=2*tf*(b^3/12); % Moment of Inertia [mm^4]
>> Mcr Theoretical=(pi/L)*sqrt(E*Ix*G*J+Cw*Ix*[(pi*E)/L] ^2)
Mcr Theoretical =
2.4184e+008
>>
>> Mcr ANSYS= 0.30757E+09; % ANSYS-Critical Moment [N.mm]
>>
>> Error1=[abs(Mcr ANSYS-Mcr Theoretical)/Mcr ANSYS]*100
Error1=
21.3710
>>
>> Error2=[abs(Mcr Theoretical-Mcr ANSYS)/Mcr Theoretical]*100
Error2 =
27.1795
>>
>> Average Error=( Error1+ Error2)/2
```

```
Average Error Convergence =
24.2752
```

A.12. Analysis-2.1.3.4 M_{cr} and E-1.3.4 Calculations

```
>> E=210000; G=80769; % Elastic/Shear M. [N/mm^2]
>> b=220;tf=14; hw=420;tw=10; h=434;L=8000; % Geometric Dimensions [mm]
>> J=(1/3)*[2*b*tf^3+h*tw^3]; % Torsional Constant [mm^4]
>> Cw=(tf*b^3*h^2)/24; % Warping Constant [mm^6]
>> Ix=2*tf*(b^3/12); % Moment of Inertia [mm^4]
>> Mcr Theoretical=(pi/L)*sqrt(E*Ix*G*J+Cw*Ix*[(pi*E)/L] ^2)
Mcr Theoretical =
2.5698e+008
>>
>> Mcr ANSYS= 0.33203E+09; % ANSYS-Critical Moment [N.mm]
>>
>> Error1=[abs(Mcr ANSYS-Mcr Theoretical)/Mcr ANSYS]*100
Error1=
22.6021
>>
>> Error2=[abs(Mcr Theoretical-Mcr ANSYS)/Mcr Theoretical]*100
Error2 =
29.2024
>>
>> Average Error=( Error1+ Error2)/2
Average Error Convergence =
25.9023
```

A.13. Analysis-2.1.4.1 M_{cr} and E-1.4.1 Calculations

```
>> E=210000; G=80769; % Elastic/Shear M. [N/mm^2]
>> b=200;tf=12; hw=400;tw=8; h=412;L=10000; % Geometric Dimensions [mm]
>> J=(1/3)*[2*b*tf^3+h*tw^3]; % Torsional Constant [mm^4]
>> Cw=(tf*b^3*h^2)/24; % Warping Constant [mm^6]
>> Ix=2*tf*(b^3/12); % Moment of Inertia [mm^4]
>> Mcr Theoretical=(pi/L)*sqrt(E*Ix*G*J+Cw*Ix*[(pi*E)/L] ^2)
Mcr Theoretical =
1.1279e+008
>>
>> Mcr ANSYS= 0.15799E+09; % ANSYS-Critical Moment [N.mm]
>>
>> Error1=[abs(Mcr ANSYS-Mcr Theoretical)/Mcr ANSYS]*100
Error1=
28.6104
>>
>> Error2=[abs(Mcr Theoretical-Mcr ANSYS)/Mcr Theoretical]*100
Error2 =
40.0765
>>
>> Average Error=( Error1+ Error2)/2
Average Error Convergence =
34.3434
```

A.14. Analysis-2.1.4.2 M_{cr} and E-1.4.2 Calculations

```
>> E=210000; G=80769; % Elastic/Shear M. [N/mm^2]
>> b=200;tf=12; hw=420;tw=10; h=432;L=10000; % Geometric Dimensions [mm]
>> J=(1/3)*[2*b*tf^3+h*tw^3]; % Torsional Constant [mm^4]
>> Cw=(tf*b^3*h^2)/24; % Warping Constant [mm^6]
```

```
>> Ix=2*tf*(b^3/12); % Moment of Inertia [mm^4]
>> Mcr Theoretical=(pi/L)*sqrt(E*Ix*G*J+Cw*Ix*[(pi*E)/L] ^2)
Mcr Theoretical =
1.2312e+008
>>
>> Mcr ANSYS= 0.17697E+09; % ANSYS-Critical Moment [N.mm]
>>
>> Error1=[abs(Mcr ANSYS-Mcr Theoretical)/Mcr ANSYS]*100
Error1=
30.4280
>>
>> Error2=[abs(Mcr Theoretical-Mcr ANSYS)/Mcr Theoretical]*100
Error2 =
43.7360
>>
>> Average Error=( Error1+ Error2)/2
Average Error Convergence =
37.0820
```

A.15. Analysis-2.1.4.3 M_{cr} and E-1.4.3 Calculations

```
>> E=210000; G=80769; % Elastic/Shear M. [N/mm^2]
>> b=220;tf=14; hw=400;tw=8; h=414;L=10000; % Geometric Dimensions [mm]
>> J=(1/3)*[2*b*tf^3+h*tw^3]; % Torsional Constant [mm^4]
>> Cw=(tf*b^3*h^2)/24; % Warping Constant [mm^6]
>> Ix=2*tf*(b^3/12); % Moment of Inertia [mm^4]
>> Mcr Theoretical=(pi/L)*sqrt(E*Ix*G*J+Cw*Ix*[(pi*E)/L] ^2)
Mcr Theoretical =
1.7618e+008
>>
>> Mcr ANSYS= 0.24608E+09; % ANSYS-Critical Moment [N.mm]
```

```
>>
>> Error1=[abs(Mcr ANSYS-Mcr Theoretical)/Mcr ANSYS]*100
Error1=
28.4049
>>
>> Error2=[abs(Mcr Theoretical-Mcr ANSYS)/Mcr Theoretical]*100
Error2 =
39.6743
>>
>> Average Error=( Error1+ Error2)/2
Average Error Convergence =
34.0396
```

A.16. Analysis-2.1.4.4 M_{cr} and E-1.4.4 Calculations

```
>> E=210000; G=80769; % Elastic/Shear M. [N/mm^2]
>> b=220;tf=14; hw=420;tw=10; h=434;L=10000; % Geometric Dimensions [mm]
>> J=(1/3)*[2*b*tf^3+h*tw^3]; % Torsional Constant [mm^4]
>> Cw=(tf*b^3*h^2)/24; % Warping Constant [mm^6]
>> Ix=2*tf*(b^3/12); % Moment of Inertia [mm^4]
>> Mcr Theoretical=(pi/L)*sqrt(E*Ix*G*J+Cw*Ix*[(pi*E)/L] ^2)
Mcr Theoretical =
1.8773e+008
>>
>> Mcr ANSYS= 0.26565E+09; % ANSYS-Critical Moment [N.mm]
>>
>> Error1=[abs(Mcr ANSYS-Mcr Theoretical)/Mcr ANSYS]*100
Error1=
29.3319
>>
>> Error2=[abs(Mcr Theoretical-Mcr ANSYS)/Mcr Theoretical]*100
```

```
Error2 =
41.5067
>>
>> Average Error=( Error1+ Error2)/2
Average Error Convergence =
35.4193
```

A.17. Analysis-2.2.1.1 P_{cr} and E-2.1.1 Calculations

```
>> E=210000; G=80769; % Elastic/Shear M. [N/mm^2]
>> b=200;tf=12; hw=400;tw=8; h=412;L=4000; % Geometric Dimensions [mm]
>> J=(1/3)*[2*b*tf^3+h*tw^3]; % Torsional Constant [mm^4]
>> Cw=(tf*b^3*h^2)/24; % Warping Constant [mm^6]
>> Ix=2*tf*(b^3/12); % Moment of Inertia [mm^4]
>> Pcr Theoretical=(4.013/L^2)*sqrt(G*J*E*Ix)
Pcr Theoretical =
7.1650e+004
>>
>> Pcr ANSYS= 71124; % ANSYS-Critical Force [N]
>>
>> Error1=[abs(Pcr ANSYS-Pcr Theoretical)/Pcr ANSYS]*100
Error1=
0.7401
>>
>> Error2=[abs(Pcr Theoretical-Pcr ANSYS)/Pcr Theoretical]*100
Error2 =
0.7346
>>
>> Average Error=( Error1+ Error2)/2
Average Error Convergence =
0.7374
```

A.18. Analysis-2.2.1.2 P_{cr} and E-2.1.2 Calculations

```
>> E=210000; G=80769; % Elastic/Shear M. [N/mm^2]
>> b=200;tf=12; hw=420;tw=10; h=432;L=4000; % Geometric Dimensions [mm]
>> J=(1/3)*[2*b*tf^3+h*tw^3]; % Torsional Constant [mm^4]
>> Cw=(tf*b^3*h^2)/24; % Warping Constant [mm^6]
>> Ix=2*tf*(b^3/12); % Moment of Inertia [mm^4]
>> Pcr Theoretical=(4.013/L^2)*sqrt(G*J*E*Ix)
Pcr Theoretical =
7.9948e+004
>>
>> Pcr ANSYS= 79670; % ANSYS-Critical Force [N]
>>
>> Error1=[abs(Pcr ANSYS-Pcr Theoretical)/Pcr ANSYS]*100
Error1=
0.3493
>>
>> Error2=[abs(Pcr Theoretical-Pcr ANSYS)/Pcr Theoretical]*100
Error2 =
0.3481
>>
>> Average Error=( Error1+ Error2)/2
Average Error Convergence =
0.3487
```

A.19. Analysis-2.2.1.3 P_{cr} and E-2.1.3 Calculations

```
>> E=210000; G=80769; % Elastic/Shear M. [N/mm^2]
>> b=220;tf=14; hw=400;tw=8; h=414;L=4000; % Geometric Dimensions [mm]
```

```
>> J=(1/3)*[2*b*tf^3+h*tw^3]; % Torsional Constant [mm^4]
>> Cw=(tf*b^3*h^2)/24; % Warping Constant [mm^6]
>> Ix=2*tf*(b^3/12); % Moment of Inertia [mm^4]
>> Pcr Theoretical=(4.013/L^2)*sqrt(G*J*E*Ix)
Pcr Theoretical =
11.199e+004
>>
>> Pcr ANSYS= 110740; % ANSYS-Critical Force [N]
>>
>> Error1=[abs(Pcr ANSYS-Pcr Theoretical)/Pcr ANSYS]*100
Error1=
1.1300
>>
>> Error2=[abs(Pcr Theoretical-Pcr ANSYS)/Pcr Theoretical]*100
Error2 =
1.1173
>>
>> Average Error=( Error1+ Error2)/2
Average Error Convergence =
1.1236
```

A.20. Analysis-2.2.1.4 P_{cr} and E-2.1.4 Calculations

```
>> E=210000; G=80769; % Elastic/Shear M. [N/mm^2]
>> b=220;tf=14; hw=420;tw=10; h=434;L=4000; % Geometric Dimensions [mm]
>> J=(1/3)*[2*b*tf^3+h*tw^3]; % Torsional Constant [mm^4]
>> Cw=(tf*b^3*h^2)/24; % Warping Constant [mm^6]
>> Ix=2*tf*(b^3/12); % Moment of Inertia [mm^4]
>> Pcr Theoretical=(4.013/L^2)*sqrt(G*J*E*Ix)
Pcr Theoretical =
12.043e+004
```

```
>>
>> Pcr ANSYS= 118800; % ANSYS-Critical Force [N]
>>
>> Error1=[abs(Pcr ANSYS-Pcr Theoretical)/Pcr ANSYS]*100
Error1=
1.3744
>>
>> Error2=[abs(Pcr Theoretical-Pcr ANSYS)/Pcr Theoretical]*100
Error2 =
1.3558
>>
>> Average Error=( Error1+ Error2)/2
Average Error Convergence =
1.3651
```

A.21. Analysis-2.2.2.1 P_{cr} and E-2.2.1 Calculations

```
>> E=210000; G=80769; % Elastic/Shear M. [N/mm^2]
>> b=220;tf=12; hw=400;tw=8; h=412;L=6000; % Geometric Dimensions [mm]
>> J=(1/3)*[2*b*tf^3+h*tw^3]; % Torsional Constant [mm^4]
>> Cw=(tf*b^3*h^2)/24; % Warping Constant [mm^6]
>> Ix=2*tf*(b^3/12); % Moment of Inertia [mm^4]
>> Pcr Theoretical=(4.013/L^2)*sqrt(G*J*E*Ix)
Pcr Theoretical =
3.1845e+004
>>
>> Pcr ANSYS= 31642; % ANSYS-Critical Force [N]
>>
>> Error1=[abs(Pcr ANSYS-Pcr Theoretical)/Pcr ANSYS]*100
Error1=
0.6403
```

```
>>
>> Error2=[abs(Pcr Theoretical-Pcr ANSYS)/Pcr Theoretical]*100
Error2 =
0.6363
>>
>> Average Error=( Error1+ Error2)/2
Average Error Convergence =
0.6383
```

A.22. Analysis-2.2.2.2 P_{cr} and E-2.2.2 Calculations

```
>> E=210000; G=80769; % Elastic/Shear M. [N/mm^2]
>> b=200;tf=12; hw=420;tw=10; h=432;L=6000; % Geometric Dimensions [mm]
>> J=(1/3)*[2*b*tf^3+h*tw^3]; % Torsional Constant [mm^4]
>> Cw=(tf*b^3*h^2)/24; % Warping Constant [mm^6]
>> Ix=2*tf*(b^3/12); % Moment of Inertia [mm^4]
>> Pcr Theoretical=(4.013/L^2)*sqrt(G*J*E*Ix)
Pcr Theoretical =
3.5533e+004
>>
>> Pcr ANSYS= 35444; % ANSYS-Critical Force [N]
>>
>> Error1=[abs(Pcr ANSYS-Pcr Theoretical)/Pcr ANSYS]*100
Error1=
0.2499
>>
>> Error2=[abs(Pcr Theoretical-Pcr ANSYS)/Pcr Theoretical]*100
Error2 =
0.2493
>>
>> Average Error=( Error1+ Error2)/2
```

```
Average Error Convergence =
0.2496
```

A.23. Analysis-2.2.2.3 P_{cr} and E-2.2.3 Calculations

```
>> E=210000; G=80769; % Elastic/Shear M. [N/mm^2]
>> b=220;tf=14; hw=400;tw=8; h=414;L=6000; % Geometric Dimensions [mm]
>> J=(1/3)*[2*b*tf^3+h*tw^3]; % Torsional Constant [mm^4]
>> Cw=(tf*b^3*h^2)/24; % Warping Constant [mm^6]
>> Ix=2*tf*(b^3/12); % Moment of Inertia [mm^4]
>> Pcr Theoretical=(4.013/L^2)*sqrt(G*J*E*Ix)
Pcr Theoretical =
4.9774e+004
>>
>> Pcr ANSYS= 49276; % ANSYS-Critical Force [N]
>>
>> Error1=[abs(Pcr ANSYS-Pcr Theoretical)/Pcr ANSYS]*100
Error1=
1.0105
>>
>> Error2=[abs(Pcr Theoretical-Pcr ANSYS)/Pcr Theoretical]*100
Error2 =
1.0004
>>
>> Average Error=( Error1+ Error2)/2
Average Error Convergence =
1.0054
```

A.24. Analysis-2.2.2.4 P_{cr} and E-2.2.4 Calculations

```
>> E=210000; G=80769; % Elastic/Shear M. [N/mm^2]
>> b=220;tf=14; hw=420;tw=10; h=434;L=6000; % Geometric Dimensions [mm]
>> J=(1/3)*[2*b*tf^3+h*tw^3]; % Torsional Constant [mm^4]
>> Cw=(tf*b^3*h^2)/24; % Warping Constant [mm^6] >> Ix=2*tf*(b^3/12); % Moment
of Inertia [mm^4]
>> Pcr Theoretical=(4.013/L^2)*sqrt(G*J*E*Ix)
Pcr Theoretical =
5.3526e+004
>>
>> Pcr ANSYS= 53130; % ANSYS-Critical Force [N]
>>
>> Error1=[abs(Pcr ANSYS-Pcr Theoretical)/Pcr ANSYS]*100
Error1=
0.7448
>>
>> Error2=[abs(Pcr Theoretical-Pcr ANSYS)/Pcr Theoretical]*100
Error2 =
0.7393
>>
>> Average Error=( Error1+ Error2)/2
Average Error Convergence =
0.7420
```

A.25. Analysis-2.2.3.1 Pcr and E-2.3.1 Calculations

```
>> E=210000; G=80769; % Elastic/Shear M. [N/mm^2]
>> b=200;tf=12; hw=400;tw=8; h=412;L=8000; % Geometric Dimensions [mm]
>> J=(1/3)*[2*b*tf^3+h*tw^3]; % Torsional Constant [mm^4]
>> Cw=(tf*b^3*h^2)/24; % Warping Constant [mm^6]
```

```
>> Ix=2*tf*(b^3/12); % Moment of Inertia [mm^4]
>> Pcr Theoretical=(4.013/L^2)*sqrt(G*J*E*Ix)
Pcr Theoretical =
1.7913e+004
>>
>> Pcr ANSYS= 17805; % ANSYS-Critical Force [N]
>>
>> Error1=[abs(Pcr ANSYS-Pcr Theoretical)/Pcr ANSYS]*100
Error1=
0.6043
>>
>> Error2=[abs(Pcr Theoretical-Pcr ANSYS)/Pcr Theoretical]*100
Error2 =
0.6007
>>
>> Average Error=( Error1+ Error2)/2
Average Error Convergence =
0.6025
```

A.26. Analysis-2.2.3.2 Pcr and E-2.3.2 Calculations

```
>> E=210000; G=80769; % Elastic/Shear M. [N/mm^2]
>> b=200;tf=12; hw=420;tw=10; h=432;L=8000; % Geometric Dimensions [mm]
>> J=(1/3)*[2*b*tf^3+h*tw^3]; % Torsional Constant [mm^4]
>> Cw=(tf*b^3*h^2)/24; % Warping Constant [mm^6]
>> Ix=2*tf*(b^3/12); % Moment of Inertia [mm^4]
>> Pcr Theoretical=(4.013/L^2)*sqrt(G*J*E*Ix)
Pcr Theoretical =
1.9987e+004
>>
>> Pcr ANSYS= 19944; % ANSYS-Critical Force [N]
```

```
>>
>> Error1=[abs(Pcr ANSYS-Pcr Theoretical)/Pcr ANSYS]*100
Error1=
0.2159
>>
>> Error2=[abs(Pcr Theoretical-Pcr ANSYS)/Pcr Theoretical]*100
Error2 =
0.2155
>>
>> Average Error=( Error1+ Error2)/2
Average Error Convergence =
0.2157
```

A.27. Analysis-2.2.3.3 P_{cr} and E-2.3.3 Calculations

```
>> E=210000; G=80769; % Elastic/Shear M. [N/mm^2]
>> b=220;tf=14; hw=400;tw=8; h=414;L=8000; % Geometric Dimensions [mm]
>> J=(1/3)*[2*b*tf^3+h*tw^3]; % Torsional Constant [mm^4]
>> Cw=(tf*b^3*h^2)/24; % Warping Constant [mm^6]
>> Ix=2*tf*(b^3/12); % Moment of Inertia [mm^4]
>> Pcr Theoretical=(4.013/L^2)*sqrt(G*J*E*Ix)
Pcr Theoretical =
2.7998e+004
>>
>> Pcr ANSYS= 27730; % ANSYS-Critical Force [N]
>>
>> Error1=[abs(Pcr ANSYS-Pcr Theoretical)/Pcr ANSYS]*100
Error1=
0.9658
>>
>> Error2=[abs(Pcr Theoretical-Pcr ANSYS)/Pcr Theoretical]*100
```

```
Error2 =
0.9566
>>
>> Average Error=( Error1+ Error2)/2
Average Error Convergence =
0.9612
```

A.28. Analysis-2.2.3.4 Pcr and E-2.3.4 Calculations

```
>> E=210000; G=80769; % Elastic/Shear M. [N/mm^2]
>> b=220;tf=14; hw=420;tw=10; h=434;L=8000; % Geometric Dimensions [mm]
>> J=(1/3)*[2*b*tf^3+h*tw^3]; % Torsional Constant [mm^4]
>> Cw=(tf*b^3*h^2)/24; % Warping Constant [mm^6]
>> Ix=2*tf*(b^3/12); % Moment of Inertia [mm^4]
>> Pcr Theoretical=(4.013/L^2)*sqrt(G*J*E*Ix)
Pcr Theoretical =
3.0108e+004
>>
>> Pcr ANSYS= 29934; % ANSYS-Critical Force [N]
>>
>> Error1=[abs(Pcr ANSYS-Pcr Theoretical)/Pcr ANSYS]*100
Error1=
0.5820
>>
>> Error2=[abs(Pcr Theoretical-Pcr ANSYS)/Pcr Theoretical]*100
Error2 =
0.5786
>>
>> Average Error=( Error1+ Error2)/2
Average Error Convergence =
0.5803
```

A.29. Analysis-2.2.4.1 Pcr and E-2.4.1 Calculations

```
>> E=210000; G=80769; % Elastic/Shear M. [N/mm^2] >> b=200;tf=12; hw=400;tw=
h=412;L=10000; % Geometric Dimensions [mm]
>> J=(1/3)*[2*b*tf^3+h*tw^3]; % Torsional Constant [mm^4]
>> Cw=(tf*b^3*h^2)/24; % Warping Constant [mm^6]
>> Ix=2*tf*(b^3/12); % Moment of Inertia [mm^4]
>> Pcr Theoretical=(4.013/L^2)*sqrt(G*J*E*Ix)
Pcr Theoretical =
1.1464e+004
>>
>> Pcr ANSYS= 11396; % ANSYS-Critical Force [N]
>>
>> Error1=[abs(Pcr ANSYS-Pcr Theoretical)/Pcr ANSYS]*100
Error1=
0.5972
>>
>> Error2=[abs(Pcr Theoretical-Pcr ANSYS)/Pcr Theoretical]*100
Error2 =
0.5937
>>
>> Average Error=( Error1+ Error2)/2
Average Error Convergence =
0.5955
```

A.30. Analysis-2.2.4.2 Pcr and E-2.4.2 Calculations

```
>> E=210000; G=80769; % Elastic/Shear M. [N/mm^2]
>> b=200;tf=12; hw=420;tw=10; h=432;L=10000; % Geometric Dimensions [mm]
```

```
>> J=(1/3)*[2*b*tf^3+h*tw^3]; % Torsional Constant [mm^4]
>> Cw=(tf*b^3*h^2)/24; % Warping Constant [mm^6]
>> Ix=2*tf*(b^3/12); % Moment of Inertia [mm^4]
>> Pcr Theoretical=(4.013/L^2)*sqrt(G*J*E*Ix)
Pcr Theoretical =
1.2792e+004
>>
>> Pcr ANSYS= 12777; % ANSYS-Critical Force [N]
>>
>> Error1=[abs(Pcr ANSYS-Pcr Theoretical)/Pcr ANSYS]*100
Error1=
0.1152
>>
>> Error2=[abs(Pcr Theoretical-Pcr ANSYS)/Pcr Theoretical]*100
Error2 =
0.1151
>>
>> Average Error=( Error1+ Error2)/2
Average Error Convergence =
0.1152
```

A.31. Analysis-2.2.4.3 Pcr and E-2.4.3 Calculations

```
>> E=210000; G=80769; % Elastic/Shear M. [N/mm^2]
>> b=220;tf=14; hw=400;tw=8; h=414;L=10000; % Geometric Dimensions [mm]
>> J=(1/3)*[2*b*tf^3+h*tw^3]; % Torsional Constant [mm^4]
>> Cw=(tf*b^3*h^2)/24; % Warping Constant [mm^6]
>> Ix=2*tf*(b^3/12); % Moment of Inertia [mm^4]
>> Pcr Theoretical=(4.013/L^2)*sqrt(G*J*E*Ix)
Pcr Theoretical =
1.7919e+004
```

```
>>
>> Pcr ANSYS= 17751; % ANSYS-Critical Force [N]
>>
>> Error1=[abs(Pcr ANSYS-Pcr Theoretical)/Pcr ANSYS]*100
Error1=
0.9442
>>
>> Error2=[abs(Pcr Theoretical-Pcr ANSYS)/Pcr Theoretical]*100 Error2 =
0.9354
>>
>> Average Error=( Error1+ Error2)/2
Average Error Convergence =
0.9398
```

A.32. Analysis-2.2.4.4 Pcr and E-2.4.4 Calculations

```
>> E=210000; G=80769; % Elastic/Shear M. [N/mm^2]
>> b=220;tf=14; hw=420;tw=10; h=434;L=10000; % Geometric Dimensions [mm]
>> J=(1/3)*[2*b*tf^3+h*tw^3]; % Torsional Constant [mm^4]
>> Cw=(tf*b^3*h^2)/24; % Warping Constant [mm^6] >> Ix=2*tf*(b^3/12); % Moment
of Inertia [mm^4]
>> Pcr Theoretical=(4.013/L^2)*sqrt(G*J*E*Ix)
Pcr Theoretical =
1.9269e+004
>>
>> Pcr ANSYS= 19161; % ANSYS-Critical Force [N]
>>
>> Error1=[abs(Pcr ANSYS-Pcr Theoretical)/Pcr ANSYS]*100
Error1=
0.5650
>>
```

```
>> Error2=[abs(Pcr Theoretical-Pcr ANSYS)/Pcr Theoretical]*100
Error2 =
0.5618
>>
>> Average Error=( Error1+ Error2)/2
Average Error Convergence =
0.5634
```

APPENDIX B: ANSYS VON MISES STRESS SIMULATIONS

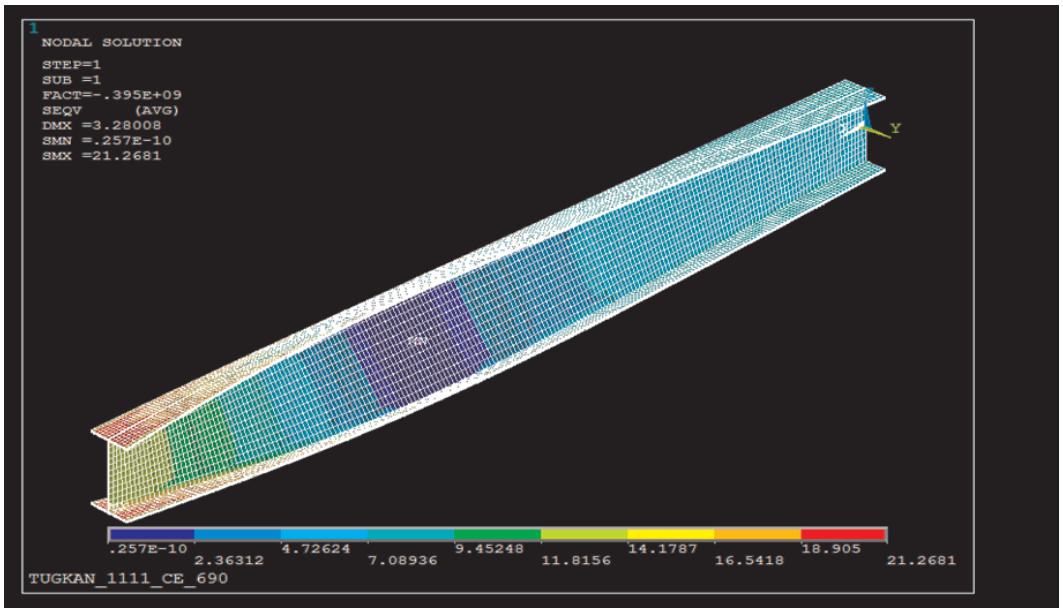

Figure B.1. ANSYS Von Mises Stress Simulation of Analysis-1111.

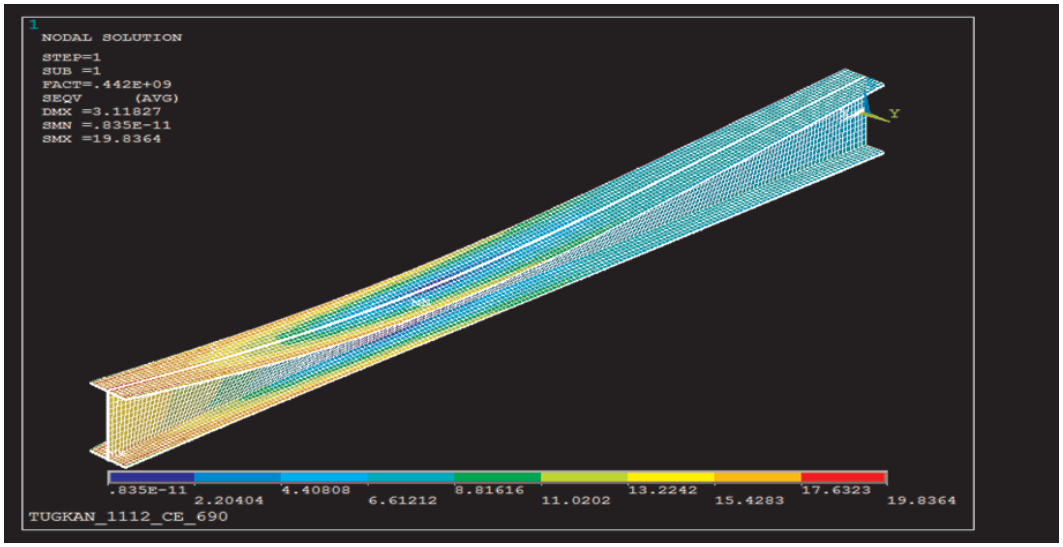

Figure B.2. ANSYS Von Mises Stress Simulation of Analysis-1112.

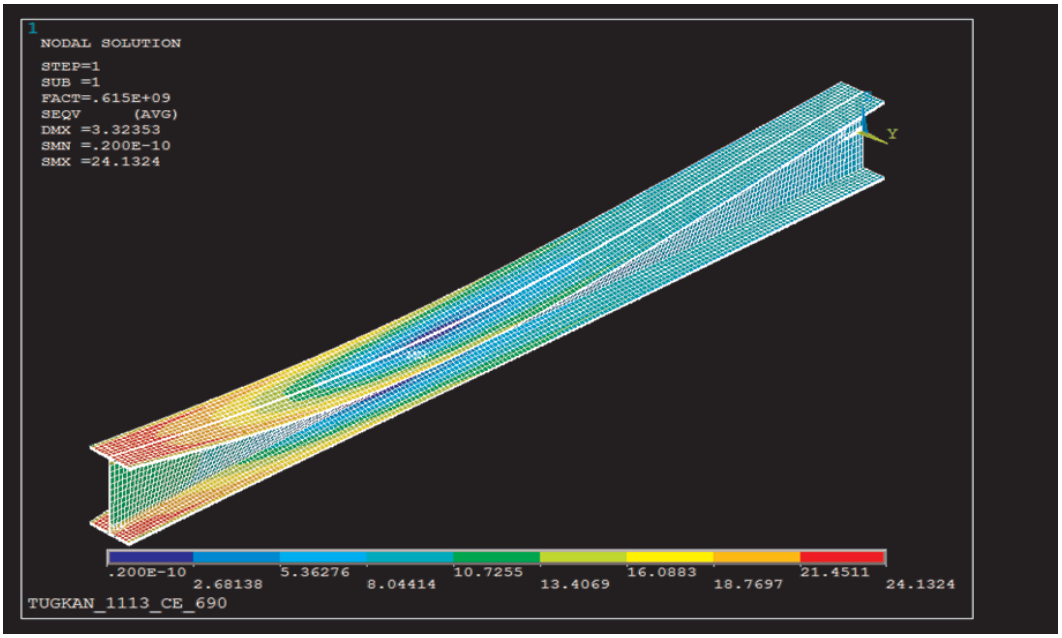

Figure B.3. ANSYS Von Mises Stress Simulation of Analysis-1113.

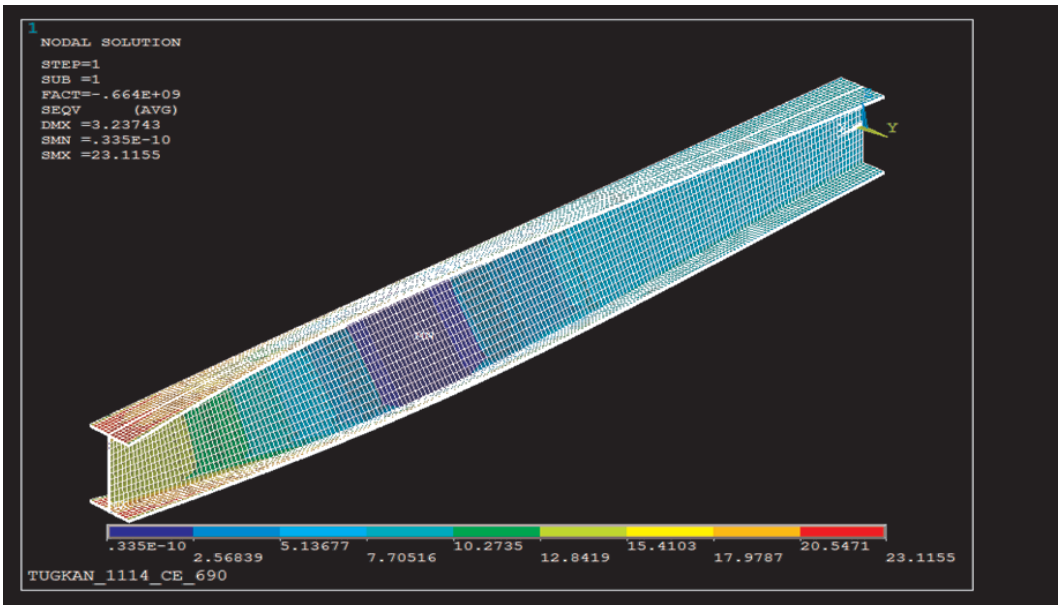

Figure B.4. ANSYS Von Mises Stress Simulation of Analysis-1114.

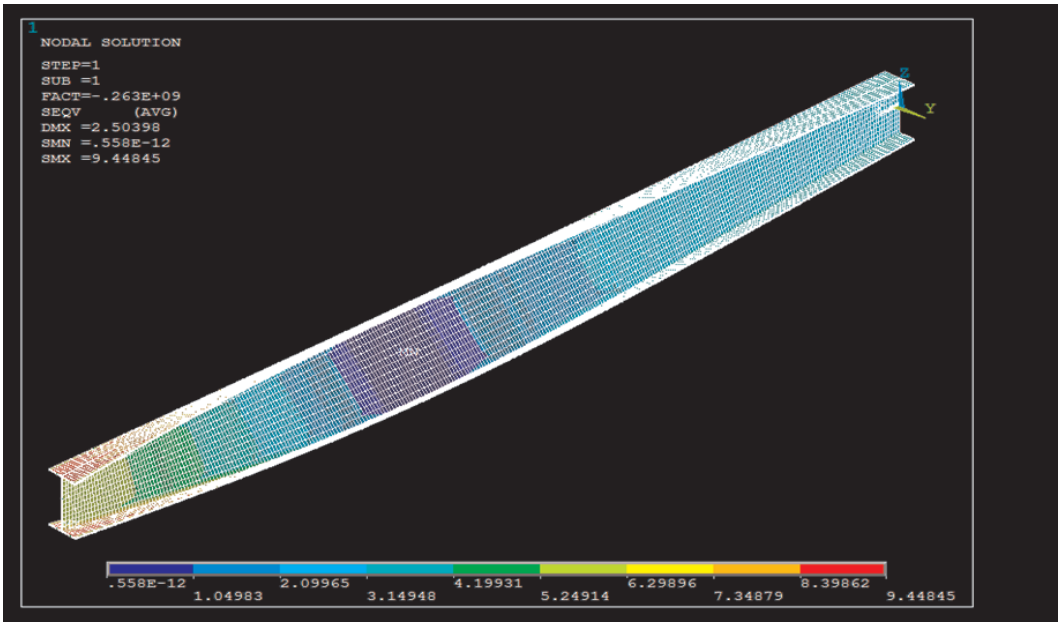

Figure B.5. ANSYS Von Mises Stress Simulation of Analysis-1121.

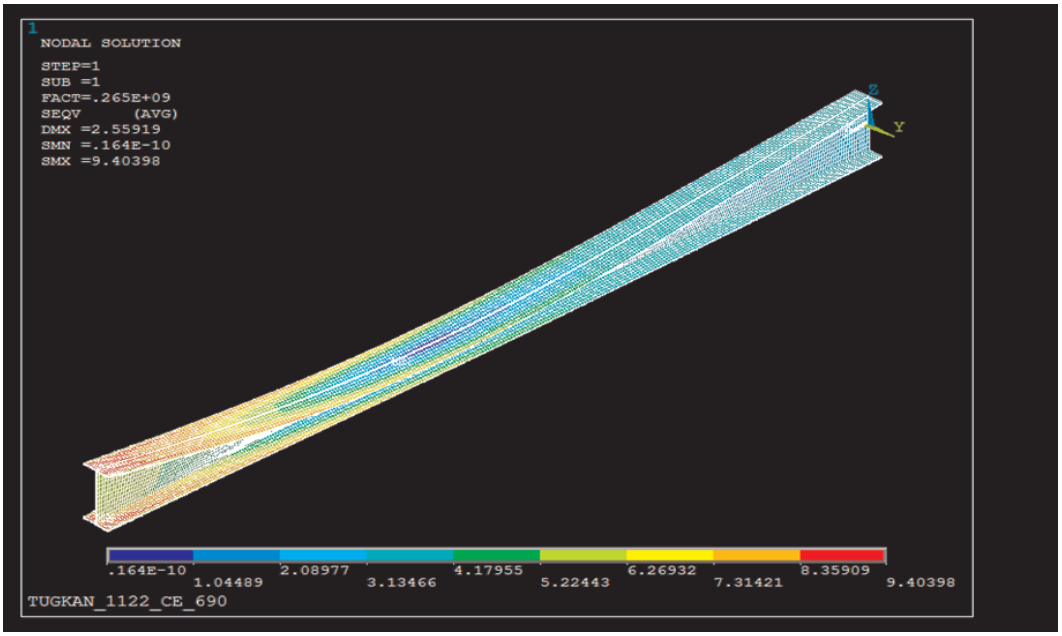

Figure B.6. ANSYS Von Mises Stress Simulation of Analysis-1122.

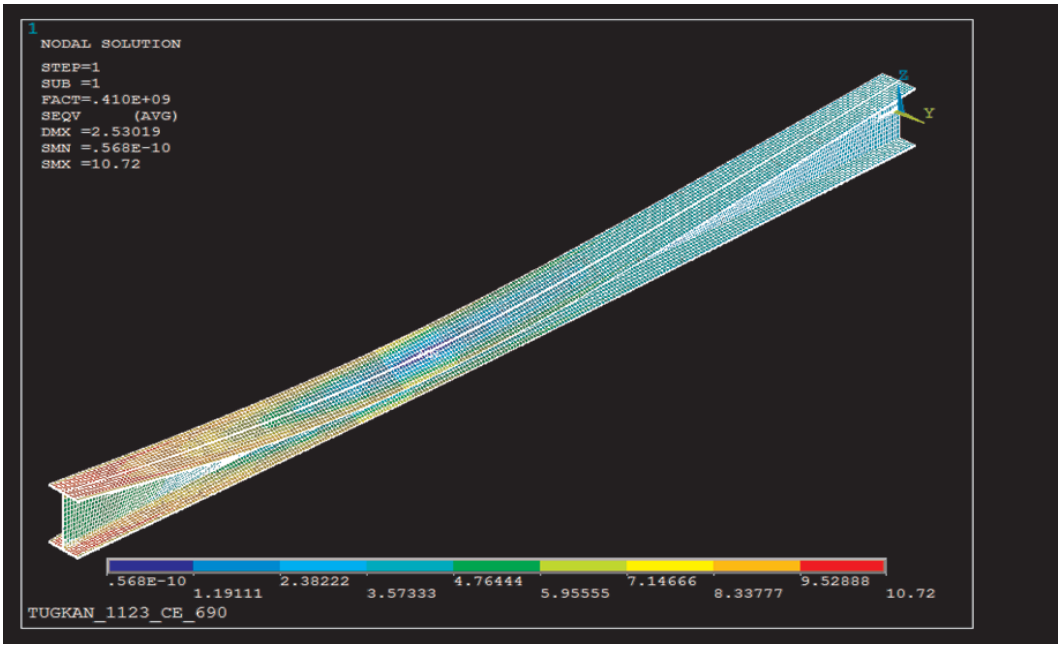

Figure B.7. ANSYS Von Mises Stress Simulation of Analysis-1123.

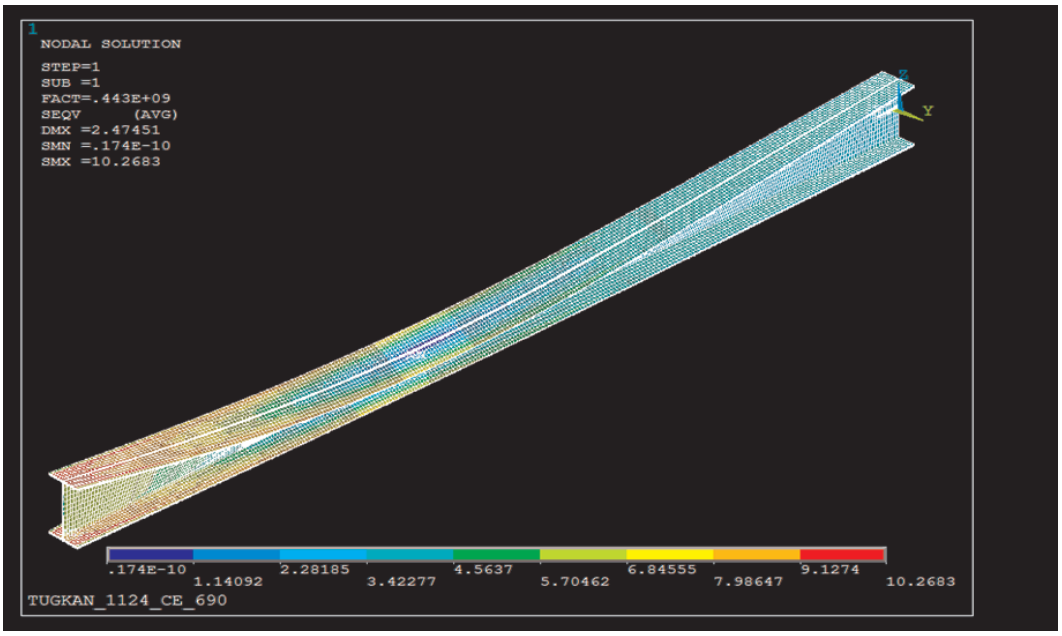

Figure B.8. ANSYS Von Mises Stress Simulation of Analysis-1124.

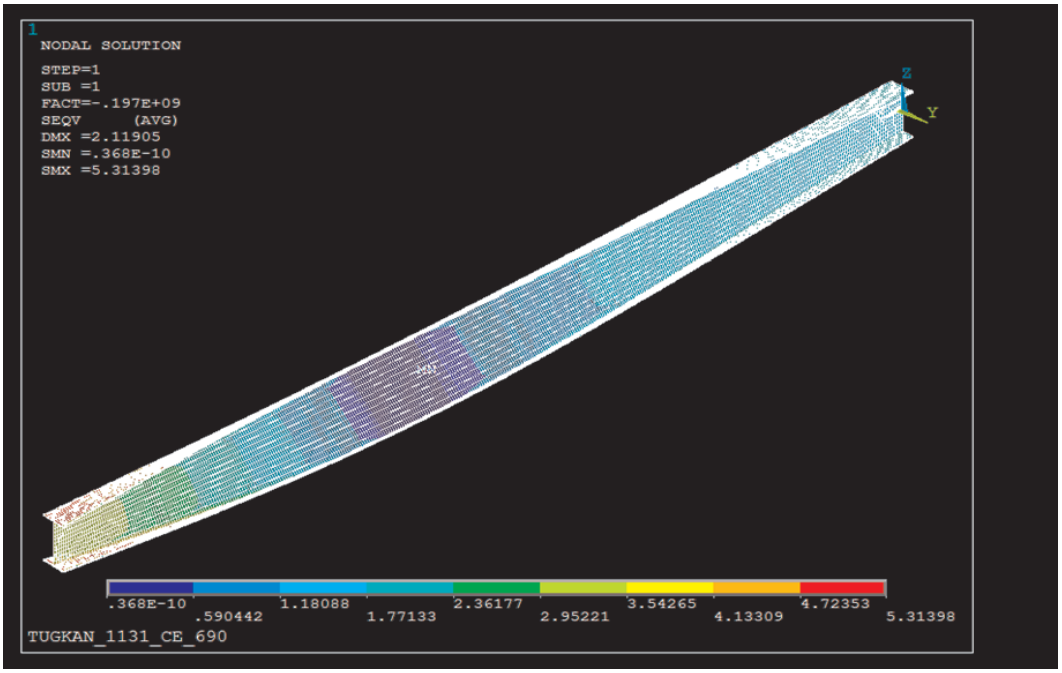

Figure B.9. ANSYS Von Mises Stress Simulation of Analysis-1131.

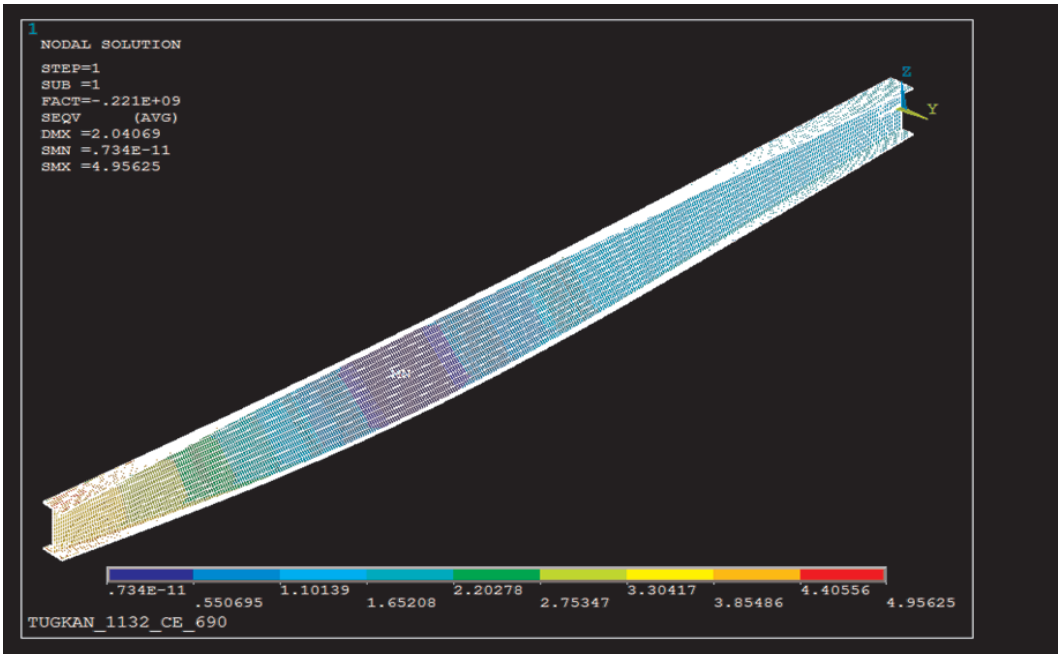

Figure B.10. ANSYS Von Mises Stress Simulation of Analysis-1132.

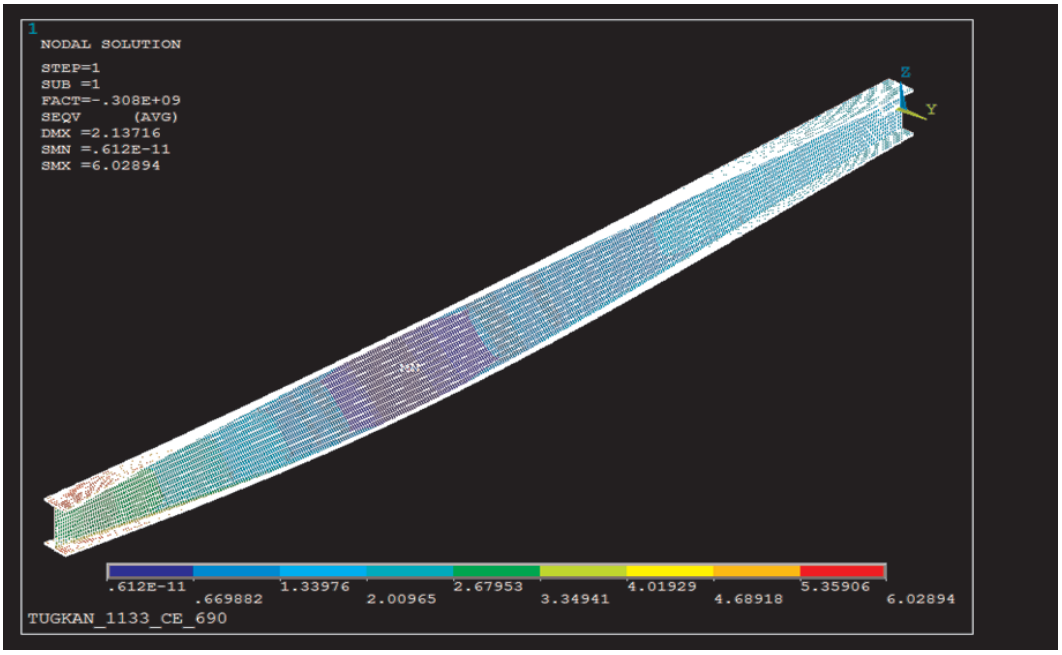

Figure B.11. ANSYS Von Mises Stress Simulation of Analysis-1133.

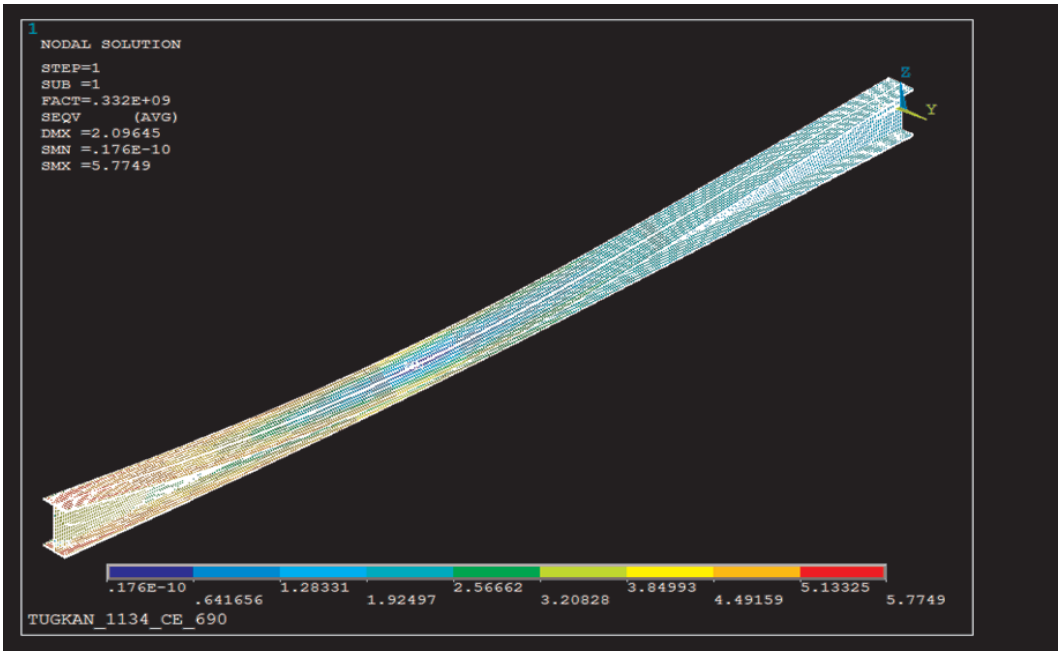

Figure B.12. ANSYS Von Mises Stress Simulation of Analysis-1134.

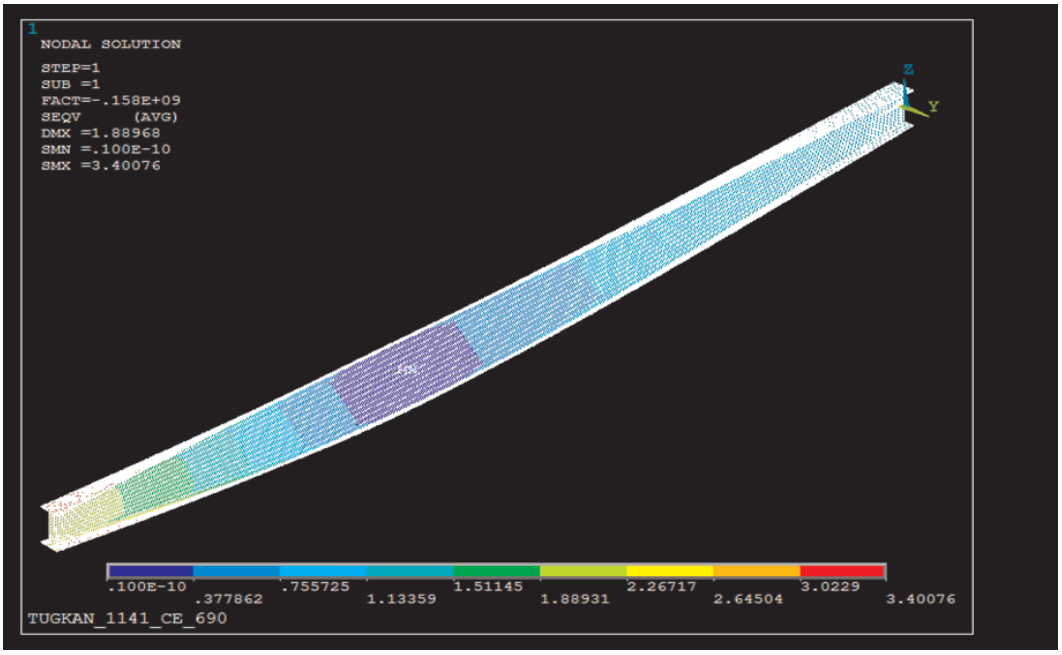

Figure B.13. ANSYS Von Mises Stress Simulation of Analysis-1141.

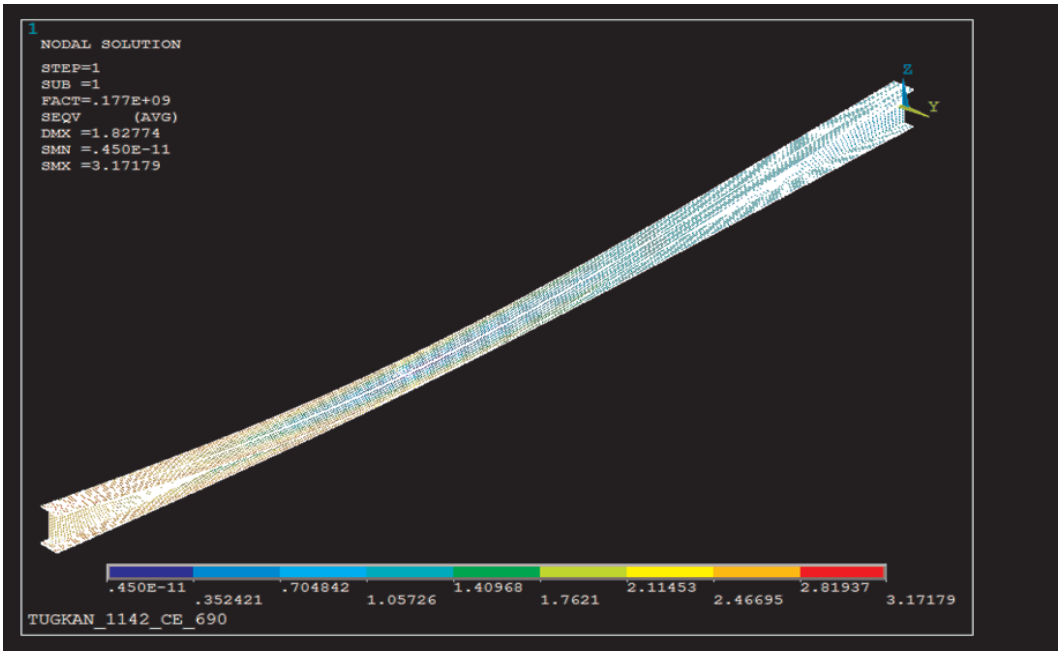

Figure B.14. ANSYS Von Mises Stress Simulation of Analysis-1142.

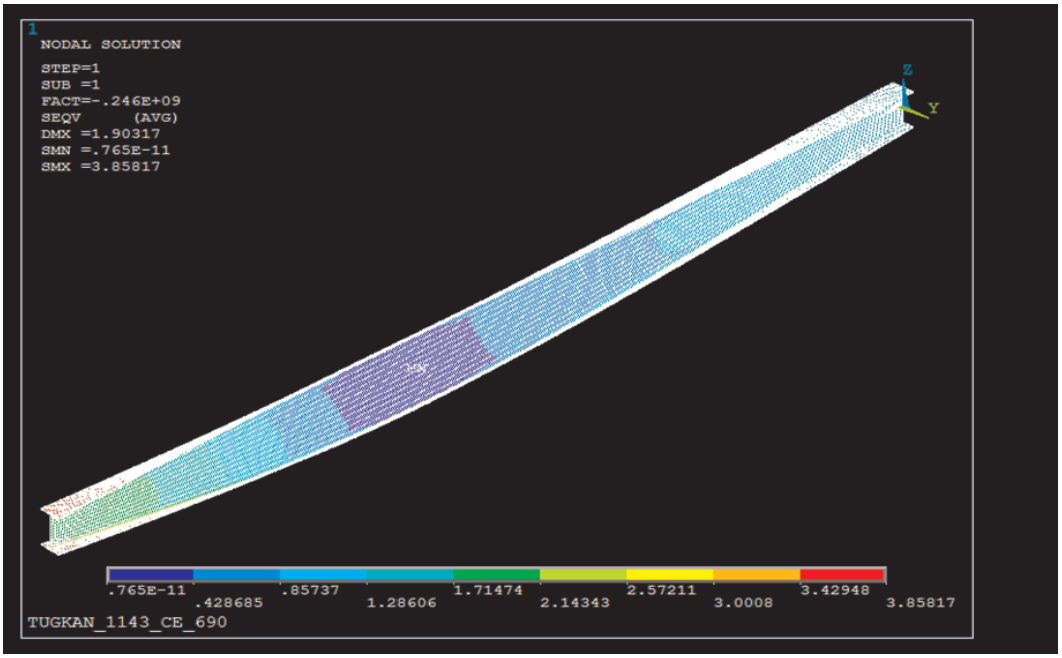

Figure B.15. ANSYS Von Mises Stress Simulation of Analysis-1143.

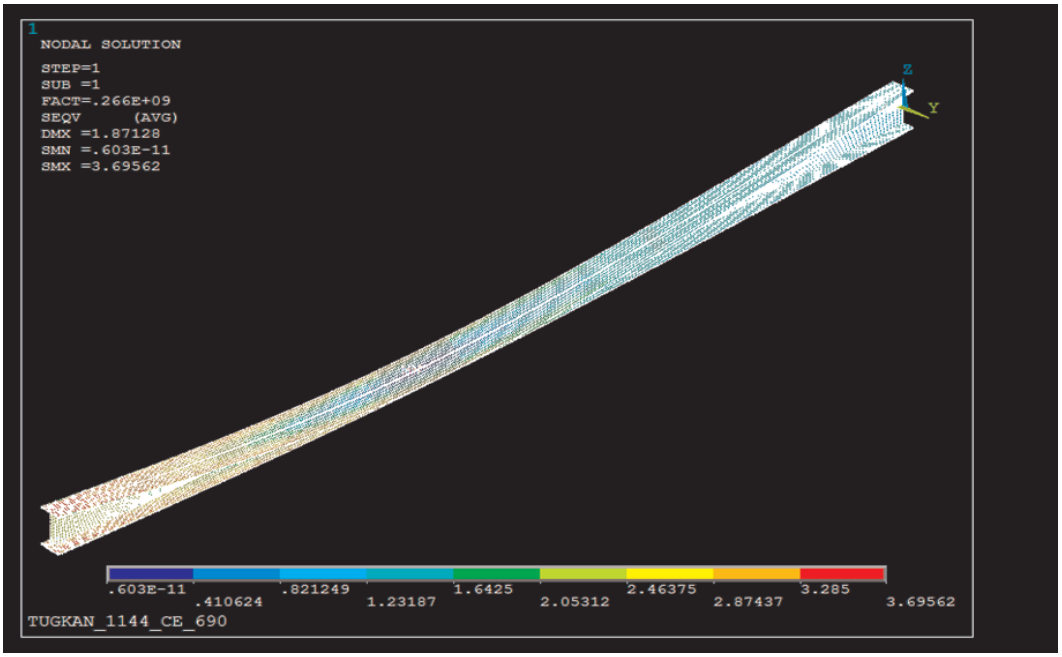

Figure B.16. ANSYS Von Mises Stress Simulation of Analysis-1144.

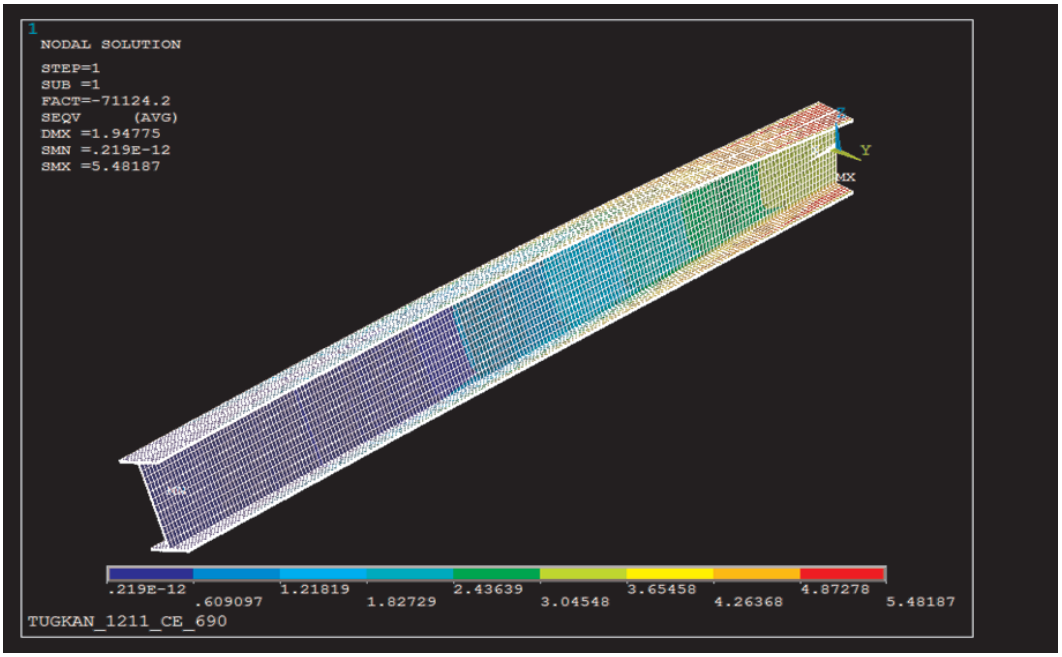

Figure B.17. ANSYS Von Mises Stress Simulation of Analysis-1211.

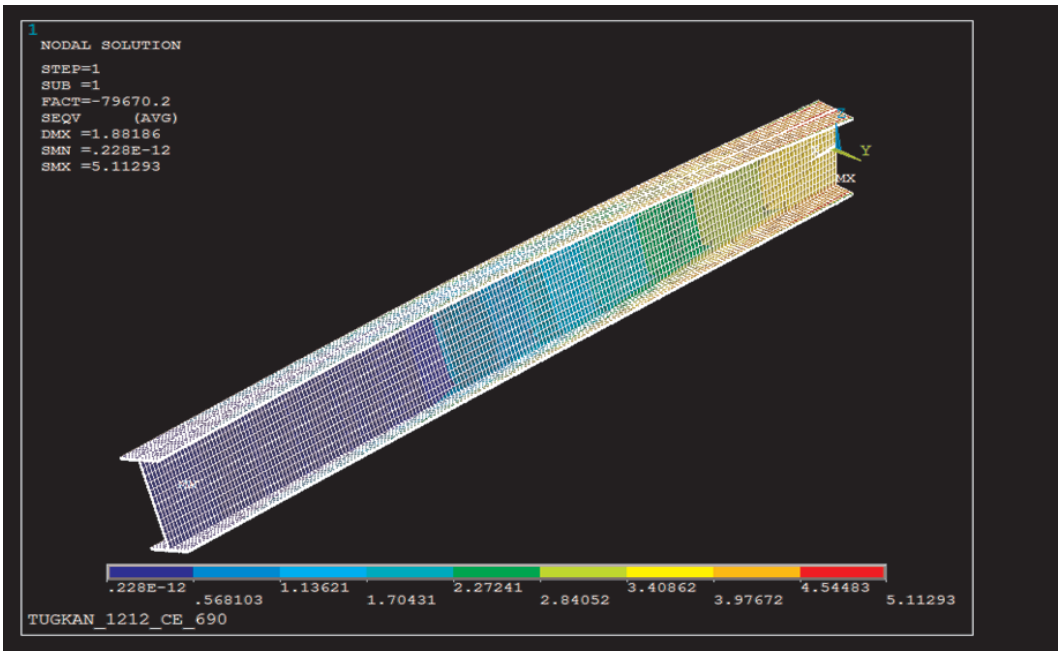

Figure B.18. ANSYS Von Mises Stress Simulation of Analysis-1212.

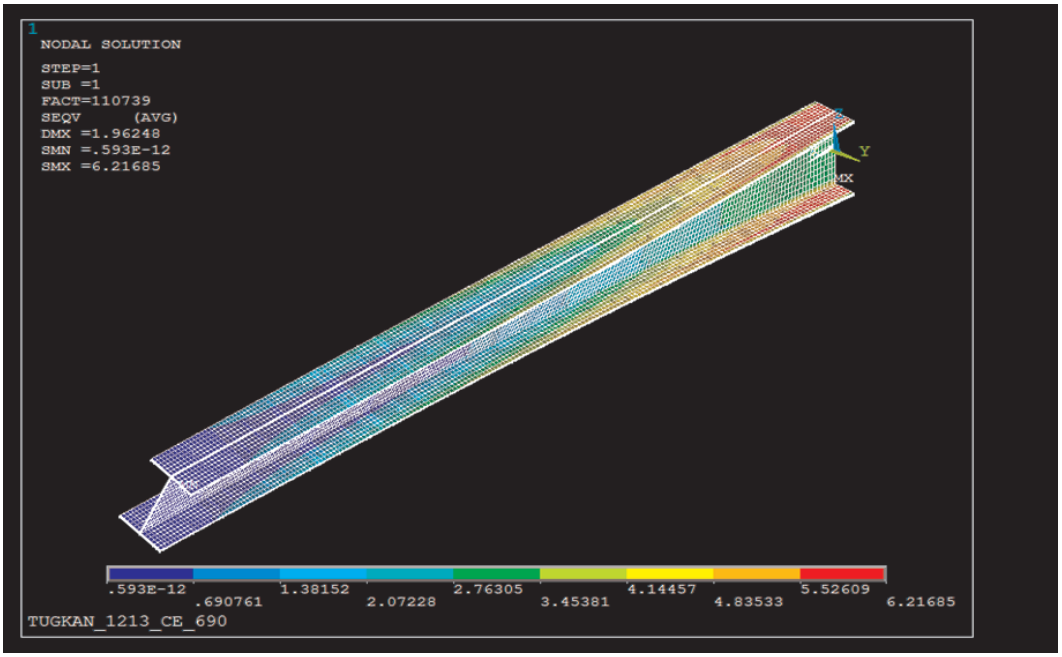

Figure B.19. ANSYS Von Mises Stress Simulation of Analysis-1213.

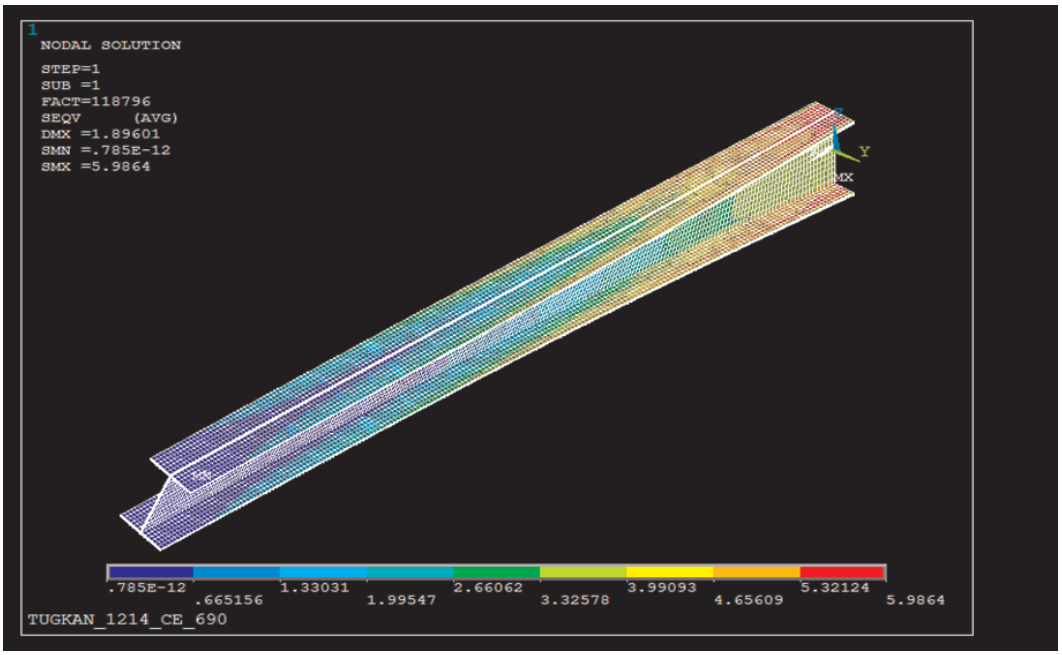

Figure B.20. ANSYS Von Mises Stress Simulation of Analysis-1214.

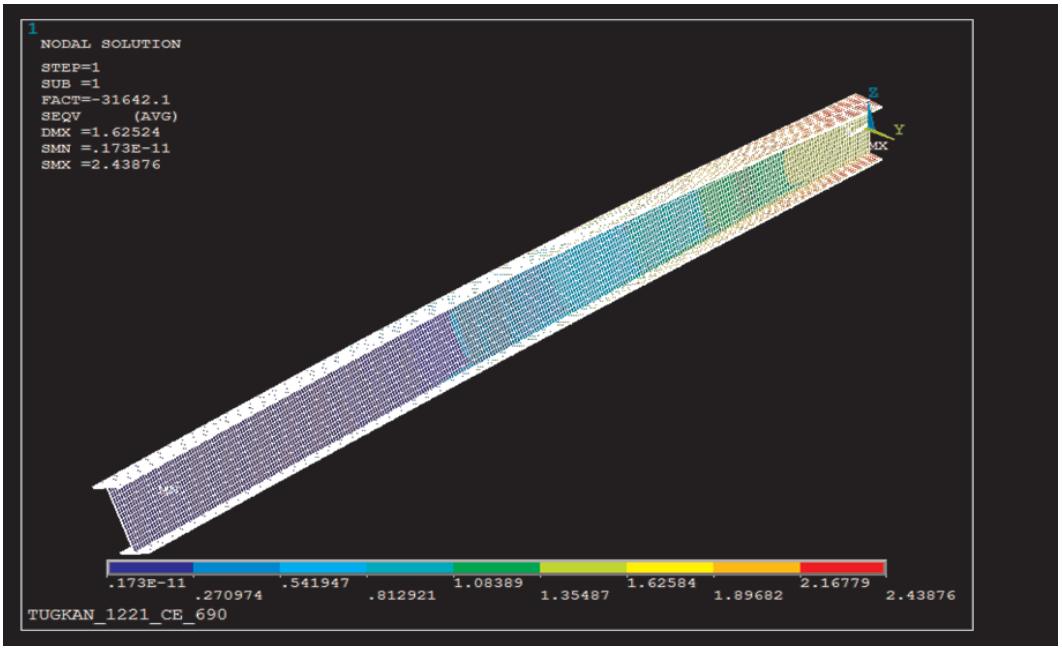

Figure B.21. ANSYS Von Mises Stress Simulation of Analysis-1221.

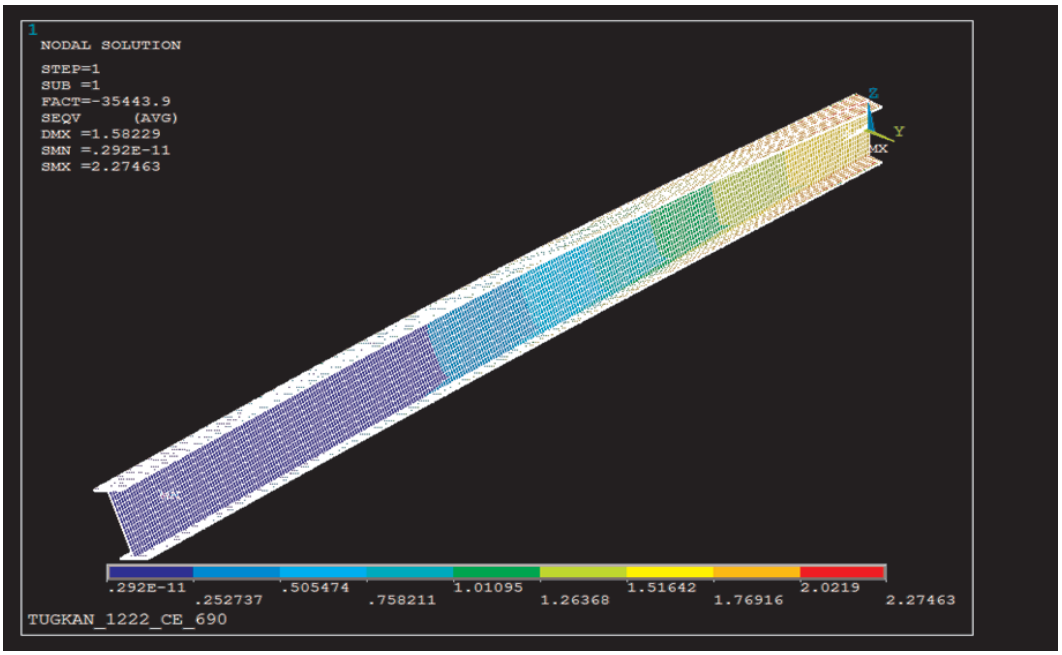

Figure B.22. ANSYS Von Mises Stress Simulation of Analysis-1222.

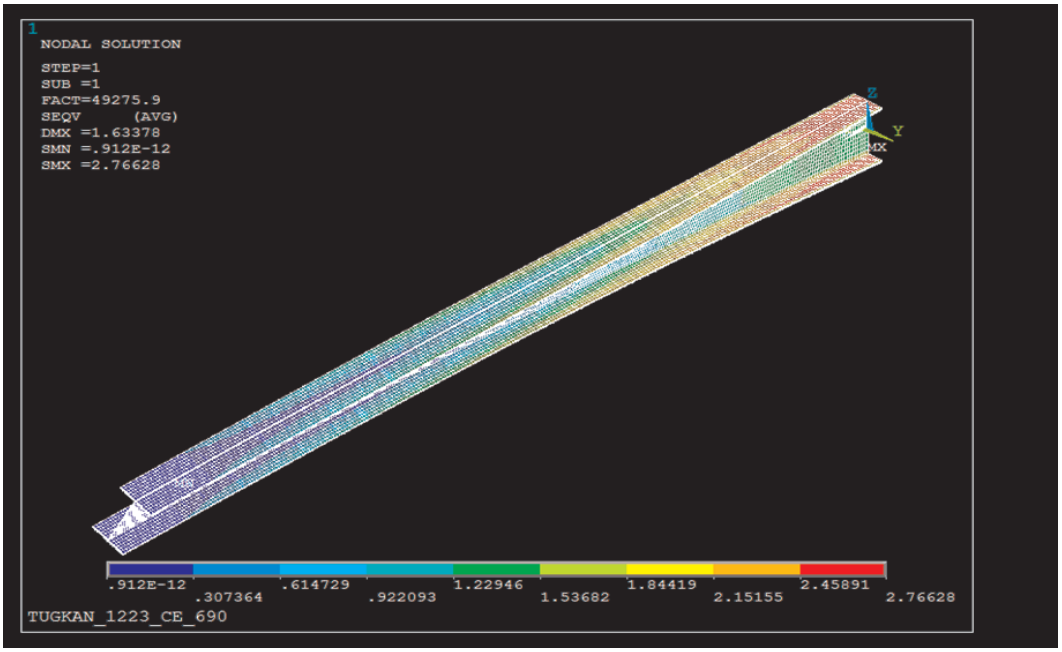

Figure B.23. ANSYS Von Mises Stress Simulation of Analysis-1223.

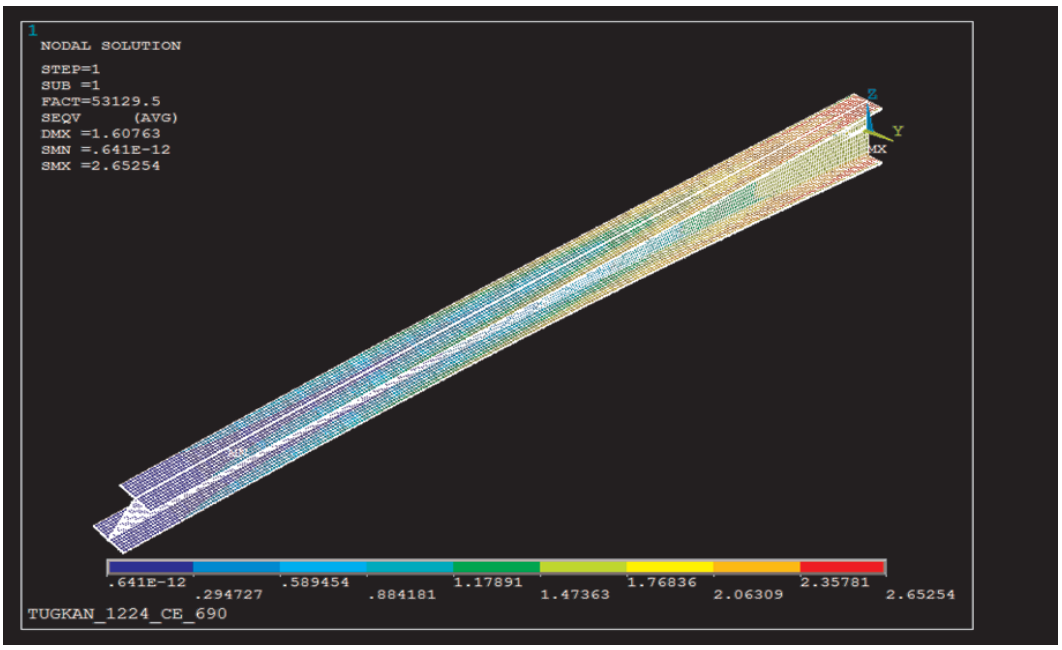

Figure B.24. ANSYS Von Mises Stress Simulation of Analysis-1224.

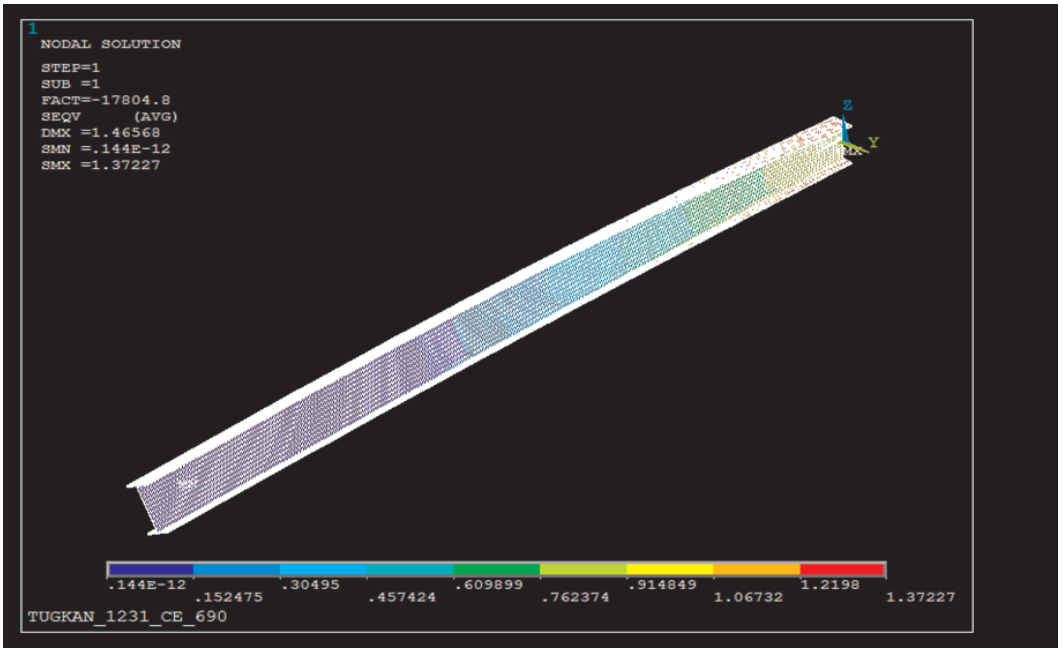

Figure B.25. ANSYS Von Mises Stress Simulation of Analysis-1231.

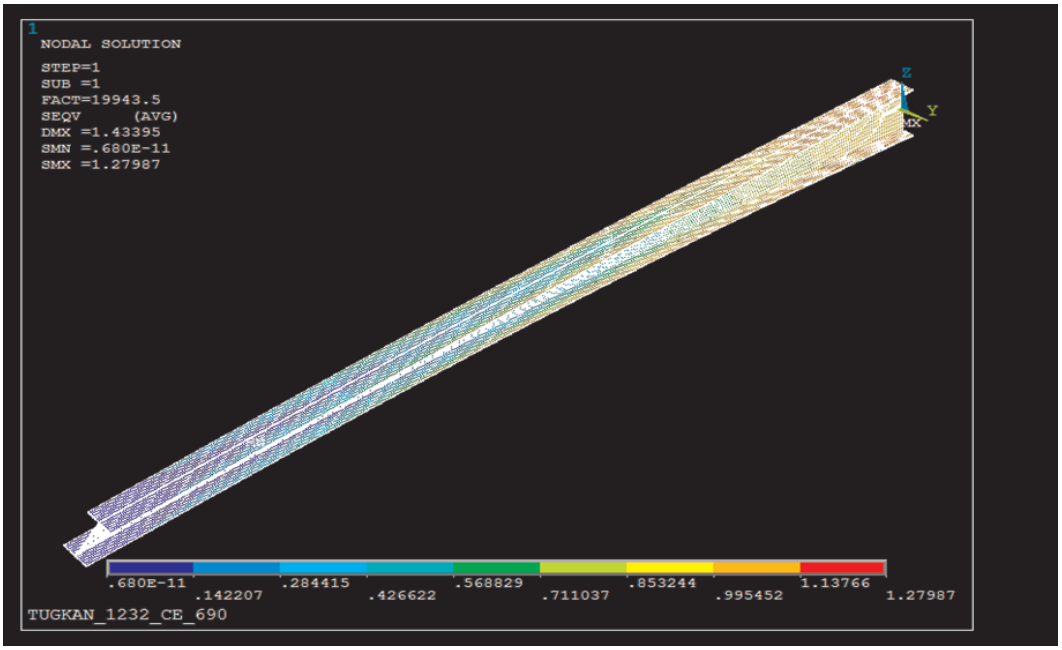

Figure B.26. ANSYS Von Mises Stress Simulation of Analysis-1232.

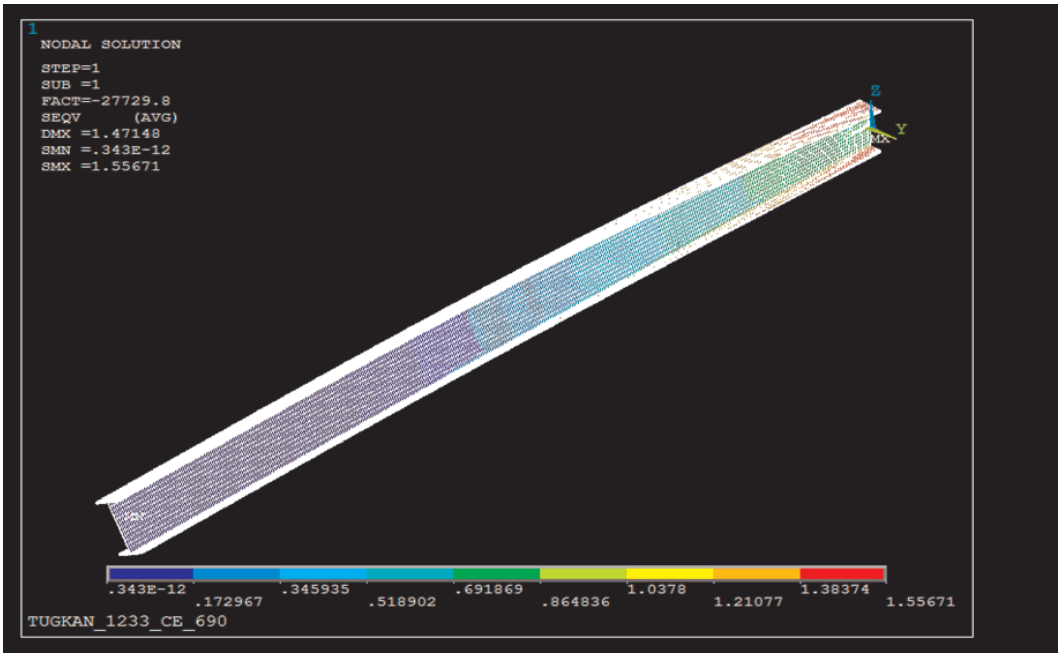

Figure B.27. ANSYS Von Mises Stress Simulation of Analysis-1233.

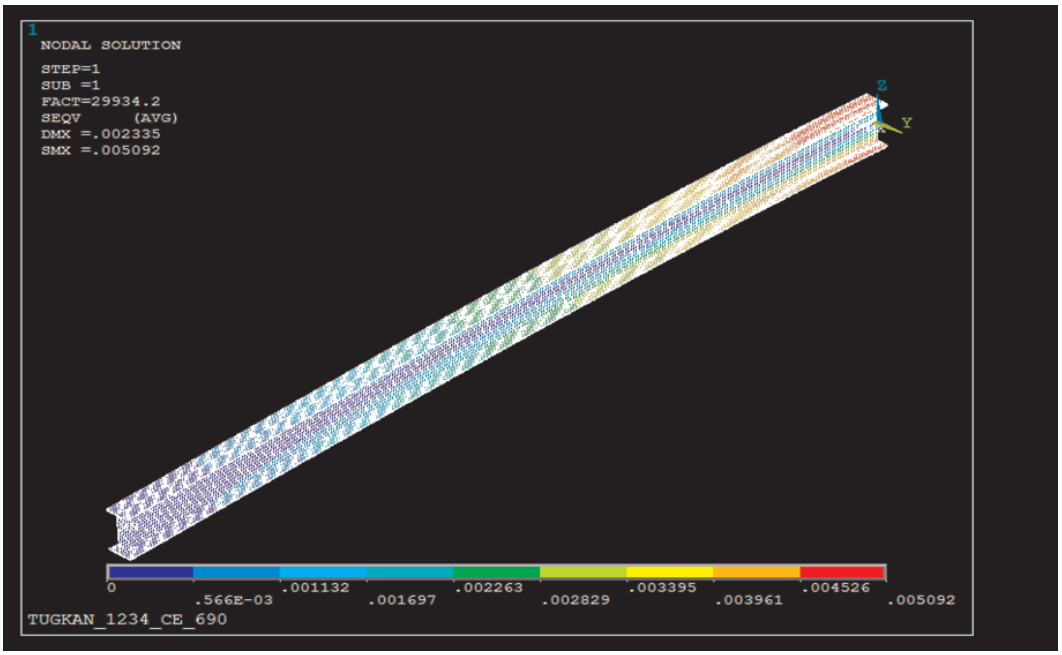

Figure B.28. ANSYS Von Mises Stress Simulation of Analysis-1234.

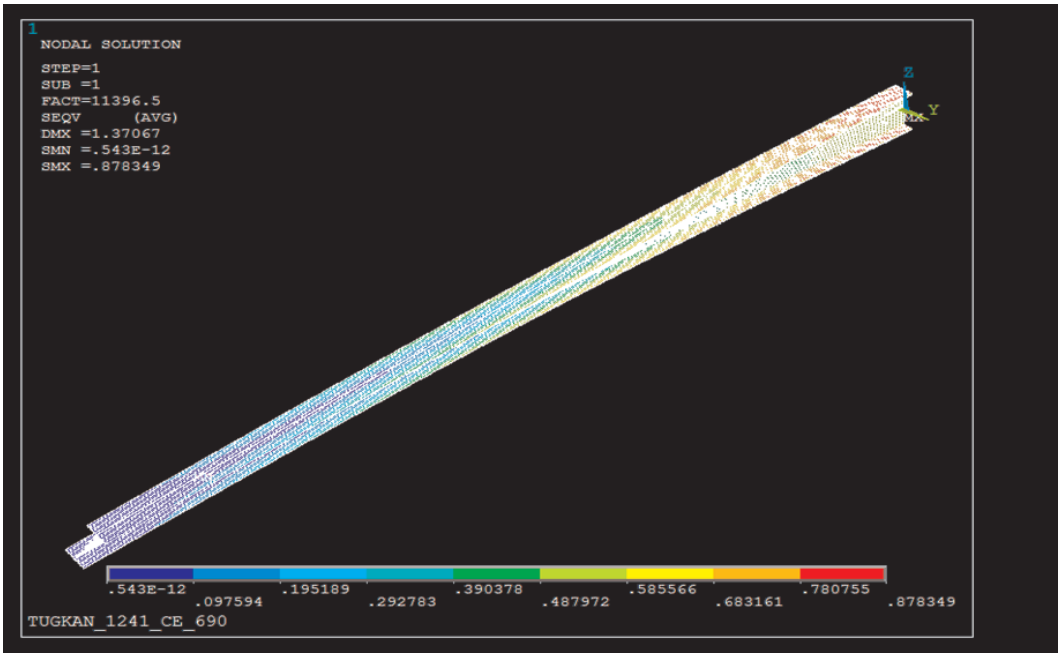

Figure B.29. ANSYS Von Mises Stress Simulation of Analysis-1241.

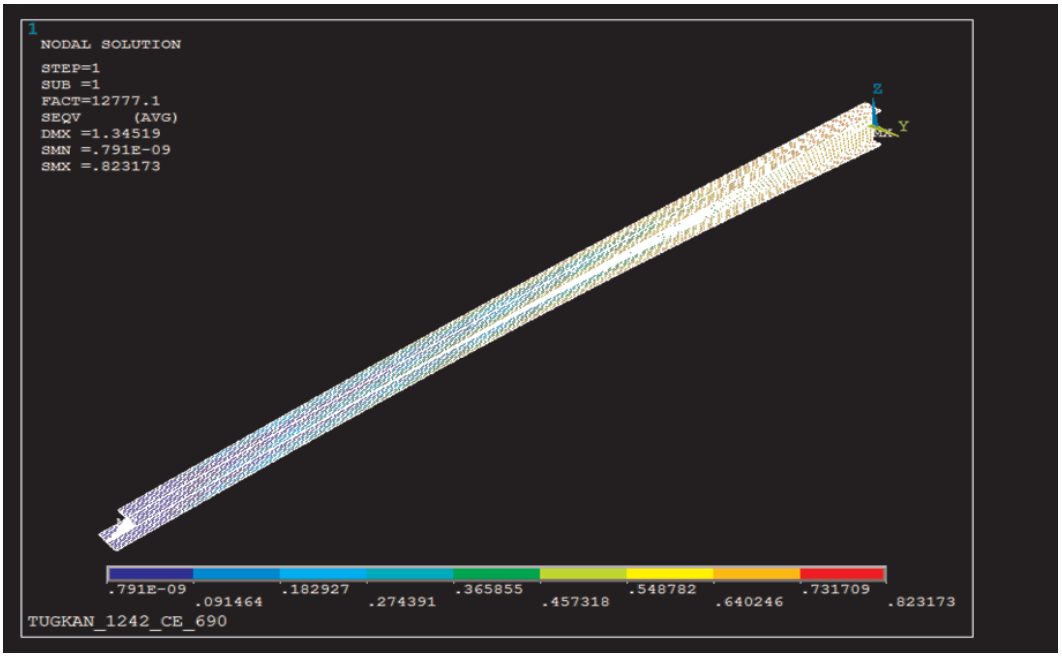

Figure B.30. ANSYS Von Mises Stress Simulation of Analysis-1242.

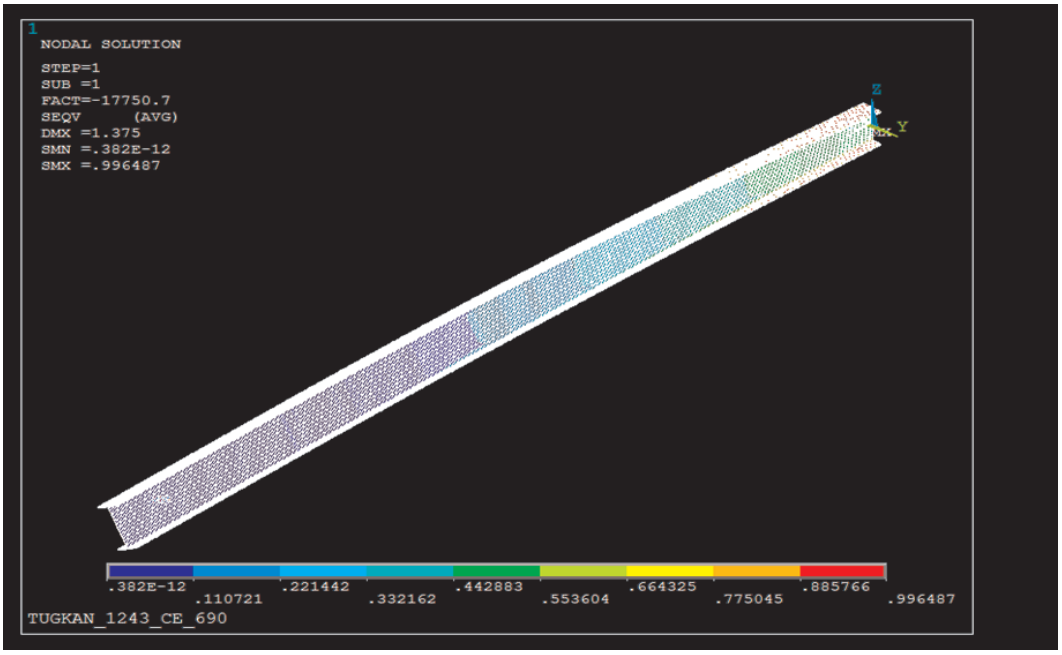

Figure B.31. ANSYS Von Mises Stress Simulation of Analysis-1243.

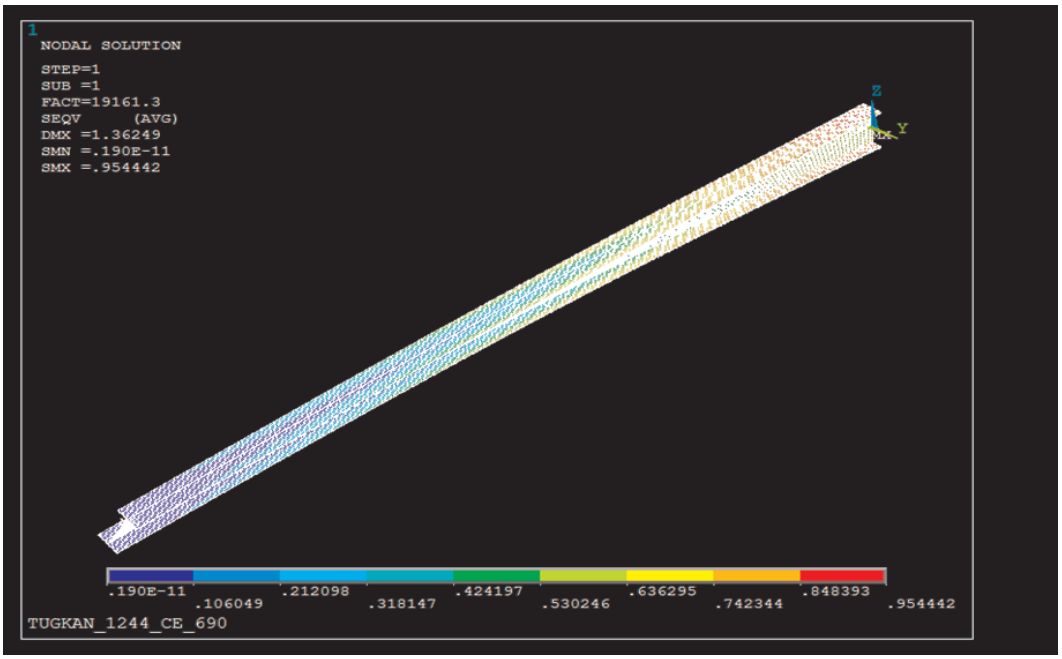

Figure B.32. ANSYS Von Mises Stress Simulation of Analysis-1244.

REFERENCES

1. Galambos, T.V., A.E. Surovek, "Structural Stability of Steel", Concepts and Applications for Structural Engineers, Vol. 1, pp. 236-288, 2008.

2. Chajes, A., "Principles of Structural Stability Theory", Vol. 1, pp. 195-236, 1974.

3. Salmon, C.G., J.E. Johnson., F.A. Malhas, "Steel Structures Design and Behaviour", Emphasizing Load and Resistance Factor Design, Vol. 5, pp. 431-494, 2009.

4. Timoshenko, S.P., J.M. Gere, "Theory of Elastic Stability", Vol. 2, pp. 251-277, 2009.

5. American Institute of Steel Construction (AISC), "Load and Resistance Factor Design Specification for Structural Steel Buildings", AISC, Chicago, usa, 1999.

6. Gambhir, M.L., "Stability Analysis and Design of Structures", Vol. 2, pp. 162-284, 2010.

7. Moaveni, S., "Finite Element Analysis", Theory and Application with ANSYS, Vol. 1, pp. 216-261, 1999.

8. Stolarski, T., Y. Nakasone., S. Yoshimoto., "Engineering Analysis with ANSYS Software", Vol. 2, pp. 143-213, 2006.

9. Madenci, E., İ. Güven, "The Finite Element Method and Applications in Engineering Using ANSYS", Vol. 2, pp. 216-324, 2007.

10. ANSYS User Guide, "Lateral Torsional Buckling Beam-189" , Technology Drive Canonsburg, PA, ANSYS Inc, 1978.

11. ConSteel 8 Manuel, "Lateral Torsional Buckling", ConSteel Solutions Ltd. Budapest, 2009.